

Oliver Rhodes

Nardobakken Studentboliger

Performance of a Prefabricated Vertical Drain System

Trondheim, June 2019

PROJECT THESIS: TBA4900

Supervisor: Arnfinn Emdal

Department of Civil and Transport Engineering
Norwegian University of Science and Technology (NTNU)



NTNU – Trondheim
Norwegian University of
Science and Technology

Preface

This thesis is submitted as part of the MSc in Geotechnics and Geohazards at The Norwegian University of Science and Technology (NTNU).

The reasearch was undertaken at the in the geotechnical department at NTNU, under the supervision of Arnfinn Emdal. Data was provided by Rambøll in Trondheim.

Trondheim, June 2019

A handwritten signature in black ink, appearing to read 'O. Rhodes', with a stylized flourish at the end.

Oliver Rhodes

Acknowledgment

I would like to thank Arnfinn Emdal for his help during the project, and Per Arne Wangen at Rambøll for providing the data.

I would also like to thank the graduating class of 2019, whose company helped motivate me throughout the semester. And finally, thanks goes to my friends and family who have supported me during my time at NTNU. I leave a richer man for the experiences we've shared.

O.J.R.

Summary and Conclusions

The project site in Nardo is underlain by a thick sequence of soft clays. An evaluation of site investigation data alongside a thorough review of the site history has produced a strong geological and geotechnical model. The study site is located at the base of a shallow slope, underlain by Dry Crust, Landslide Deposits, Quick Clay, and Marine Clay. The top of the slope is capped with river deposits.

A combination of laboratory and insitu testing has provided parameters for the back-analysis of a prefabricated vertical drain system using settlement and pore pressure observations for verification.

Use of prefabricated vertical drains was analysed by back calculation of consolidation parameters and inserted into closed-form analytical solutions, before more sophisticated numerical methods were utilised to model the drain system using non-linear parameters and a staged construction sequence.

A soft soil creep model was utilised for the analysis that was able to calculate settlements mostly to within $\pm 8\text{mm}$, equating to an average percentage error of $\pm 15\%$. The calculated pore pressures aligned closely with measured values also although initial excess pore pressures were slightly under-estimated.

A good understanding of the stress history enabled the creep model to be used confidently, although some inaccuracies were introduced when averaging previous overburden pressure along the sloping ground.

It is concluded that the drains provided a good means of accelerating consolidation and providing additional stability to foundation soils. An interesting observation that the drains increased groundwater to a close to hydrostatic condition highlighting that care must be taken when designing a deep drainage system if pore pressures are significantly greater than hydrostatic, as a decrease in stability may result.

Contents

Preface	i
Acknowledgment	ii
Summary and Conclusions	iii
Aacronyms	x
1 Introduction	1
1.1 Background	1
1.2 Objectives	2
1.3 Limitations	2
1.4 Approach	2
1.5 Structure of the Report	3
2 Site Context	4
2.1 Site Location and Description	4
2.2 Geology and Topography	5
2.3 Landslides in the Local Area	6
2.4 Stress History	7
2.4.1 Inferred Over-consolidation	8
3 Nardobakken Site Conditions	9
3.1 Data Sources	9
3.2 Soil Layering	10
3.3 Index Tests	11
3.4 Oedometer Stiffness	13
3.4.1 Permeability	14
3.5 Shear Strength	15
3.6 Landslide Hazard and Proposed Remediation	16
4 Literature Review for Precompression and Prefabricated Vertical Drains	17
4.1 Introduction	17

4.2	Primary Consolidation	17
4.3	Secondary Consolidation/Creep	18
4.4	Consolidation under surcharge	20
4.5	Radial Drainage due to Prefabricated Vertical Drains	20
4.6	Design Considerations for Vertical Drains	21
4.6.1	Other Considerations	22
4.7	Plane-Strain Permeability Equivalence	22
5	Construction Sequence and Monitoring	25
5.1	Sequence of Events	25
5.2	PVD Installation and Specification	26
5.3	Filling	27
5.4	Pore Pressure Monitoring	27
5.5	Ground Settlement Monitoring	28
6	Modelling of a Single Drain	31
6.1	Parameters	31
6.2	Back-Calculation of Horizontal Coefficient of Consolidation, C_h	32
6.2.1	C_h from Settlement Data	32
6.2.2	C_h from Pore Pressure Data	33
6.3	Single Drain Analytical Solution	34
6.4	Finite Element Solution	35
6.4.1	Boundary Conditions	36
6.4.2	Mesh	36
6.4.3	Governing Theory	36
6.4.4	Plane-Strain Finite Element Formulation	37
6.5	Comparison of Axisymmetric and Plane Strain Formulations	37
6.6	Limitations of Analytical Method	39
7	Numerical Models	41
7.1	Geometry	41
7.2	Mesh	41
7.3	Loading	43
7.4	Groundwater Calculations	43
7.5	Mohr-Coulomb Soil Parameters	44
7.6	Soft Soil Creep Model	44
7.7	SSC Compression Parameters	46
7.8	SSC Strength	47

7.9	Permeability Parameters	48
8	Numerical Analysis Results	50
8.1	Initial Loads	50
8.2	Pore Pressure Dissipation	51
8.2.1	Comparison of Pore Pressure Dissipation with and without PVD	52
8.3	Settlements	52
8.4	Lateral Displacements	52
8.5	Safety	56
9	Conclusions and Discussion	59
9.1	Summary and Conclusions	59
9.2	Discussion of Results	59
9.2.1	Uncertainty of the Ground Conditions	59
9.2.2	Accuracy of the Numerical Model	60
9.2.3	Efficacy as a Slope Stabilisation Technique	60
9.3	Recommendations for Future Work	61
	Bibliography	62
A	Site Plan and Slope Profiles	66
B	Interpreted Site Investigation Data	67

List of Figures

2.1	Areal photo of project site	4
2.2	Geology map of Trondheim	5
2.3	Geology map of the site	5
2.4	Landslide event in Othilienborg, reproduced from Sand (1999)	6
2.5	Landslide event in Lerkendal, reproduced from Sand (1999)	6
2.6	Change in ground level between 1951 and 2018	7
3.1	Investigation points referenced within this report	10
3.2	Moisture content and Atterberg limits	12
3.3	Unit weight	12
3.4	Plasticity and liquidity indices	12
3.5	Initial void ratio	12
3.6	Oedometers plotted as effective stress - void index	14
3.7	Vertical permeability from CRS oedometers	15
4.1	Principle of secondary consolidation (Bjerrum, 1972)	19
4.2	Principle of conversion between radial flow and plane flow permeability; from Indraratna and Redana (2000)	23
5.1	Cross section of PVD and mandrel	26
5.2	Piezometer pore pressures before and after PVD installation with corresponding hydrostatic profiles	28
5.3	Piezometer pore pressures before, during and after PVD installation	28
5.4	Principle sketch of settlement plate used	30
6.1	caption	32
6.2	caption	32
6.3	Unit cell finite element geometry	35
6.4	Pore pressure dissipation for analytical, axisymmetric FE, and plane-strain FE methods	38

6.5	Settlements for analytical, axisymmetric FE, and plane-strain FE methods	38
6.6	Comparison of analytical solution and field measurements	40
6.7	Comparison of analytical solution and field measurements, optimised paramters	40
7.1	Profile A model and boundaries	42
7.2	Profile A stress points and nodes	42
7.3	Profile B model and boundaries	42
7.4	Profile B stress points and nodes	42
7.5	Profile C model and boundaries	42
7.6	Profile C stress points and nodes	42
7.7	The reference surface and equivalent mean stresses after (Stolle et al., 1999)	45
7.8	Oedometer test and simulation C2 5.4m	47
7.9	Oedometer test and simulation C2 6.35m	47
7.10	Oedometer test and simulation C2 7.4m	47
7.11	Oedometer test and simulation C2 10.3m	47
7.12	Oedometer test and simulation C2 11.4m	47
7.13	CAUC triaxial test simulation and laboratory results C2, 6.45m and 6.6m	48
7.14	CAUC and CAUP triaxial test simulation and laboratory results C2, 10.4m and 10.55m	48
7.15	CAUC triaxial test simulation and laboratory results C2, 11.5m and 11.6m	48
7.16	CAUC triaxial test simulation and laboratory results for Quick Clay C2, 7.5m and 7.6m	48
8.1	Principal stresses, K_0 calculation	51
8.2	Principal stresses, drained null step	51
8.3	Pore pressure at position A2	53
8.4	Pore pressure at position C1	53
8.5	Pore pressure at position C2	53
8.6	Excess pore pressures after filling without PVD	54
8.7	Excess pore pressures after 267 days consolidation without PVD	54
8.8	Excess pore pressures after filling with PVD installed	54
8.9	Excess pore pressures after 265 days consolidation with PVD installed	54
8.10	Predicted and measured settlements Section A	55
8.11	Predicted and measured settlements Section B	55
8.12	Predicted and measured settlements Section C	55
8.13	Predicted settlements at Kiwi	55
8.14	Settlement along Profile A, with and without PVD	56
8.18	Comparison of lateral displacements at 15m from the fill centre-line, with and without PVD	56

8.15 Normalised lateral displacements along Profile A	58
8.16 Normalised lateral displacements along Profile B	58
8.17 Normalised lateral displacements along Profile C	58

List of Tables

3.1	Parameters derived from the CRS oedometers	13
3.2	Summary of triaxial test results	16
5.1	Properties and dimensions of PVD and mandrel	26
5.2	Summary of piezometer readings during construction	27
6.1	Parameters for unit cell analysis	31
6.2	C_h back calculated from settlement data	33
6.3	C_h back-calculated from pore pressure readings	34
6.4	Equivalent plane strain permeability values	37
7.1	Summary of generated meshes	43
7.2	Staged construction summary	43
7.3	Mohr-Coulomb paramters for soils not subject to creep	44
7.4	Compression parameters for SSC model	46
7.5	Strength parameters for SSC model	47
7.6	Permeability parameters	49
8.1	Factor of safety against base failure	57
B.1	Summary of soundings referenced within this study	68

Acronyms

CAUC Consolidated Anisotropic Undrained Compression triaxial test

CAUP Consolidated Anisotropic Undrained Passive triaxial test

CPT Cone Penetration Test

CRS Constant Rate of Strain

moh Meters above sea level (Norwegian: meter over havet)

POP Previous Overburden Pressure

PSD Particle Size Distribution

PVD Prefabricated Vertical Drain

SSC Soft Soil Creep model

Chapter 1

Introduction

Prefabricated vertical drains (PVD) are a common method to accelerate the consolidation process by exploiting the faster rate of radial consolidation, as compared to vertical consolidation. This is particularly useful at sites underlain by deep, soft, fine-grained soils. This report aims to compare and evaluate the various calculation methods based on a study of observations from a site in Nardo, Trondheim. At this site, PVD were installed beneath a crushed rock fill which was constructed to serve as both a slope stabilisation measure and foundation of a medium rise student accommodation block.

1.1 Background

The project site is located in Nardo, Trondheim at the base of a shallow slope. This slope comprises marine clay, capped with sand and gravel deposits and is located in an area containing quick clays and where landsliding has occurred historically. The general slope is approximately 11° with some localised cuttings related to previous construction works e.g. retail facilities and car parking.

The author has previously undertaken an analysis of slope stability, in which a factor of safety was below the required 1.4 in the total stress situation, and as such it was necessary to improve stability to enable future construction works. The most appropriate means of stabilising the slope was with a counter-fill with PVD to accelerate settlement and provide additional stability to the foundation soils.

An analysis of the filling and consolidation has been undertaken, initially using one-dimensional radial consolidation theory to model a single drain. This has then been developed into two, one-dimensional, finite element models in axisymmetry, and equivalent plane-strain. Finally

a two-dimensional, plane-strain model was used to model the performance of the multi-drain system.

1.2 Objectives

The main objectives of this project are

1. Review site history and all relevant test data for evaluation of soil behaviour
2. Literature study of pre-compression with prefabricated vertical drains
3. Develop appropriate axisymmetric and plane-strain models that are able to reproduce the geometry, loading, and measured pore pressures and settlements at the project site
4. Compare the results to measured values and conclude on the performance of the model

1.3 Limitations

The field values of settlement and pore pressure are available for the respective periods of 267 days and 179 days following the final fill level being reached. Pore pressures have largely dissipated, though some settlement appears to continue.

Considerable uncertainty exists about the exact loading sequence during the construction works as very vague timings were provided by the contractor. A 'best fit' of the sequence of works has been produced from pore pressure readings from three piezometers at one end of the site. Moving away from this position creates greater uncertainty about when each stage of construction was carried out.

All the settlement plates, and the piezoemeters on one slope profile, were read at a relatively large time intervals therefore initial settlement curves, and initial excess pore pressures were not recorded. Verification of the calculation results is therefore limited in some areas.

1.4 Approach

A thorough background study of the project area will be carried out using available data sources in order to determine the stress history.

A site investigation report will be considered, and soil parameters will be derived from interpreted laboratory test reports.

A literature review of pre-loading and prefabricated vertical drains will be carried out and an analytical solution for site project site will be created. Consideration will be give to the merits and limitations of such a model and ways to improve it using numerical methods will be described.

A numerical model incorporating non-linear soil behaviour will be used to model the project site when subjected to a staged construction, the results of which shall be critiqued.

1.5 Structure of the Report

The rest of the report is structured as follows:

Chapter 2 - Description of the site area and local geological history

Chapter 3 - Site investigation data and interpretation

Chapter 4 - Literature review and theory for prefabricated vertical drains, pre-loading, and surcharging including relevant soil mechanics theory

Chapter 5 - Construction sequence and monitoring data is presented and described

Chapter 6 - Modelling of a single drain using closed form and numerical methods

Chapter 7 - Description of the 2D numerical model, input parameters, geometry, and loading

Chapter 8 - Results of the 2D numerical model

Chapter 9 - Discussion of the results of the numerical analysis, conclusions, and recommendations for further work

Chapter 2

Site Context

This chapter serves to give a context to the study site by reviewing the local geological history and topography. The stress history is considered to be one of the most important factors affecting rates of consolidation therefore attention shall be paid to it.

2.1 Site Location and Description

The study site is located in Nardo, Trondheim within a valley with hills to the east and west. The valley base forms a shallow decline trending to the north and along the road, Torbjørn Bratts Veg.



Figure 2.1: Areal photo of project site

The area shown in red in Figure 2.1 is a car park to the rear of a Kiwi store. Development works require the re-profiling of this area and placement of a crushed rock fill that will act to stabilise

the shallow slope to the west and act as the foundation of a mid-rise student accommodation block.

2.2 Geology and Topography

The quaternary geology of the Trondheim region is relatively well studied. The Fennoscandian ice sheet laid down moraines over Greenstone bedrock some 13,000 years ago (Reite et al., 1982). As the icesheet began to retreat some 10,000 years ago, the lower lying areas of Trondheim remained below the marine limit with the melting ice sheet providing a source of sediment allowing for the deposition of thick marine clays (Reite et al., 1999). Simultaneous to deposition, stress relief from the glacial retreat caused isostatic uplift resulting in a land rise on the order of several hundred meters (NGU, 2013).

The previous marine limit was approximately 175m above existing sea level, whilst Nardo is at +60moh, indicating this area was located in a maximum water depth of some 115m.

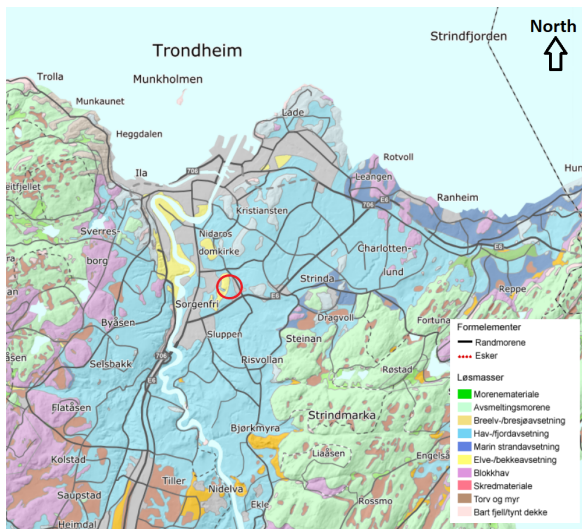


Figure 2.2: Geology map of Trondheim

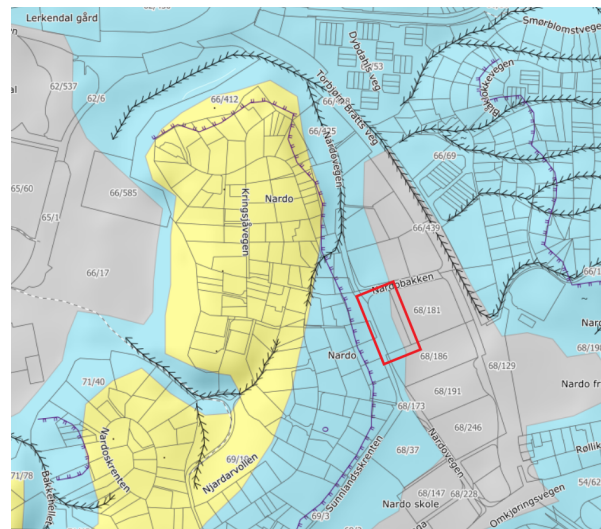


Figure 2.3: Geology map of the site

Figures 2.2 and 2.3 show the quaternary geology (with the study site shown as a red boundary). Thick marine clays are mapped as the predominant geology of the area, with the hill to the west being capped with sand river deposits from the former course of the Nidelva. Grey shading indicates anthropogenic deposits, i.e. filling in relation to construction of buildings/roads. Additionally, quick clay hazard mapping shows the site to lie within a quick clay susceptible zone.

Figure 2.3 shows flow channels in the surrounding area. These channels correlate very strongly to the present day topography which comprises hills to the west and east of the site, and a valley that trends on a north western direction.

2.3 Landslides in the Local Area

Work by [Sand \(1999\)](#) has traced the history of landsliding across Trondheim. The key findings of his study, as well as interpretation with respect to the Nardo study site have been summarised in this section.

Some 4000 to 4500 years ago the Nidelva was located to the east of its present day location. River erosion caused several short duration landslide events in the area between Sluppen Ridge and Stavne Leangen Bridge (south of Nardo). Approximately 10m of historic slide debris has been proven in this area and dating of the slide material indicated the slides happened ca.2200 years ago. In Othilienborg (immediately south east of Nardo), some 2.5m of slide material is present from slide events ca.600 to 700 years ago.

Between Sundlandskrenten and Gloschaugen (north of the Nardo) there is a valley causing a break in plateau. At the base of the valley, 3.5m of slide debris was proven in one location, dated to some 1800 years ago. Original ground level is thought to have been 55moh to 75moh in Gloschaugen and Sundlandskrenten respectively, with the present day valley bottom at 40moh.

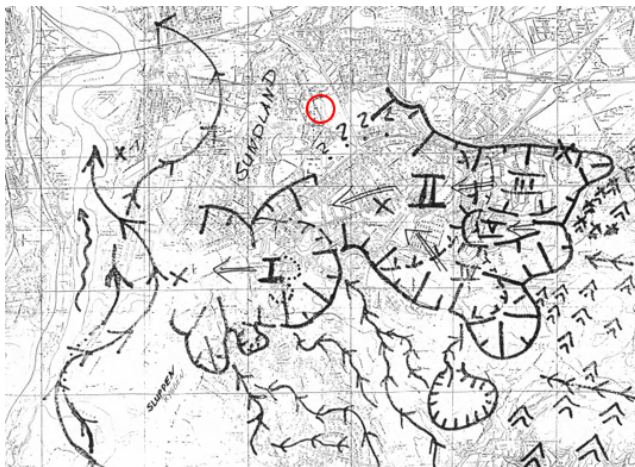


Figure 2.4: Landslide event in Othilienborg, reproduced from [Sand \(1999\)](#)

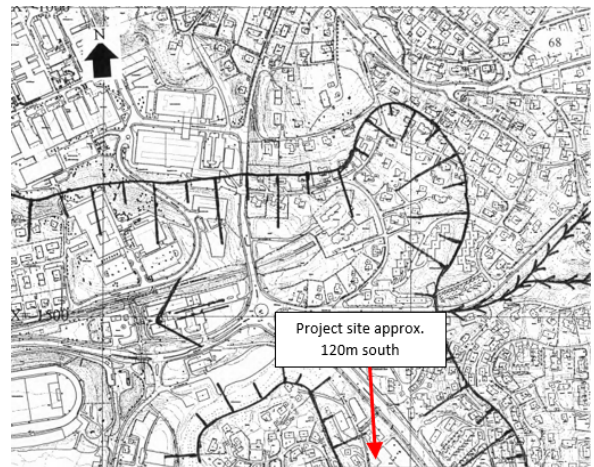


Figure 2.5: Landslide event in Lerkendal, reproduced from [Sand \(1999\)](#)

Figures 2.4 and 2.5 show that slope failures occurred around Nardo and the resulting debris flowed out to the north and west. Quick clay slides have extremely long run-out distances ([Strand et al., 2017](#)); transporting and depositing material over large distances. Therefore Nardo may be underlain by landslide debris of not only unknown thickness, but also unknown composition.

2.4 Stress History

Ground level contours have been traced from the 1951 survey of Trondheim. It is noted that elevations on the 1951 map had to be increased by 0.76m due to a change of datum. The map shows a general fall in gradient across the site in a north eastern direction. The south west of the PVD area is at approximately 64moh, and the north east at approximately 61moh. The fall of approx 4m is consistent along the approx 30m width of the site, giving a slope angle of some 8° and continues as such for a further approx 50m to the base of the valley, coincident with Torbjorn Brats Veg.

Contemporary mapping shows that a cut was made into the slope for the construction of Kiwi to a level of 58moh to 59moh.

The contours traced from the 1951 map were imported into the computer programme Surfer along with contemporary surveys undertaken prior to construction activities. The change in ground level has been contoured, showing little to no change on the south western boundary, increasing to -3.5m to -4m, i.e. cut on the north eastern boundary of the study site.

Across the Kiwi building footprint, some 0m to 3.5m excavation was also noted. The cut created a maximum slope angle of approximately 15° within the study site.



Figure 2.6: Change in ground level between 1951 and 2018

The 1951 map has a contour interval of 2m, whereas the contemporary survey is 1m. Slight discrepancies in road positions were noted when re-scaling and overlaying the two maps, thought to be caused by inaccuracies in mapping. However, the overlay was centred around Nardo and

so the error introduced for this purpose is minimal.

Comparison of the pre and post construction surveys the net change in ground level across the PVD area can be seen to range from 1.3m to 3.3m. It must be noted that benching was used in order to construct on the hillside, therefore the change in ground level is not equivalent to the thickness of fill placed.

The net ground level change has also been contoured from the 1951 map and post construction survey. It shows that change in terrain is a net decrease in the north east of some -1m to -1.8m, and a net increase in the south west of some 0.6m to 1.4m. The centre line of the long section of the filled area has little net change in terrain level.

2.4.1 Inferred Over-consolidation

The site history suggests that the Marine Clay initially formed a plateau across the whole area at approximately 70moh and was subsequently eroded to level less than the present day (i.e. below 59moh) by the Nidelva. A landslide event then occurred, and an accumulation of debris has created the existing local topography which was locally re-profiled for development. This gives evidence for a normally consolidated layer of Landslide Debris, underlain by a moderately over-consolidated Marine Clay.

Previous overburden pressure (POP) for the Landslide Debris might vary in the range of 20kPa to 70kPa due to gravity loading. POP in the deeper Marine Clay may be up to 200kPa, though this will depend in some extent to the amount of pre-landslide erosion.

Chapter 3

Nardobakken Site Conditions

The purpose of this chapter is to set out the ground conditions of the study site and to describe and quantify the pertinent geotechnical properties and soil behaviour.

3.1 Data Sources

A site investigation completed by Rambøll in May 2017 is the main source of site-specific data. In addition, several historic ground investigations both on and off-site have been incorporated where necessary. An overview plan showing the locations of site investigation points referenced within this report is given in Figure 3.1. An enlarged version of this plan along with the three slope profiles, A, B, and C has been enclosed in Appendix A for greater clarity.

The geotechnical parameters have been obtained based on all available and relevant data for the site. The interpreted laboratory test results and CPTU profiles are enclosed in Appendix B.

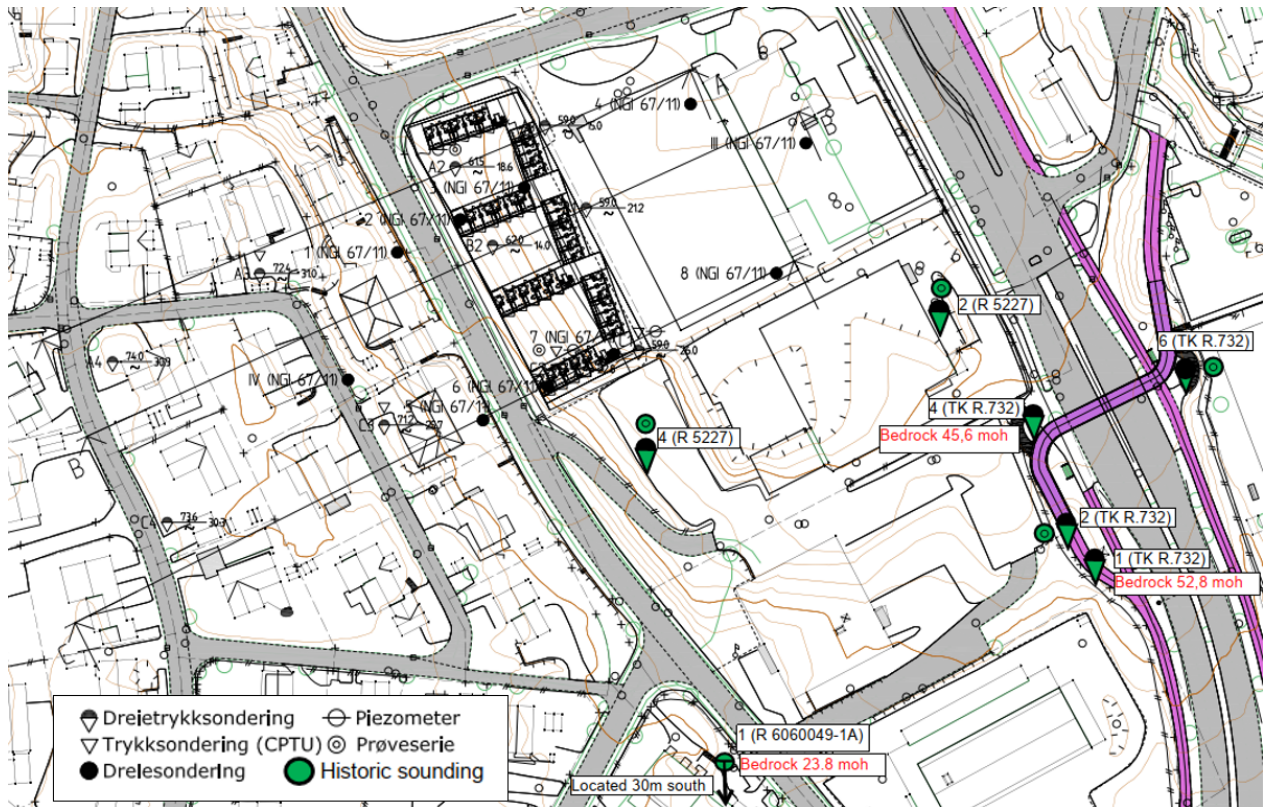


Figure 3.1: Investigation points referenced within this report

3.2 Soil Layering

It was identified that study site is underlain by the following sequence of soils:

- (S) Sand/gravelly sand - river deposits strata dipping to the west
- (DC) Dry Crust - desiccated Marine Clay, maximum 2m thickness
- (LD) Landslide Debris (marine clay) - 'young' marine clay deposited onto lower levels from landslide events several hundred to several thousand years ago
- (QC) Quick Clay - very high sensitivity clay within the lower half of the Marine Clay (landslide debris) unit
- (MC) Marine clay (undisturbed) - 'older' marine clay, not affected by previous landslides

The contact between S and LD was identified at an elevation of ca. 65moh, above the foundation level of the fill.

The distinction between the LD and QC was based on profiles of undrained shear strength and sensitivity.

The distinction between LD/QC and MC is based on compressibility and void index as a measure of soil structure and ageing.

The depth to bedrock was not proven beneath the site. Soundings in the surround areas have recorded bedrock elevation to range drastically between 52.8moh and 23.8moh. The on-site soundings extended below the levels of nearby shallow bedrock and therefore a deeper level has been assumed for the site. For the purposes of this study, a level of 20moh will be assumed, giving a total thickness of some 40m of clay.

3.3 Index Tests

Index tests comprising moisture content, Atterberg Limits, and unit weight were performed on clay soils retrieved using a 54mm piston sampler. The initial voids ratio (e_0) was computed from the moisture content (w) and unit weight (γ). Grain specific gravity (G_s) was assumed to be 2.75.

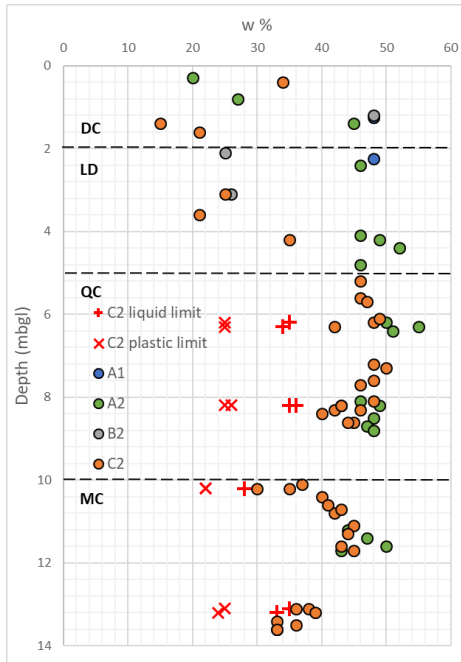


Figure 3.2: Moisture content and Atterberg limits

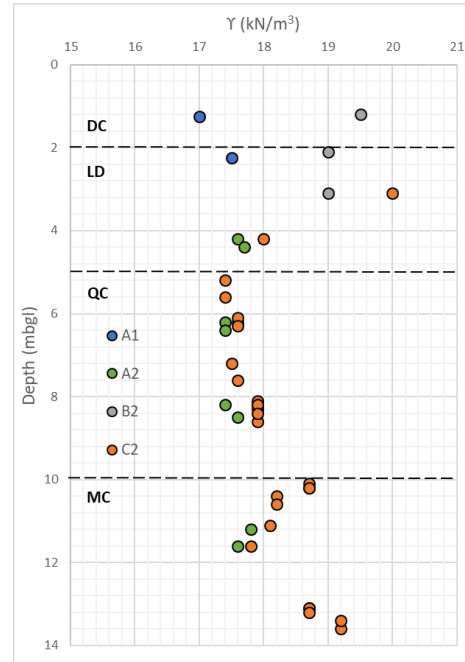


Figure 3.3: Unit weight

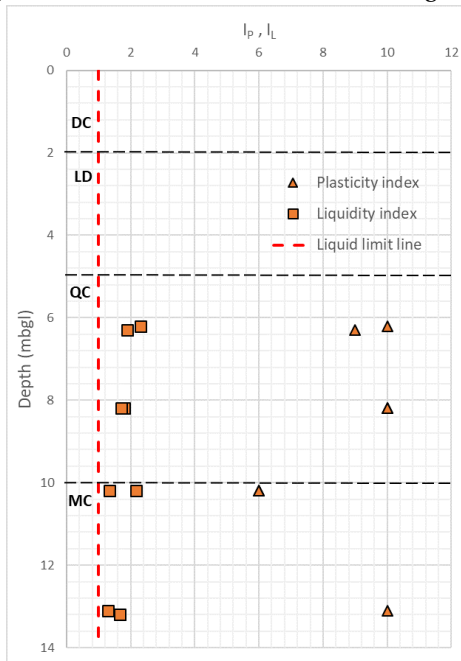


Figure 3.4: Plasticity and liquidity indices

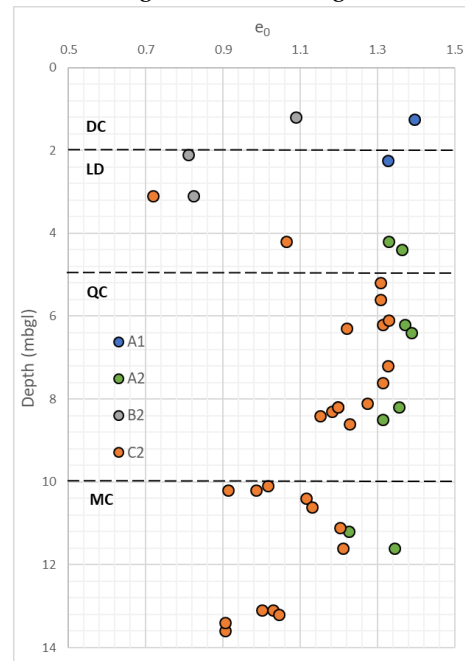


Figure 3.5: Initial void ratio

The profiles shown in Figures 3.2 to 3.5 show a large scatter of in all data within the Dry Crust and Landslide Deposits. Both w and e_0 are seen to be fairly consistent with depth within the Quick Clay, and decreasing with depth within the Marine Clay, suggesting a less open structure. Atterberg Limits within the Quick Clay and Marine Clay all show a low plasticity clay, and moisture contents always above the liquid limit.

Particle size distribution from investigations approximately 100m east of the project site [Kom-mune \(1988\)](#) identified clays at between 0.2m and 7m depth comprised of 0-1% gravel, 3-12% sand, 66-72% silt and 21-25% clay.

3.4 Oedometer Stiffness

The oedometer stiffness parameters have been obtained based on five continuous rate of strain (CRS) tests. The strain rate generally ranged 0.4 %/hr to 1.2%/hr, and pore pressure ratio was generally <0.15.

The oedometer modulus is taken as:

$$M = \frac{d\sigma'}{d\epsilon} \quad (3.1)$$

Where:

$$\sigma' = \sigma - \frac{2}{3}u_b$$

Depth (m)	Elevation (moh)	σ'_{v0} (kPa)	e_0	p'_c (kPa)	M_{oc} (kPa)	m_{oc}	m_{nc}	C_v (m ² /yr)
5.40	58.10	72.5	1.307	120	2500	33.06	13.61	1.4
6.35	57.15	79.5	1.274	132	4300	47.62	17.24	6.5
7.40	56.10	88	1.313	100	2700	31.05	15.38	3.3
10.30	53.20	112	1.130	165	6300	76.32	15.15	25
11.40	52.10	121	1.209	210	6800	42.34	15.04	7

Table 3.1: Parameters derived from the CRS oedometers

Table 3.1 shows the consolidation parameters determined from the CRS, with the interpretations enclosed in Appendix B.

It was identified that yielding of the sample typically coincides with a large, sudden increase in pore pressure, u_b , suggesting that yielding occurs with brittle, contractant soil behaviour. This is further evidenced by the large deformations occurring at p'_c showing that destructuring of the soil occurs.

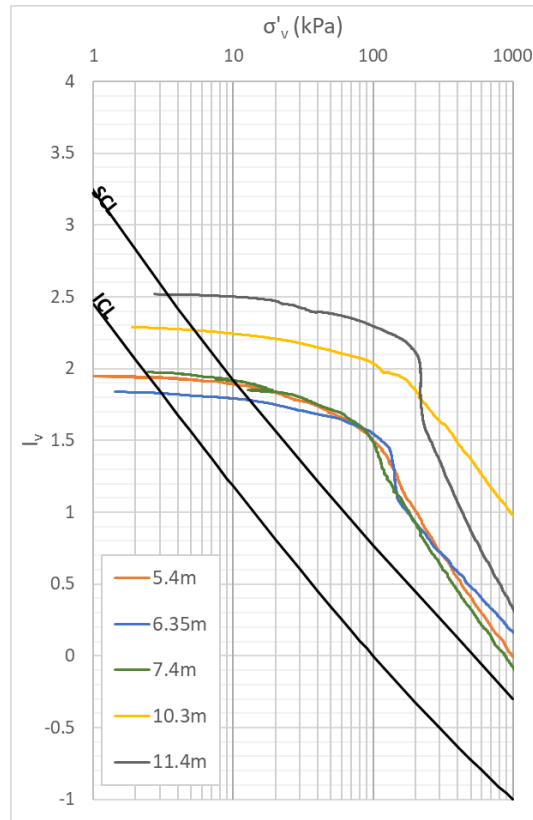


Figure 3.6: Oedometers plotted as effective stress - void index

Figure 3.6 shows the void index as a function of vertical effective stress. Void index is a measure of the structure/ageing of a soil as a result of geological processes with greater void ratio indicating greater structural resistance (Burland, 1990). It is clear that the resistance is greater within samples taken at 10.3m and 11.4m and thus the structure and ageing is greater at these depths.

3.4.1 Permeability

Permeability has been interpreted from CRS tests according to:

$$k = \frac{\partial H}{\partial t} \frac{H \gamma_w}{2u_b} \quad (3.2)$$

Where $\frac{\partial H}{\partial t}$ is an imposed constant.

Due to the change in compressibility and deformation of the assumed pore pressure isochrone, Equation 3.2 does not reliably predict vertical permeability. The calculated value will represent the lower-bound of the true value (Tavenas et al., 1983a). This effect is pronounced particularly at stress levels close to yield due to destructuring of the clay.

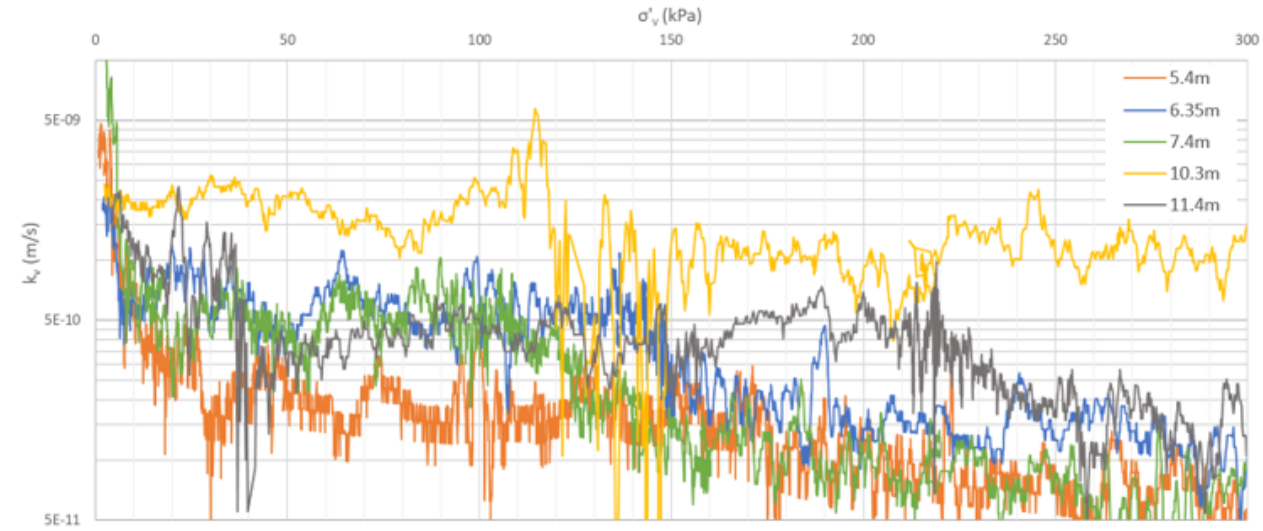


Figure 3.7: Vertical permeability from CRS oedometers

Figure 3.7 shows vertical permeability of 5×10^{-10} m/s is a reasonable average value. However, significantly higher initial permeabilities are seen, as well significantly lower values at stresses beyond p'_c . No obvious trend between vertical permeability and depth is observed.

3.5 Shear Strength

Shear strength parameters have been interpreted from both triaxial testing and CPTU profiles. The test results, included in full in Appendix B, show an initial small dilatancy followed contraction and softening to failure. A post-peak, residual strength can be observed, though this contrast in strength would probably be greater in samples of higher quality (Karlsrud and Hernandez-Martinez, 2013). That is to say that peak in-situ shear strength is likely to be greater than that measured in the triaxial cell. Sample disturbance is greatest in the quick clay samples where the change in void ratio during consolidation corresponds to 'poor' sample quality Lunne et al. (1997). The remaining samples of lower sensitivity Marine Clay and Landslide deposits are all characterised as 'good' to 'very good' sample quality.

Depth (m)	Type	Su (kPa)	c' (kPa)	ϕ	de/e0	Quality	Strata
6.45	CAUC	28	3	28	0.021	VGOOD	LD
6.6	CAUC	26	3	28	0.025	VGOOD	LD
7.5	CAUC	30	4	23	0.058	POOR	QC
7.6	CAUC	35	4	22	0.055	POOR	QC
10.4	CAUC	36	6	26	0.08	POOR	MC
10.55	CAUP	20	5	21	0.024	VGOOD	MC
11.5	CAUC	48	5	27	0.034	GOOD	MC
11.6	CAUC	50	5	26	0.033	GOOD	MC

CAUC - anisotropically consolidated undrained compression

CAUP - anisotropically consolidated undrained passive (extension)

Table 3.2: Summary of triaxial test results

3.6 Landslide Hazard and Proposed Remediation

The author has previously studied the slope stability for the site. Both limit equilibrium and finite element methods calculated critical safety factors of safety of 1.26 in the undrained condition and 1,54 in the drained condition.

The undrained analysis identified that sliding would occur at the contact between QC and MC. The rupture surface would follow the boundary between an upper softer layer and lower firmer layer, suggesting that reactivation of previously failed material by retrogressive failure was the mechanism to be considered. The likely trigger is shear stress changes within the sensitive material caused by construction activities e.g. unloading from basement excavation.

The analysis revealed a requirement to increase the safety factor in accordance with current code of practice (NVE, 2014). The proposed methodology is to place rockfill counterfill at the toe of the slope, thereby increasing the restoring moments within the slope. Subsequent analysis of this revealed an increase the safety factor to 1.44. Additionally, consolidation beneath the fill would result in an increased shear strength on the passive side of the failure surface, though this was not accounted for in the analysis.

Chapter 4

Literature Review for Precompression and Prefabricated Vertical Drains

In this chapter, relevant theory for the study of consolidation under an applied load with radial drainage is compiled. It is intended to give background to the issues associated with consolidation analyses, and introduce methods of analysis.

4.1 Introduction

Pre-compression is a common ground improvement technique whereby post-construction settlements are partially or fully compensated prior to construction by applying load to the foundation soils and allowing consolidation to take place. This approach is particularly beneficial for thick deposits of soft clay are present which prohibit deep foundation solutions. However, loading of soft clays will create prohibitively long consolidation times of the order of several years, or even more. For this reason pre-loading is often combined with installation of vertical drainage which creates a reduced drainage path length. Additionally, since the consolidation now occurs with radial drainage, the typically higher rate of horizontal permeability of sedimentary clays is exploited.

This chapter is a summary of previous work on pre-compression and vertical drains in soft clays.

4.2 Primary Consolidation

Primary consolidation is driven by dissipation of excess pore pressures that are generated by application of load. The dissipation leads to an increase in effective stress, volumetric strain of

the soil and settlement of the overlying structure. The strain at any time is therefore controlled by the hydraulic conductivity of the soil.

Within typical engineering problems, for example embankments on soft ground, soft soils with high compressibility and low permeability may lead to settlements spanning several years to tens of years or even more [Bjerrum \(1972\)](#).

4.3 Secondary Consolidation/Creep

Secondary consolidation under constant effective stress occurs as a result of a redistribution of internal forces within a soil's structure. The strains occurring from primary and secondary consolidation occur simultaneously and cannot be separated ([Terzaghi et al., 1996](#)). However, in the initial period following a change in effective stress, the contribution of creep to total strains is relatively small with the creep contribution increasing with time.

[Bjerrum \(1972\)](#) proposed that creep strains develop due to void ratio, overburden pressure in logarithmic time cycles as in Figure [4.1](#).

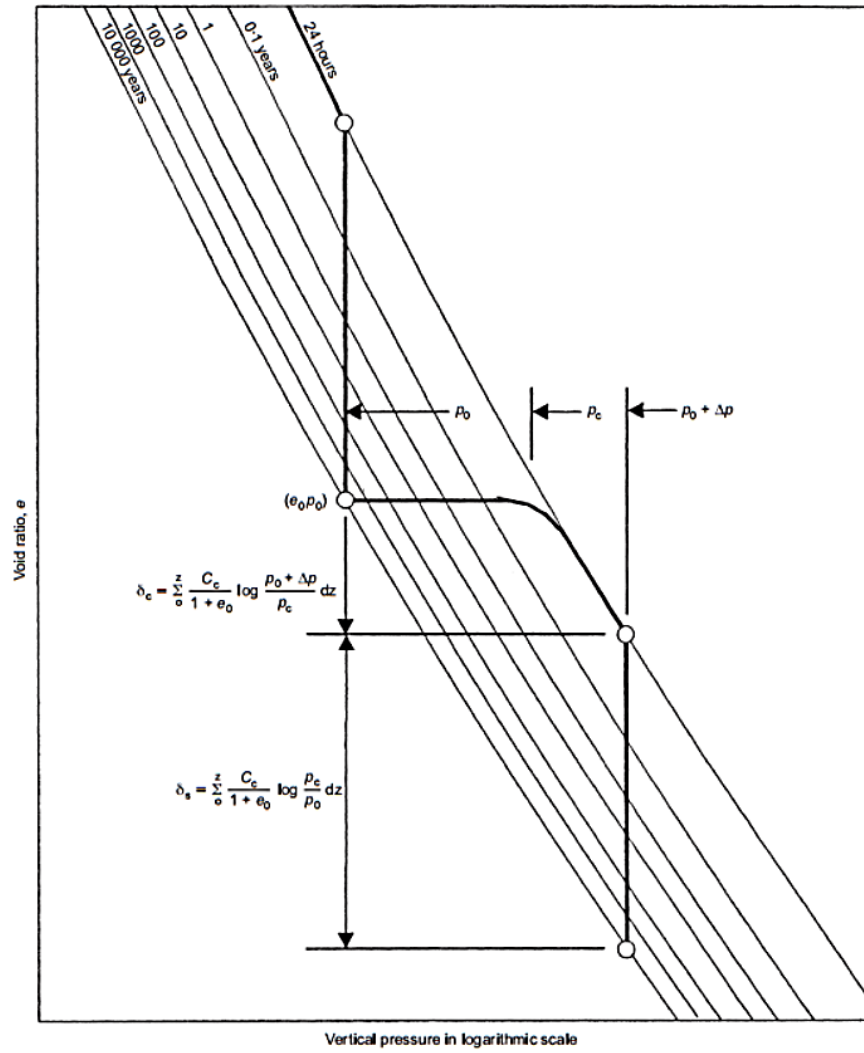


Figure 4.1: Principle of secondary consolidation (Bjerrum, 1972)

There are two main hypotheses for when creep strains develop, as pointed out by (Ladd et al., 1977). Hypothesis A says that creep occurs at the end of primary consolidation, whereas hypothesis B states that it occurs during primary consolidation due to a structural viscosity. Hypothesis A is considered to be an empirical criterion and a pragmatic solution for routine design.

Hypothesis A is untrue for soils stressed beyond preconsolidation stresses, and there is a wealth of data to demonstrate that Hypothesis B is true in the general case (Degago et al. (2011)). This further highlights the importance of understanding stress history and soil structure when applying creep models.

4.4 Consolidation under surcharge

The process of consolidation by pre and surcharge loading is explained in this section. What is considered is the application of a pre-load to the ground surface with an additional surcharge applied with the intention of accelerating compression and compensating secondary compression.

Johnson (1970), defined the degree of consolidation in the one dimensional case at the time of surcharge removal for normally consolidated soils:

$$U_{f+s} = \frac{\left(1 - c_\alpha \log \frac{t_{sc}}{t_p}\right) \log \left(1 + \frac{p_f}{p_0}\right) + \frac{c_\alpha}{C_c} (1 + e_0) \log \frac{t_{sc}}{t_p}}{\log \left(1 + \frac{p_s}{p_0} \left(1 + \frac{p_s}{p_f}\right)\right)} \quad (4.1)$$

Where

C_c is the coefficient of primary compression in $\log \sigma'$ stress

C_α is the coefficient of secondary compression in $\log \sigma'$ stress

p_0 is the initial stress level

p_f is the final stress level

p_s is the surcharge stress level

This gives the degree of consolidation under the centre-line of a loaded area which gives a conservative estimate as the edges will consolidate more rapidly.

Using this theory it is possible to predict rate of consolidation in the one-dimensional case for a normally consolidated soil. However, the weakness of this method is that it does not account for p_c of a normally consolidated soil and thus engineering judgement and previous experience is required for the selection of appropriate input parameters.

Some account of geological influence factors is made when using drainage path length to determine t_p . In this way, intermediate drainage layers can be accounted for.

4.5 Radial Drainage due to Prefabricated Vertical Drains

Prefabricated vertical drains (PVD) are typically 3mm to 5mm thickness and 100mm width and can be installed into foundation soils to great depth. They are installed by various methods, most typically by a closed-end steel mandrel which may be driven into the soil by hydraulic rams (static) or vibratory/drop weight (dynamic).

Barron (1948) and Kjellman (1948) were the first to develop equations for the consolidation of soils with vertical drains. The former compared both the free-strain and equal strain cases and found the difference in results between these two methods to be of little practical importance. The free strain solution was then further developed by Hansbo (1981) to include the effects of smear zone and well resistance and it was proven that the average degree of consolidation can be found by:

$$\bar{U} = 1 - \frac{\bar{u}}{\bar{u}_0} = 1 - e^{-8T_h/\mu_s} \quad (4.2)$$

Where:

$T_h = \frac{C_h t}{D^2}$ is the time factor in radial drainage

$C_h = \frac{k_h M}{\gamma_w}$ is the coefficient of consolidation for horizontal flow

$D = 1.05 \cdot S$ is the diameter of the influence zone of the drain based on the field spacing, S

$\mu = \frac{n^2}{n^2-1} \ln(n) - 0.75 + \frac{1}{n^2} - \frac{1}{4n^2}$ smear and well resistance not accounted for

$\mu_s = \nu + \pi z(2l - z) \frac{k_h}{q_w} (1 - \frac{1}{n^2})$ smear zone and well resistance accounted for

$\nu = \frac{n^2}{n^2-s^2} \ln \frac{n}{s} - \frac{3}{4} + \frac{s^2}{4n^2} + \frac{k_h}{k'_h} \frac{n^2-s^2}{n^2} \ln(s)$

$n = \frac{D}{d_w}$ is the ratio of the diameter of the influence zone to the diameter of the well

$s = \frac{d_s}{d_w}$ is the ratio of the diameter of the smear zone to the diameter of the well

k_h and k'_h are the horizontal permeability in undisturbed and remoulded zones, respectively

q_w is the discharge capacity of the drain

This allows for a systematic review of the effect of smear and well resistance, but only linear soil properties are used, therefore separate calculations must be undertaken when soil properties vary spatially or temporally.

4.6 Design Considerations for Vertical Drains

There are several factors which must be considered for the design of vertical drains, most significant of which are the installation effects.

Pore pressures generated by installing PVD are not well studied. Studies on cone penetration testing indicate that the ratio of excess pore pressure to initial vertical effective stress would be greater than unity at a radial distance of $2d_m$ (Levadoux and Baligh, 1980).

Installing PVD generates high octahedral strains which generates a remoulded 'smear' zone surrounding the drain. The strain may decrease to less than 2% at a distance greater $2d_m$, where d_m is the diameter of the mandrel (Levadoux and Baligh, 1980). Empirical evidence indicates the diameter of the smear zone ranges $1.5 - 3d_m$ Jamiolkowski et al. (1983), Holtz et al. (1991), Indraratna and Redana (2000) which is dependant installation methods, and soil plasticity.

The effect of well resistance must also be considered as a soil element draining horizontally to a boundary condition where excess pore pressure during consolidation process is zero cannot happen in a saturated well. Additionally, the drain itself has a finite discharge capacity, however the effect of this is negligible for discharge capacities greater than $100m^3/year$ (Holtz, 1987)

4.6.1 Other Considerations

The selection of filter sleeve must consider the soil retention (piping resistance), soil filtration (clogging resistance), as well as permeability of the filter. Siltation/clogging of the drain and filter sleeve will reduce the performance of the drain system over time. Additionally, the well discharge may be reduced due a reduction in core volume from lateral earth pressures (Holtz, 1987).

Biological/chemical degradation may also be of concern in particularly problematic ground.

Bjerrum (1972) showed that increasing the drainage of the soil will increase the rate of primary consolidation, however it does not affect the magnitude of total long-term settlements.

4.7 Plane-Strain Permeability Equivalence

In order to maintain an equivalent continuity of flow as in the axisymmetric (radial flow) case, then the horizontal permeability in the plane-strain case must be factored. This principle is shown diagrammatically in Figure 4.2.

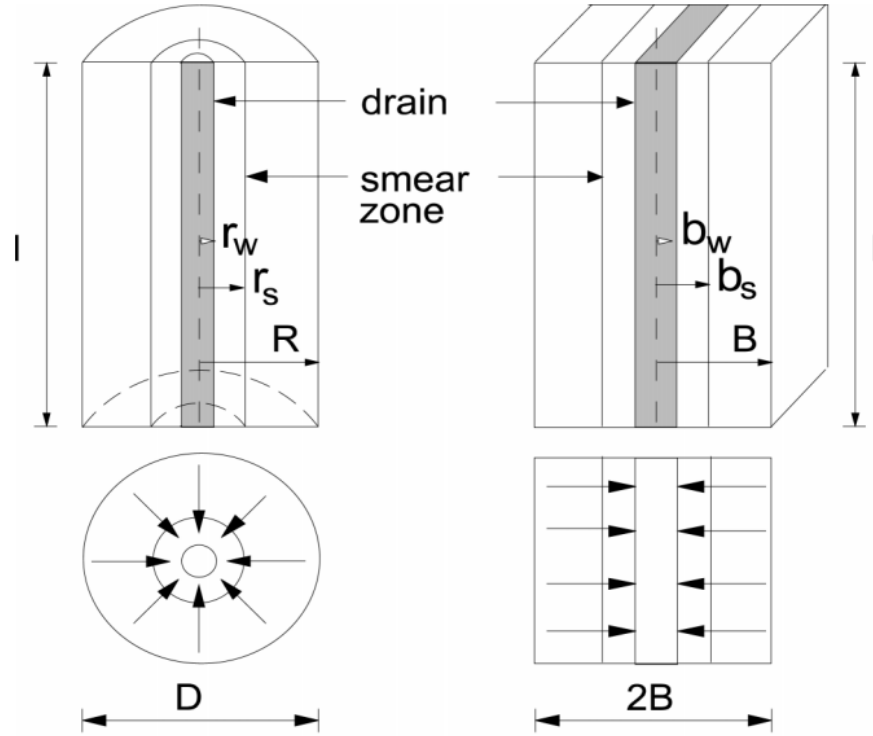


Figure 4.2: Principle of conversion between radial flow and plane flow permeability; from [Indraratna and Redana \(2000\)](#)

The basic assumption is that the dimensionless time, permeability, and shape functions must all share the same equivalence. That is:

$$\frac{T_{hp}}{T_h} = \frac{k_{hp}}{k_h} \frac{R^2}{B^2} = \frac{\mu_p}{\mu} \quad (4.3)$$

Where subscript p denoted a plane-strain parameter, and R and B are the radius and width of the axisymmetric and plane-strain unit cell respectively, as shown in Figure 4.2.

Indraratna and Redana (1997; 2000) proposed a solution in which the drain spacings and time factors in both the axisymmetric and plane-strain models are equal and the permeability adjusted for the plane-strain case to represent radial drainage. The method incorporates a defined smear zone with separate permeability to the undisturbed soil.

The horizontal permeability in plane strain is derived as:

$$k_{hp} = \frac{k_h \left(\alpha + \beta \frac{k_{hp}}{k'_{hp}} + \theta(2lz - z^2) \right)}{\ln\left(\frac{n}{s}\right) + \frac{k_h}{k'_h} \ln(s) - 0.75 + \pi(2lz - z^2) \frac{k_h}{q_w}} \quad (4.4)$$

Where

$$\alpha = \frac{2}{3} - \frac{2b_s}{B} \left(1 - \frac{b_s}{B} + \frac{b_s^2}{3B^2} \right)$$

$$\beta = \frac{1}{B^2} (b_s - b_w)^2 + \frac{b_s}{3B^3} (3b_w^2 - b_s^2)$$

$$\theta = \frac{2k_{hp}^2}{k'_{hp} B q_z} \left(1 - \frac{b_w}{B} \right)$$

And

$$q_z = \frac{2}{\pi B} q_w$$

And

The dimensions of the unit cell, i.e. R and B are kept constant between the two cases.

It can be seen that Equation 4.4 does not explicitly define the permeability parameters k_{hp} and k'_{hp} , thus the parameters obtained from analytical solutions are used as an input. An initial value of plane strain horizontal permeability is calculated from:

$$\frac{k_{hp}}{k_h} = \frac{0.67}{\ln(n) - 0.75} \quad (4.5)$$

Which is a special case of equation 4.4 where the effect of smear and well resistance are omitted. This value is then used as a starting point for iteration.

Chapter 5

Construction Sequence and Monitoring

The sequence of construction works and monitoring shall be described in this section. Where some uncertainty exists, the sequence of events is considered as the most likely with respect to relative timings.

5.1 Sequence of Events

Exact dates of when fill was placed across the site are not available. The sequence of events has been determined based on broad timescales provided by the contractor, supported by evidence from pore pressure and settlement monitoring.

The sequence of events known to have been carried out are as follows:

1. Site clearance, topsoil strip, excavate to foundation - 07/05/18 to 11/05/18. Pore pressure data indicates this to have occurred on 08/05/18
2. Placement of working platform - ca. 50cm of crushed stone - 14/05/18 to 18/05/18. Pore pressure data indicates this to have occurred on 15/05/18
3. Installation of PVD to 25m below terrain by static, closed-end, steel mandrel - 04/06/18 to 08/06/18. Pore pressure data indicates this to have occurred on 08/06/18
4. Placement of ca. 3m of fill 25/06/18 to 06/07/18. Pore pressure data indicates this to have occurred on 21/06/18
5. Monitoring of pore pressures and surface settlements - data until 17/12/18 and 15/03/19 respectively

At the time of reporting the surcharge load is understood to be the top 1m of fill and will be removed in late 2019/2020, (some months after this study).

Site Clearance

In order to enable construction, the top ca.0.2m of topsoil was removed and benches cut into the slope to provide a level surface on which heavy plant can operate.

Working Platform

A working platform was placed over the site to create sufficient bearing capacity for the PVD installation plant. The platform was composed of crushed rock of grain size 2mm to 32mm and ranged in thickness from 0.5m to 1m.

5.2 PVD Installation and Specification

MembraDrain MD 88H PVD were installed by BAT Cofra. The drains are composed of a polypropylene core wrapped in a non-woven geotextile filter sleeve. The installation method was with closed-end, static, rectangular-section, steel mandrel, and driven to 25m below terrain. The specifications of the drains and mandrel are given in Figure 5.1 and Table 5.1.

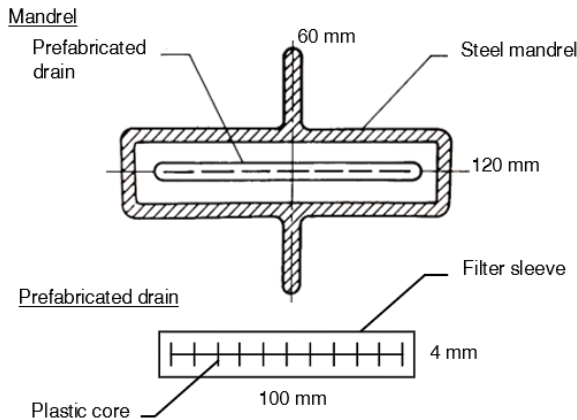


Figure 5.1: Cross section of PVD and mandrel

Drain properties	
Width (mm)	100
Thickness (mm)	4
Discharge capacity (m ³ /day)	3
Filter Properties	
Opening size (μm)	79
Permeability (m/day)	3400
Mandrel Dimensions	
Width (mm)	120
Thickness (mm)	60
Wall thickness (mm)	10

Table 5.1: Properties and dimensions of PVD and mandrel

5.3 Filling

The fill is understood to comprise a well-compacted crushed rock of grain size 22mm to 120mm with <1% fine grained material. Unit weight is assumed to be $\gamma = 20\text{kN/m}^3$.

The fill was placed and compacted in layers, and based on pore pressure readings, appears to have been placed in less than one week. The exact timings of fill placement has been interpreted from pore pressure measurements and as such, some uncertainty exists when discussing the site as a whole.

5.4 Pore Pressure Monitoring

The pore pressure in five vibrating wire piezometers was monitored between May 2018 and December 2018. The resolution of the data obtained during the construction phase is given in Table 5.2. Note that the installation depths refer to meters below the initial terrain i.e. at site investigation stage.

Series no.	Position	Depth (mbgl)	Elevation (moh)	Start date	End date	Data resolution
6011	A2	6	56.2	08/05/2018	04/02/2019	Monthly ¹
6012	A2	10	52.2	08/05/2018	04/02/2019	Monthly ¹
11058	C1	6	53	08/05/2018	17/12/2018	2hr
9936	C2	8	55.5	08/05/2018	17/12/2018	2hr
11059	C2	12	51.5	13/02/2018	17/12/2018	2hr ²

¹ Piezometer was read manually

² Data resolution was 1hr between 13/02/2018 and 07/06/2018

Table 5.2: Summary of piezometer readings during construction

The supplied piezometer data was uncorrected for barometric pressure and no air pressure measurement was taken during the monitoring period. The data was therefore corrected for changing pressure conditions using the nearest available weather station at Voll (approx 1.4km east of the site and at 127m elevation). Air pressure was obtained relative to sea level and corrected to the average level of installed piezometers. It is noted that this averaging of piezometer levels leads to an error of approximately $\pm 0.1\%$. This translates to a possible error in barometric pressure in the range of $\pm 1\text{kPa}$ which is not considered to be significant.

Pore pressure measurements at location A2 were only taken at monthly intervals, therefore the initial 'spike' due to undrained loading was not measured.

Figures 5.2 and 5.3 show an increase in pore pressure due to installation of PVD. Both at positions A2 and C2, an under-hydrostatic pore pressure profile is noted prior to any construction

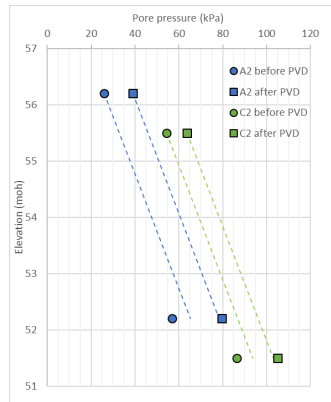


Figure 5.2: Piezometer pore pressures before and after PVD installation with corresponding hydrostatic profiles

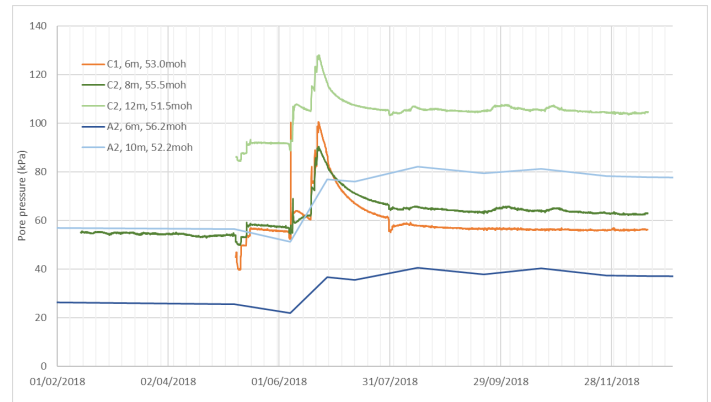


Figure 5.3: Piezometer pore pressures before, during and after PVD installation

activities. Following the installation of PVD and completion of primary consolidation, all pore pressures remained at a higher level, conforming very closely to a hydrostatic profile.

At approximately 07/06/18, a sudden increase followed by rapid decay is measured at both C1 and C2. This is probably caused by PVD installation. The magnitude of excess pore pressure is between 15kPa and 45kPa.

5.5 Ground Settlement Monitoring

A total of eight settlement plates (TP1 to TP8) were installed at original ground level prior to filling and one additional plate (TP9) installed close to the western corner of Kiwi. The locations of these plates is shown in Figure 3.1. Figure 5.4 shows the cross-section of a single plate. Settlement of the plate was monitored on a weekly basis for the first six weeks after placement of the fill, and monthly thereafter. Measurements were to the nearest millimetre.

Between 24/05/18 and 15/06/18 levels were noted to fluctuate by -0.007m and +0.04m. This change in levels occurred after site clearance and placement of the working platform but with no clear pattern between ground movements and site works. Due to this problem the data between these dates has been discounted as unreliable and settlement has been assessed from the movement measured from 22/06/18 onwards, at which time all plates registered net movements of +0.001m to -0.003m. It seems likely that ground movement before 22/06/18 were due to movement of machinery and PVD installation causing ground disturbance and deflection of the plates.

At the time of reporting, recorded settlements at positions TP1 to TP8 range from 0.036m to 0.116m. No heave has been recorded following these settlements as the surcharge load has not

yet been removed.

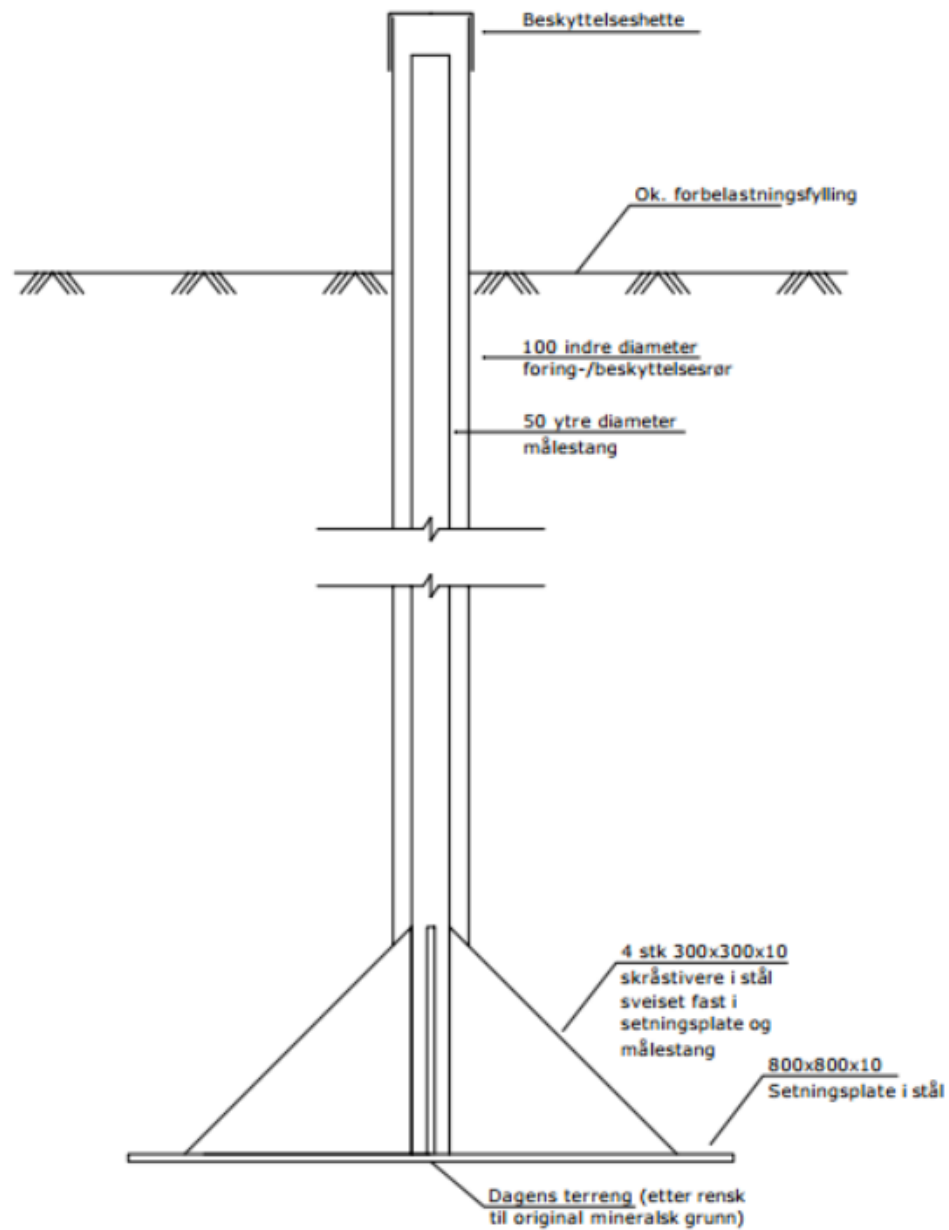


Figure 5.4: Principle sketch of settlement plate used

Chapter 6

Modelling of a Single Drain

In this section the simple case of one-dimensional compression of a single drain will be considered. An analytical, closed form solution as well as finite element methods for axisymmetric and plane-strain conditions will be compared. The purpose of this section is to show how installation effects can be accounted for and compare the results of different analysis techniques.

6.1 Parameters

Initial modelling of the drains is carried out with a linear elastic model, assuming one-dimensional compression. The elastic parameters are typical average values for the entire drain length but the lack of stress-dependant stiffness will limit the applicability with respect to real strain development.

E' (kPa)	ν	k_h (m/s)	k'_h (m/s)
6000	0.2	1.50E-09	5.00E-10

Table 6.1: Parameters for unit cell analysis

In all cases, a single unit cell has been modelled with a uniform surface load of 60kPa.

In all cases it has been assumed that the smear zone radius is equal to twice the mandrel equivalent radius, $r_s = 2r_m$. k'_h within the smear zone is assumed to be constant and equal to the vertical permeability. In reality the disturbance within the smear zone will reach a maximum at the drain boundary, decreasing to zero at the edge of the undisturbed zone, and following a non-linear distribution. Additionally, withdrawal of the mandrel will leave an air-gap along the drain length which retards initial saturation and flow into the drain. This effect will not be directly modelled and is instead accounted for by selection of an appropriate k'_h value.

k_h is assumed to be $3k'_h$.

6.2 Back-Calculation of Horizontal Coefficient of Consolidation, C_h

6.2.1 C_h from Settlement Data

The coefficient of horizontal consolidation can be back analysed using the average change in measured settlement (Asaoka, 1978). A time interval of $\Delta t = 10$ days was selected and the settlement at four time intervals was interpolated from the data.

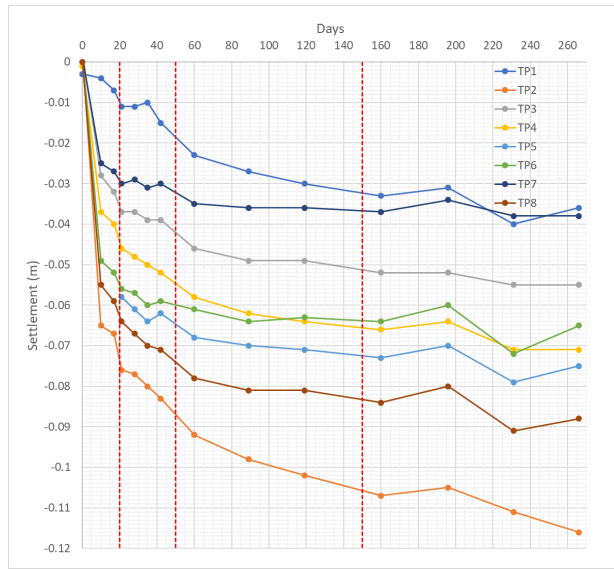


Figure 6.1: caption

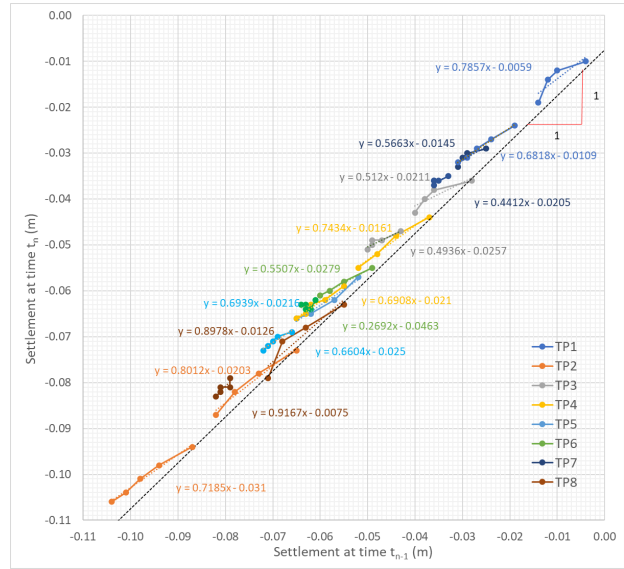


Figure 6.2: caption

Figure 6.1 shows a back calculation of C_h in two time periods, the first is between 20 and 50 days after filling, and the second is between 50 and 150 days after filling. Figure 6.2 shows the interpolated change in settlement for the normalised time for both time periods.

C_h is then found according to (Asaoka, 1978):

$$C_h = -\frac{D^2 \mu \ln(\beta)}{8 \Delta t} \quad (6.1)$$

Where:

D is the diameter of the influence zone

μ is a function of the well spacing according to Equation 4.2

β is the inclination $\Delta \delta_{tn} / \Delta \delta_{tn-1}$

	β 20 to 50 days	β 50 to 150 days
TP1	0.7857	0.6818
TP2	0.8012	0.7185
TP3	0.5120	0.4936
TP4	0.7434	0.6908
TP5	0.6939	0.6604
TP6	0.5507	0.2692
TP7	0.5663	0.4412
TP8	0.8978	0.9167
Average	0.6939	0.6090
Average (centre-line only)	0.6250	0.5285
C_h (m ² /yr)	10.0	6.8
C_h (m ² /yr)(centre-line only)	12.9	8.8

Table 6.2: C_h back calculated from settlement data

It is noted that the settlement contribution from soils beneath the base of the drains is not known. The error arising from not accounting for this is considered to be negligible over the first 30 day timescale as it will account for a very small proportion of measured settlement. However, this effect may be more significant at the second, 100 day timescale.

6.2.2 C_h from Pore Pressure Data

The equal strain solution for the dissipation of pore pressure with time at any radial distance, r , from the centre of a radially drained area is found to yield the following partial differential equation [Jamiolkowski et al. \(1983\)](#):

$$\frac{\partial \bar{u}}{\partial t} = C_h \left(\frac{1}{r} \cdot \frac{\partial u}{\partial r} + \frac{\partial^2 u}{\partial r^2} \right) \quad (6.2)$$

Substitution of the μ term from Equation 4.2 and rearrange to find C_h , the solution becomes:

$$C_h = \frac{\mu R^2}{-8 \cdot 4 \Delta t} \ln \left(\frac{u_t}{\frac{u_{t-1}}{R^2 \mu} (R^2 \ln(\frac{r}{r_w} - \frac{r^2 - r_w^2}{2}))} \right) \quad (6.3)$$

Where

Δt is the time interval between excess pore pressure measurements u_{t-1} and u_t

The calculated values in Table 6.3 represent the average value, i.e. no differentiation between the undisturbed and smear zones.

The result is a clear trend of decreasing C_h with decreasing u .

Piezometer	Time (days)	u (kPa)	C_h (m ² /yr)
C1 6m $u_0 = 44.5$ kPa	2	36.2	41.6
	6	23.6	36.0
	10	17.9	25.6
	14	14	23.5
	22	9.1	18.1
	30	6.4	15.4
C2 8m $u_0 = 27.3$ kPa	2	23.7	32.7
	6	17.4	27.8
	10	13.7	23.0
	14	11.1	21.1
	22	7.2	18.2
	30	4.8	17.2
C2 12m $u_0 = 23$ kPa	2	17.5	50.8
	6	9.2	50.7
	10	6.0	35.9
	14	4.0	34.4
	22	2.0	27.1
	30	1.0	27.1

Table 6.3: C_h back-calculated from pore pressure readings

6.3 Single Drain Analytical Solution

The average degree of consolidation at any given time has been defined according to equation 4.2.

The smear zone is defined as annulus of reduced permeability soil of radius r_s surrounding the PVD, of radius r_w . The outer, undisturbed zone extends to the outer boundary of the unit cell at a radial distance R . The numerical values of these distances are given below:

$$r_w = \frac{t_w + w_w}{\pi} = 0.0331m \quad (6.4)$$

$$r_s = 2r_m = 2 \frac{t_m + w_m}{\pi} = 0.1146m \quad (6.5)$$

$$R = 0.525S = 0.7875m \quad (6.6)$$

Where subscript w and m refer to dimensions of the PVD and mandrel respectively, given in Table 5.1.

Using the parameters in Table 6.1, C_h in the undisturbed zone and C'_h in the smear zone can be calculated. Normalising these values over the radial dimensions gives an average value within

the influence zone of $\bar{C}_h = 28.6 \text{ m}^2/\text{yr}$. This is approximately equal to the average value of each piezometer over the monitoring periods from Table 6.3 which ranged from $23.3 \text{ m}^2/\text{yr}$ to $37.7 \text{ m}^2/\text{yr}$.

The time to 90% consolidation found by rearranging gives $t_{90}=49.5$ days.

This is the theoretical value for the centre of a uniformly, vertically loaded area. A limitation of this method is in the selection of a value of C_h which of course varies between the undisturbed and smear zones.

6.4 Finite Element Solution

An axisymmetric consolidation calculation was undertaken using PLAXIS finite element code. The geometry of the problem and soil properties are kept the same as Hansbo's solution for the purposes of comparison. The centre line of the drain is the line of symmetry. This is shown in Figure 6.3.

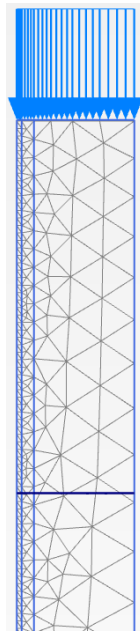


Figure 6.3: Unit cell finite element geometry

PLAXIS divides pore pressures into steady-state and excess pore pressure, with the former being assigned from a input hydrostatic condition, and the later calculated from a changing load condition.

6.4.1 Boundary Conditions

The circumference of the unit cell is specified as closed to hydraulic flow and normally fixed with respect to deformations. The base of the unit cell is also closed to hydraulic flow and fully fixed to deformations. The top surface (where load is applied) is specified as a seepage boundary and free to deform in one dimension. Thus an oedometer condition is simulated, comparable to both the analytical solution and to 1-D consolidation beneath the centre-line of a loaded area.

6.4.2 Mesh

PLAXIS automatically generates a finite element mesh based on discretisation of the input geometry. Each element consists of a 15-noded triangle.

The mesh is refined based on an input of relative element size, by way of selection of a desired coarseness. Additional automatic refinement is carried out by the programme by the local geometry which applied an implicit coarseness factor from the pint/line spacing and angles between intersecting lines. In this case the mesh is refined within the drain, and coarsened within the drain influence zone.

6.4.3 Governing Theory

The consolidation calculation in PLAXIS is carried out on the excess pore pressures. The excess pore pressure, \mathbf{u} , is calculated based on force vector nodal values multiplied by interpolation functions, \mathbf{N} (or shape functions). In this case, relevant shape functions for 15-noded triangles are used.

Strain, ϵ , is calculated from force vector nodal values multiplied by the strain interpolation matrix, \mathbf{B} which contains the spatial derivatives of the interpolation functions.

$$\begin{bmatrix} \mathbf{K} & -\mathbf{L} \\ -\mathbf{L}^T & \Delta t \mathbf{H} \end{bmatrix} \begin{bmatrix} \Delta \mathbf{v} \\ \Delta p_n \end{bmatrix} = \begin{bmatrix} 0 & 0 \\ 0 & -\Delta t \mathbf{H} \end{bmatrix} \begin{bmatrix} \mathbf{v}_0 \\ p_{n0} \end{bmatrix} + \begin{bmatrix} \Delta \mathbf{f}_n \\ \Delta t(\mathbf{q}_{n0} + \Delta \mathbf{q}_n) \end{bmatrix} \quad (6.7)$$

The stiffness matrix is:

$$\mathbf{K} = \int_v \mathbf{B}^T \mathbf{D}^e \mathbf{B} dV \quad (6.8)$$

The coupling matrix is:

$$\mathbf{L} = \int_v \mathbf{B}^T \mathbf{m} \mathbf{N} dV \quad (6.9)$$

The permeability matrix is:

$$\mathbf{H} = \int_v (\nabla \mathbf{N})^T \mathbf{k} \nabla \mathbf{N} / \gamma_w dV \quad (6.10)$$

It can be seen that at values of Δt approaching zero, so too will the diagonal term in Equation 6.7, leading to instability in the of the solution for small time intervals. Therefore time intervals must be selected with care and are dependant element size.

6.4.4 Plane-Strain Finite Element Formulation

Conversion of axisymmetric permeability to equivalent plane strain permeability is discussed in Chapter 4. This iterative method has been applied including well resistance and reduced permeability in the smear zone. The equivalent plane strain permeabilities are given below:

k_h (m/s)	1.50E-09
k_{hp} (m/s)	6.50E-10
k'_h (m/s)	5.00E-10
k'_{hp} (m/s)	7.85E-11

Table 6.4: Equivalent plane strain permeability values

It is necessary to factor horizontal permeability as the plane-strain model will not consider out of plane flow and as such it cannot contribute to pore pressure dissipation/consolidation. An implicit function is therefore used to determine an equivalent horizontal permeability which will replicate the effect of radial drainage, based on principles of continuity of flow.

6.5 Comparison of Axisymmetric and Plane Strain Formulations

A stress point at the edge of the unit cell at depth of half the drain length is compared for the three calculation methods. Additionally, settlement at the surface is also compared.

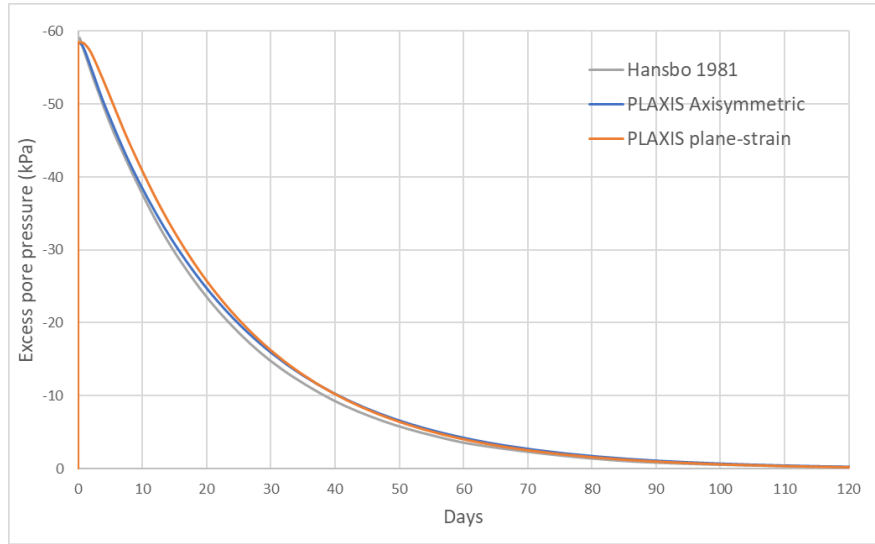


Figure 6.4: Pore pressure dissipation for analytical, axisymmetric FE, and plane-strain FE methods

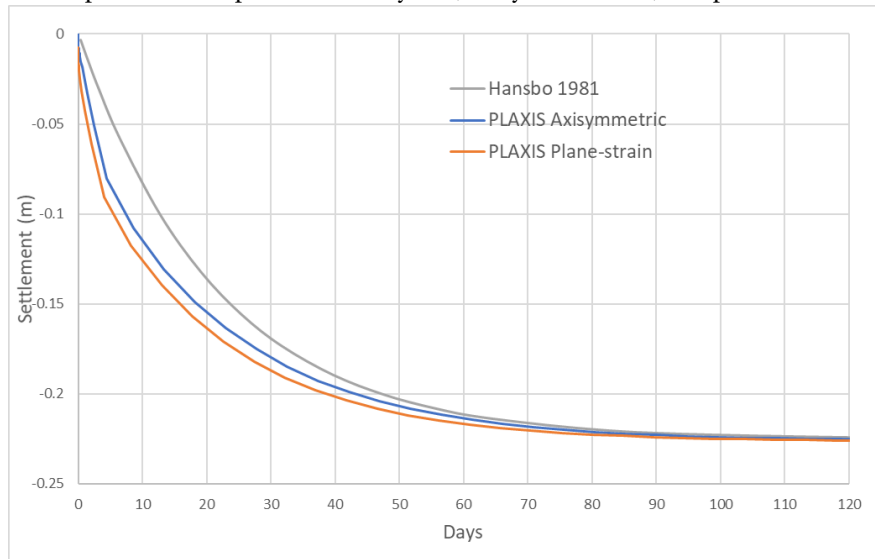


Figure 6.5: Settlements for analytical, axisymmetric FE, and plane-strain FE methods

The time taken to reach 90% consolidation, $U_{90} = 1 - u/u_0$, can be seen to match very closely between all three methods, with there being a range of just 2.9 days between the methods.

In the plane-strain case, the initial pore pressure response is not a sudden 'spike' as would be expected, but rather reduced more rounded curve is produced, with a reduced initial excess pore pressure level. The reason for this is shown when considering the critical time step, as defined below:

$$\Delta t_{critical} = \frac{l^2}{\alpha C_h} \quad (6.11)$$

Where:

l = element length

$\alpha = 80$ for a 15-noded element

Thus, the decrease of C_h in the plane-strain case results in an increase in $\Delta t_{critical}$ and therefore at time steps below this critical value, the pore pressure response is dampened.

6.6 Limitations of Analytical Method

The analytical solution is limited to linear elastic soil behaviour with a simple loading sequence with small total deformations.

By not including the non-linear behaviour of soil, the degree of consolidation in terms settlement is equal to the degree of consolidation in terms of pore pressure. In reality, rapid pore pressure changes occur for loading below p'_c and generate little settlement, whereas beyond p'_c , small changes in pore pressure generate large settlements. The significance of this becomes greater in structured clays, where collapse of the structure generates large strains.

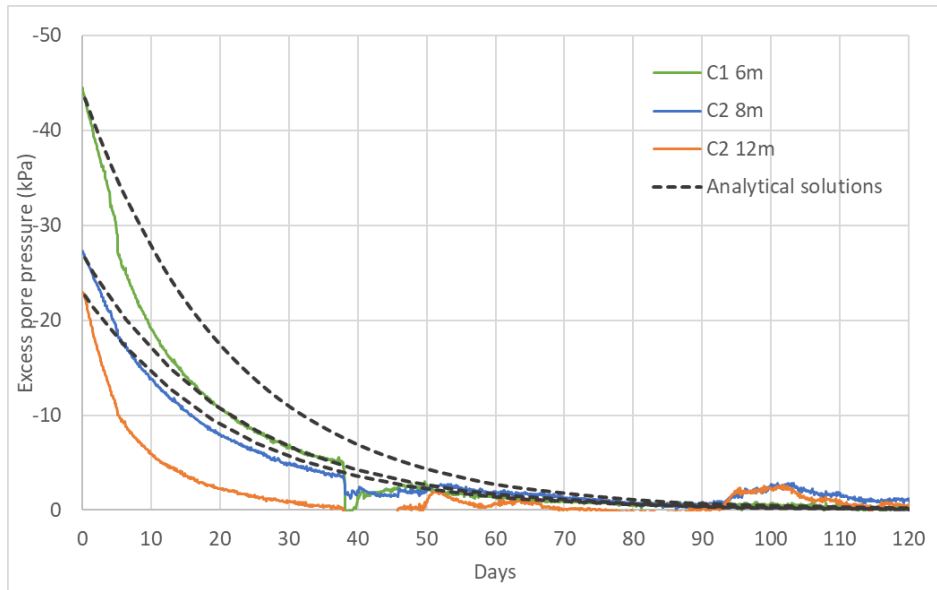


Figure 6.6: Comparison of analytical solution and field measurements

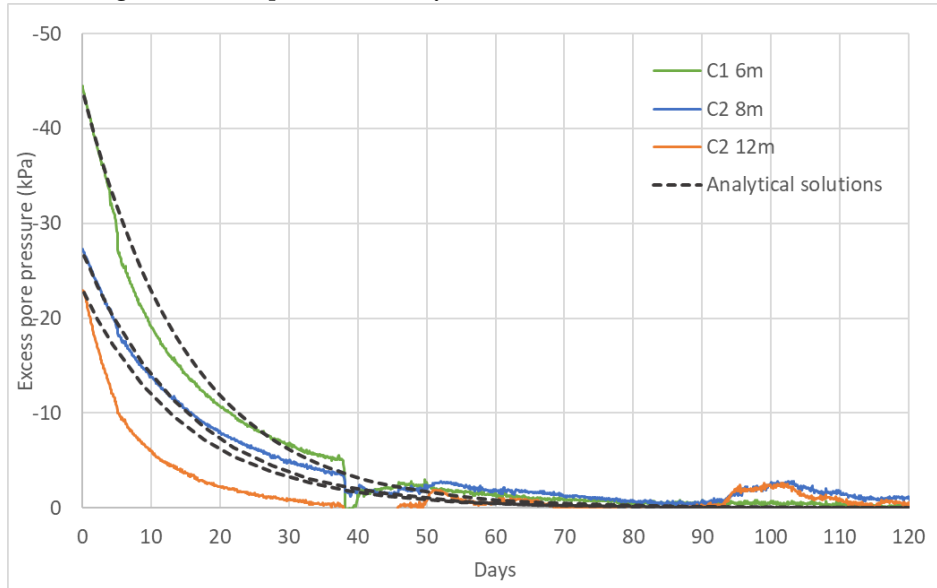


Figure 6.7: Comparison of analytical solution and field measurements, optimised parameters

Figures 6.6 and 6.7 show how optimisation of the parameters based on observed behaviour and soil layering can result in a more accurate model.

However the analytical solution does not account for non-linearity. The measured values show a higher rate of pore pressure dissipation in the initial phase and a lower rate towards the end of consolidation.

A numerical method would be better able to predict compression of these soft soils where significant non-linearity of permeability and stiffness is observed.

Chapter 7

Numerical Models

This chapter will show the methods and rationale for selection of an appropriate numerical model for the study site in order to overcome the problems of non-linearity discussed previously.

7.1 Geometry

The geometry of the problem has been determined from cross sections of the slope enclosed in Appendix A. The soil layering is based on re-interpretation of the Rambøll site investigations data contained in Appendix B including CTPU profiles and results of the laboratory testing as discussed in previous sections.

Profiles A, B and C used in the PLAXIS model are shown in Figures 7.1 to 7.6. Appropriate simplifications of the soil layering have been made, for example combining all sand and gravel soils into a single stratum. The depth to bedrock has been assumed as a horizontal, incompressible, impermeable boundary at 20moh.

The PVD, smear zone, and undisturbed soil around drains has been delineated for each PVD.

The final fill level has been taken from post-construction surveys.

7.2 Mesh

A normal mesh was generated, with a refined mesh within the PVD zone. There large range within the geometry of the size of soil units, as the smear zones are very narrow in comparison to the distance between model boundaries. Without refining the mesh in these zones a very large ratio of element length to element area is generated causing inaccuracy of the calculated result, or in the extreme, failure to converge as the stiffness matrix approaches zero.

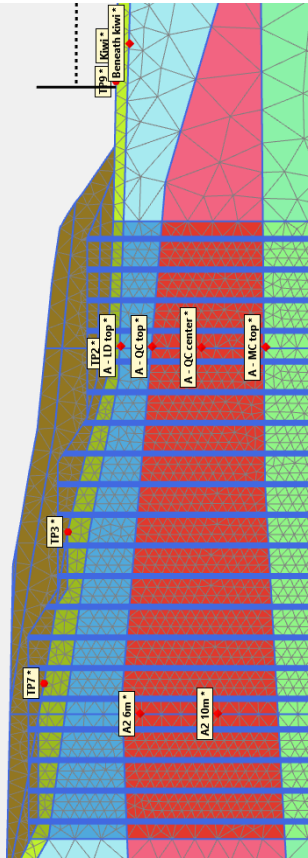


Figure 7.1: Profile A model and boundaries

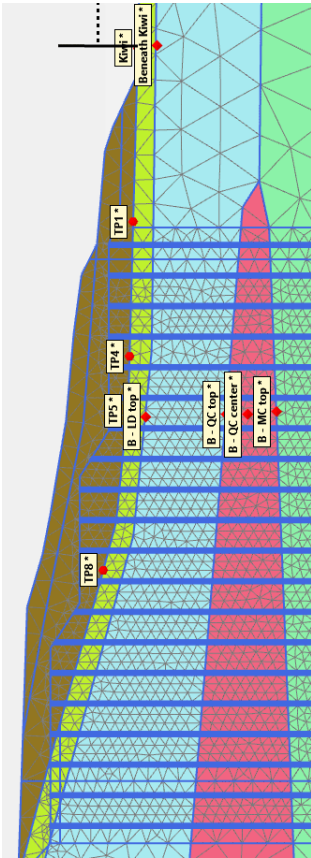


Figure 7.2: Profile A stress points and nodes

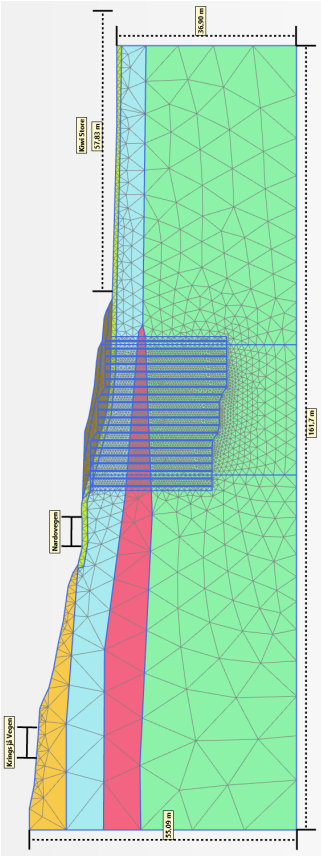


Figure 7.3: Profile B model and boundaries

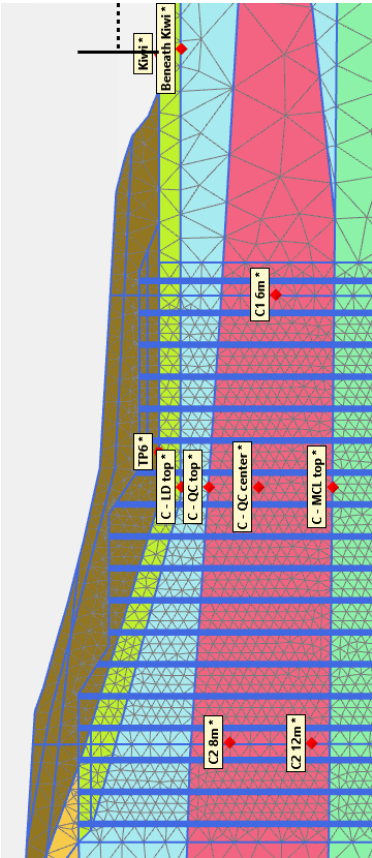


Figure 7.4: Profile B stress points and nodes

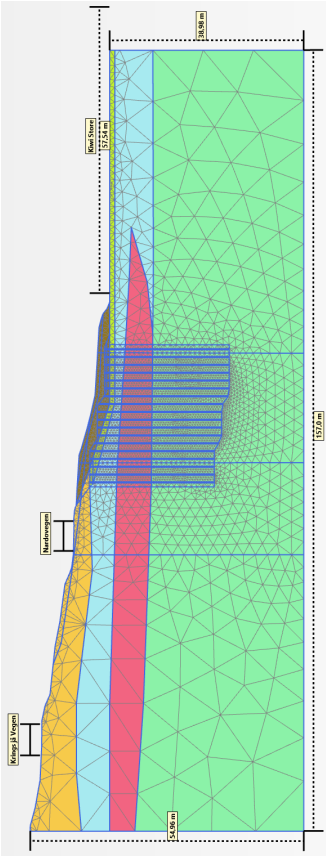


Figure 7.5: Profile C model and boundaries

Figure 7.6: Profile C stress points and nodes

Profile	No. elements	No. nodes	Max. model dimension (m)
A	14159	113949	160
B	13220	106363	162
C	12893	104010	157

Table 7.1: Summary of generated meshes

7.3 Loading

The construction phases used in the numerical models are given in Table 7.2. They fit generally with the interpretation of site activities based on the available information. Completion of filling is believed to have happened earlier on Profile A.

Phase	Loading	Profile A (days)		Profiles B + C (days)	
		Time	End	Time	End
0	Initial	0	0	0	0
1	Plastic null step	0	0	0	0
2	Site clearance	21	21	7	7
3	Working platform	4	25	25	32
4	Install PVD	6	31	11	43
5	Filling	365	396	365	408
6	Unloading	365	761	365	773

Table 7.2: Staged construction summary

With the exception of Phases 0 and 1, all were carried out as staged-construction consolidation calculations. Loads were increased linearly to the specific value across the initial time step for each stage.

The plastic null step was carried out as a drained, plastic calculation in order for the stress field to reach equilibrium which models the actual slope stresses.

7.4 Groundwater Calculations

In the initial phase, groundwater pressures is calculated by steady-state seepage with boundary conditions set on the model boundaries and positions of installed piezometers and the head set to the observed value.

When PVD are installed, groundwater pressures are re-calculated by a new hydrostatic level based on piezometers measurements

7.5 Mohr-Coulomb Soil Parameters

A Mohr-Coulomb model was selected for soils not subject to creep deformations. The selected strength, deformation and state parameters are:

Stratum	γ (kN/m ³)	e_0	c' (kPa)	ϕ	E (kPa)	ν
Fill	20	0.5	0	42	50000	0.3
Sand	19	0.5	0	35	35000	0.3
Dry Crust	18	1.3	5	26	7500	0.2

Table 7.3: Mohr-Coulomb paramters for soils not subject to creep

7.6 Soft Soil Creep Model

The soft soil creep model (SSC) was selecetd for the Landslide Deposits (LD), Quick Clay (QC) and Marine Clay (MC) due to its ability to replicate overconsolidated and normally consolidated strains.

SSC uses a linear relationship between stress-state and stiffness to predict soil hardening behaviour. It is best suited to soils where there is a high contrast between oedometer and triaxial stiffness (typically where $E_{50} > 2E_{oed}$) and thus display significant contractant behaviour at failure typical of problems related to deformations in normally consolidated to lightly overconsolidated soils.

The main benefit SSC is the use of modified compression index, λ^* , and swelling index, κ^* which are defined as:

$$\lambda^* = \frac{\lambda}{1+e} = \frac{C_c}{2.3(1+e)} = \frac{1}{m_{nc}} \quad (7.1)$$

$$\kappa^* = \frac{\kappa}{1+e} \approx \frac{2C_s}{2.3(1+e)} = \frac{1}{m_{oc}} \quad (7.2)$$

And the time-dependant stiffness parameter, μ^* which is defined as:

$$\mu^* = \frac{1}{r_s} \quad (7.3)$$

Where λ and κ are the Cam-Clay flexibility parameters in natural-log stress, The void ratio is taken as the average void ratio over the stress range over which λ^* and κ^* are to be determined.

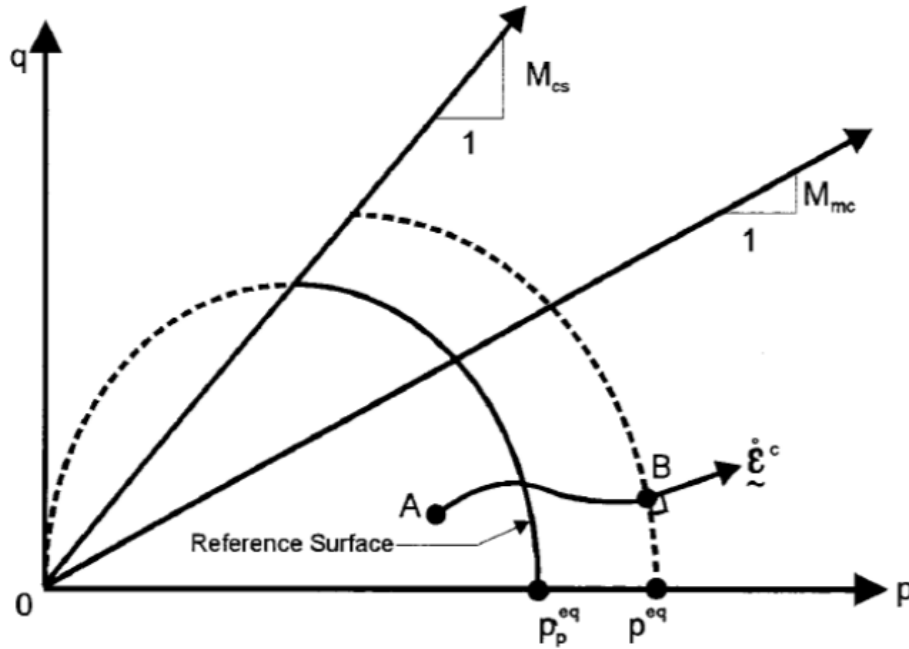


Figure 7.7: The reference surface and equivalent mean stresses after (Stolle et al., 1999)

The dimensionless time resistance number should be selected based on the soils' stress history as creep rate is far lower in the overconsolidated stress range.

The ratio λ^*/κ^* is usually in the range of 2.5 to 7, and the ratio μ^*/λ^* in the range of 0.03 to 0.07 (PLAXIS, 2018).

The Poisson's ratio in this model is a pure elastic constant, found from the ratio of horizontal to vertical stress increments:

$$\frac{v_{ur}}{1 - v_{ur}} = \frac{\Delta\sigma_{xx}}{\Delta\sigma_{yy}} \quad (7.4)$$

The creep deformations are calculated according to (Stolle et al., 1999):

$$\dot{\epsilon}_{vol} = \frac{\mu^*}{\tau} \left(\frac{p^{eq}}{p_p^{eq}} \right)^{\frac{\lambda^* - \kappa^*}{\mu^*}} = \frac{\mu^*}{\tau} \left(\frac{1}{OCR} \right)^{\frac{\lambda^* - \kappa^*}{\mu^*}} \quad (7.5)$$

Where:

p^{eq} and p_p^{eq} are the equivalent mean stresses at equivalent mean stress at p_c .

The critical-state parameter, M_{cs} , is determined by the friction angle. M is a model parameter determined by k_0^{NC} which controls the ellipse in Figure 7.7.

Failure is still defined according to a Mohr-Coulomb criterion and so perfect plastic strains are

generated when the failure criterion is met.

Destructuring of the soil is not accounted for as such strain softening in finite element analysis results in mesh dependency [Schädlich and Schweiger \(2012\)](#) with inaccuracies increasing at finer mesh sizes.

7.7 SSC Compression Parameters

Parameters κ^* and λ^* have been selected based on the laboratory test data, and adjusted in order to match the measured settlements.

The creep parameter, μ^* has been selected based on typical values of time resistance, r_s for the site area.

Stratum	γ (kN/m ³)	e_0	κ^*	λ^*	μ^*	POP (kPa)
Lanslide Deposits	18	1.3	0.016	0.075	0.0015	52
Quick Clay	18	1.3	0.016	0.075	0.0015	52
Marine Clay	19	1.1	0.012	0.05	0.0008	150

Table 7.4: Compression parameters for SSC model

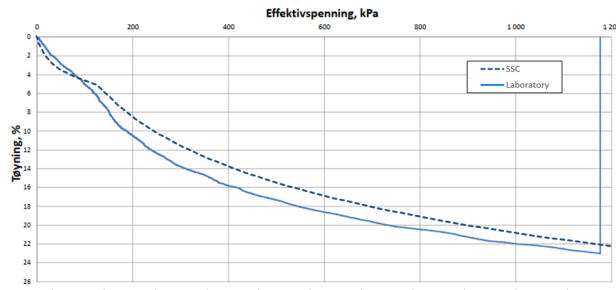


Figure 7.8: Oedometer test and simulation C2 5.4m

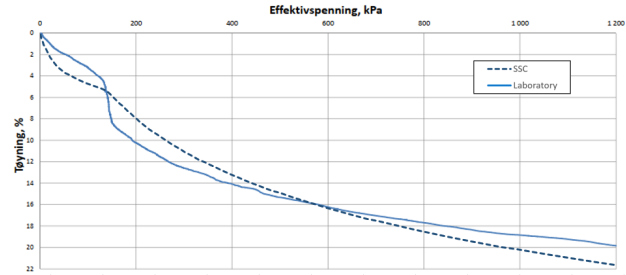


Figure 7.9: Oedometer test and simulation C2 6.35m

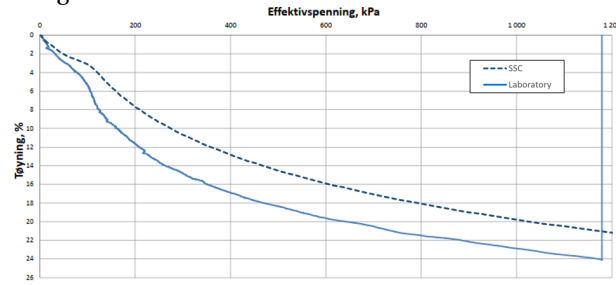


Figure 7.10: Oedometer test and simulation C2 7.4m

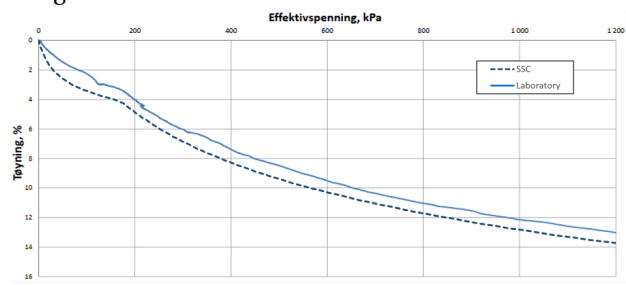


Figure 7.11: Oedometer test and simulation C2 10.3m

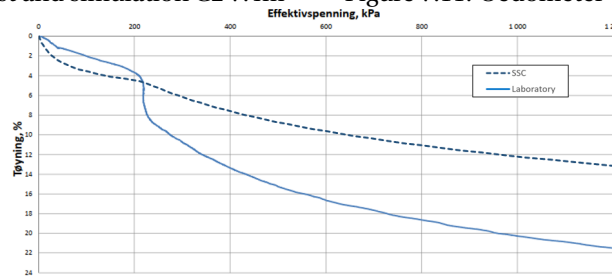


Figure 7.12: Oedometer test and simulation C2 11.4m

Validation of the parameters by simulation of CRS oedometer tests shown in Figures 7.8 to 7.12 shows a tendency for strains to be overestimated before p'_c and underestimated after p'_c as the effects of destructuring are not replicated.

7.8 SSC Strength

Strength is defined according to drained parameters according to effective stress parameters determined from the laboratory testing discussed in Chapter 3.

Stratum	ϕ	c' (kPa)
Dry Crust	26	5
Landslide Deposits	26	2
Quick Clay	24	5
Marine Clay	26	2

Table 7.5: Strength parameters for SSC model

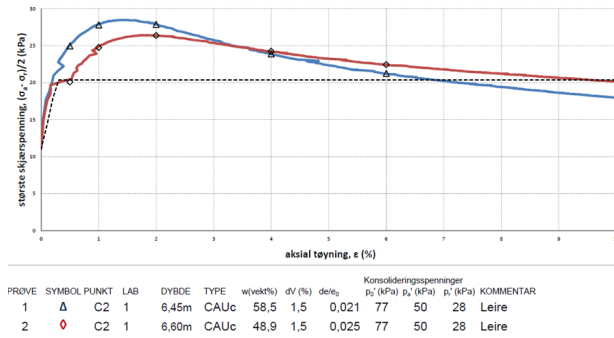


Figure 7.13: CAUC triaxial test simulation and laboratory results C2, 6.45m and 6.6m

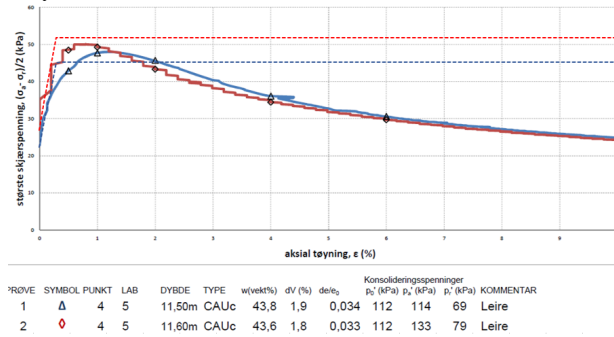


Figure 7.15: CAUC triaxial test simulation and laboratory results C2, 11.5m and 11.6m

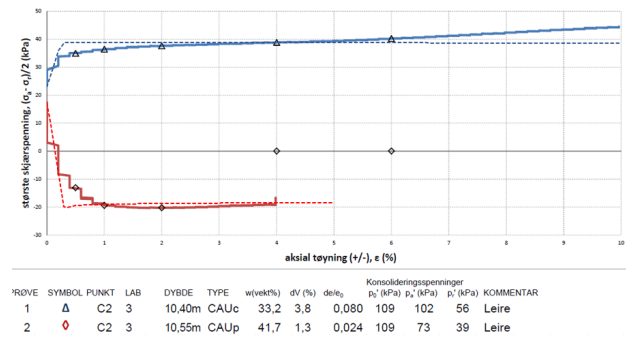


Figure 7.14: CAUC and CAUP triaxial test simulation and laboratory results C2, 10.4m and 10.55m

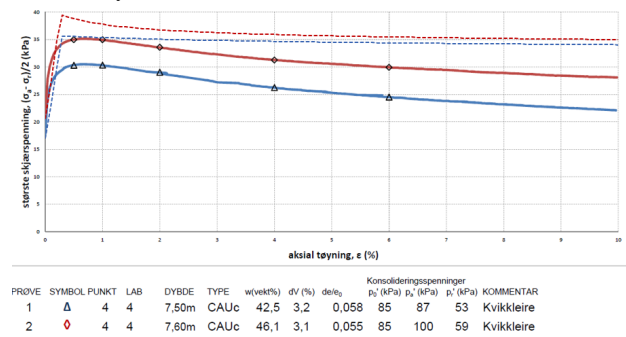


Figure 7.16: CAUC triaxial test simulation and laboratory results for Quick Clay C2, 7.5m and 7.6m

The selected strength parameters have been verified with the PLAXIS soil test function and compared to laboratory test data in Figures 7.13 to 7.16.

7.9 Permeability Parameters

Permeability has been selected based on the findings in Chapter 6. Equivalent plane strain permeabilities for the PVD zone have been calculated based on the procedure described earlier, using iteration of Equation 4.4. Stress dependency has been defined according to Tavenas et al. (1983b):

$$C_k = 0.5e_0 \quad (7.6)$$

PVD discharge capacity in plane-strain, $q_z = 4.3E-10m/s$ according to Equation 4.4, and therefore plane-strain permeability of:

$$k_v = k_h = \frac{q_z}{2b_w} = 4.3E-5m/s \quad (7.7)$$

	e_0	C_k	k_v (m/s)	k_h (m/s)	k_{hp} (m/s)	k'_{hp} (m/s)
Fill	0.5	-	5.00E-05	5.00E-05	-	-
Sand	0.5	-	5.00E-05	5.00E-05	-	-
DC, LD, QC	1.3	0.65				
Marine Clay	1.1	0.55	6.00E-10	1.80E-09	6.81E-10	1.00E-10

Table 7.6: Permeability parameters

Chapter 8

Numerical Analysis Results

In this chapter the results of the PLAXIS model are presented and discussed. The settlement and pore pressures are compared to the observed field measurements.

8.1 Initial Loads

A plastic null step was used in order to create stress equilibrium in the slope. Drained conditions were selected so that no excess pore pressures could be generated and pore pressures were calculated from steady-state groundwater flow. Total displacements remained $< 0.1\text{m}$.

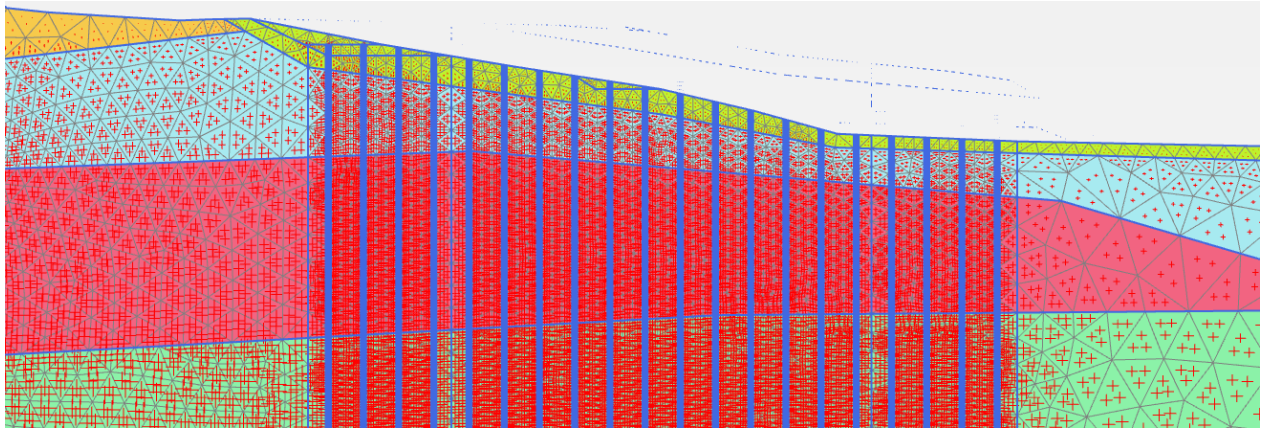
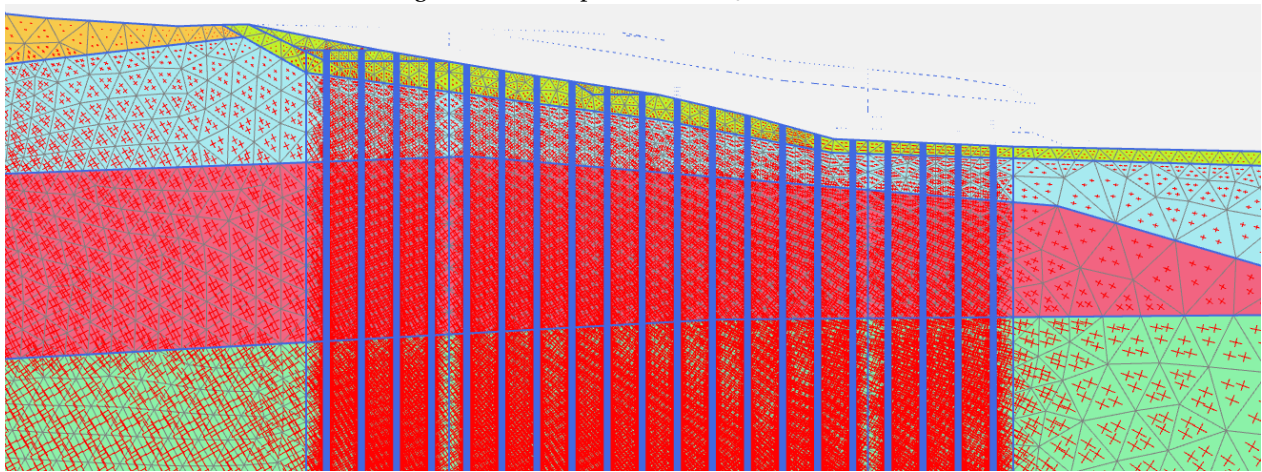
Figure 8.1: Principal stresses, K_0 calculation

Figure 8.2: Principal stresses, drained null step

Figures 8.1 and 8.2 show before and after the plastic step, which resulted in a rotation of principal stress planes.

8.2 Pore Pressure Dissipation

The pore pressured calculated by SSC model are compared to measured values from piezometers installed at depths ranging from 6m to 12m below original terrain level. Piezometers at locations C1 and C2 have a very good data resolution and so it is possible to determine specific construction activities which are shown in Figures 8.3 to 8.5 as follows:

1. Site clearance and excavation to foundation level
2. Placement of working platform layer
3. installation of PVD

4. Placement of final height of fill

The SSC model can be seen to over-predict initial pore pressures at the piezometers at 10m and 12m below terrain by some 5kPa to 10kPa throughout stages 1 and 2. This error is then removed when pore pressures are recalculated in stage 3. It can be seen that piezometers at positions C1 and C2 all slightly under-predict pore pressures at the start of stage 4. The SSC model does not replicate the gradual rise in groundwater pressure observed in C2 at 8m between stages 3 and 4. All piezometers replicate the final hydrostatic pore pressure condition observed at the end of stage 4.

8.2.1 Comparison of Pore Pressure Dissipation with and without PVD

Profile C has been used as to demonstrate the effect of PVD on excess pore pressures. Figures 8.6 to 8.9 show Profile C immediately after filling and at 267 day after filling. In both cases, immediately after filling is complete, maximum excess pore pressures are 85.5kPa. After 267 days, without PVD maximum pore pressure of 33.8kPa are within the centre of the soil mass, whereas with PVD in the centre of the soil mass $u = 0.6$ kPa.

8.3 Settlements

Total predicted settlements were calculated to be up to 125mm. In the case of loading without PVD, the time to 90% consolidation was calculated as 4.8 years to 6.3 years.

Settlement of the original terrain level was calculated for the period of 267 day after completion filling. The field settlement plates have been compared the calculated results in Figures 8.10 to 8.12. The final filling level was reached rapidly, such that relatively little consolidation occurred during placement.

Figures 8.10 to 8.12 show that the SSC model is generally able to produce similar results to the measured data, though accuracy is diminished at stress levels exceeding p'_c at which point the total settlement is usually under-estimated. The destructuring and softening of the clay is not replicated.

8.4 Lateral Displacements

Lateral displacements have been calculated for cross-sections beneath the fill area. These have been reported for various distances from the centreline of the fill with negative distances being the decreasing x-ordinate (up slope) and positive values being increases in the x-ordinate (down

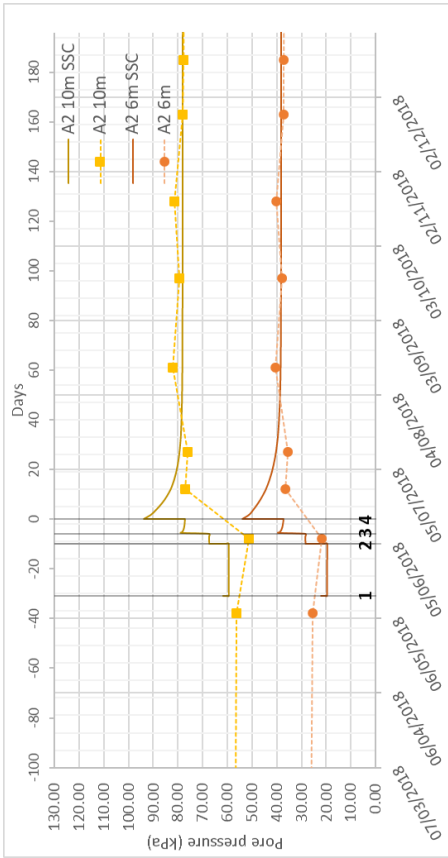


Figure 8.3: Pore pressure at position A2

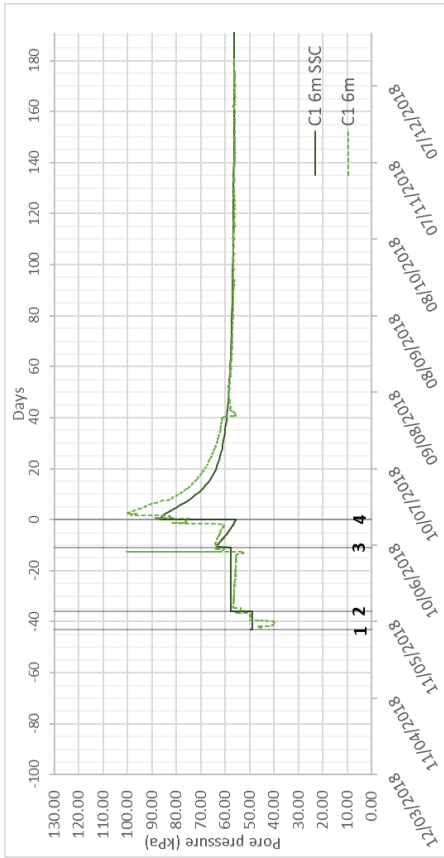


Figure 8.4: Pore pressure at position C1

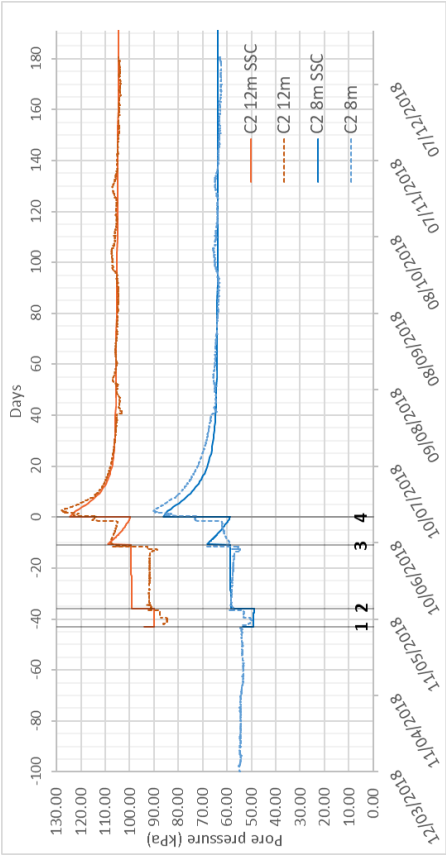


Figure 8.5: Pore pressure at position C2

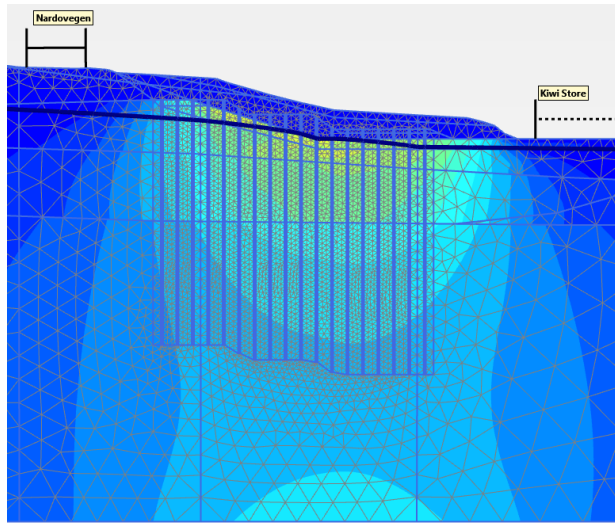


Figure 8.6: Excess pore pressures after filling without PVD

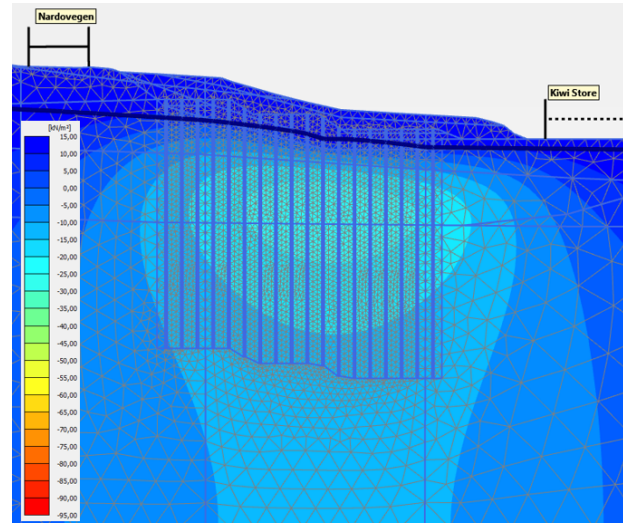


Figure 8.7: Excess pore pressures after 267 days consolidation without PVD

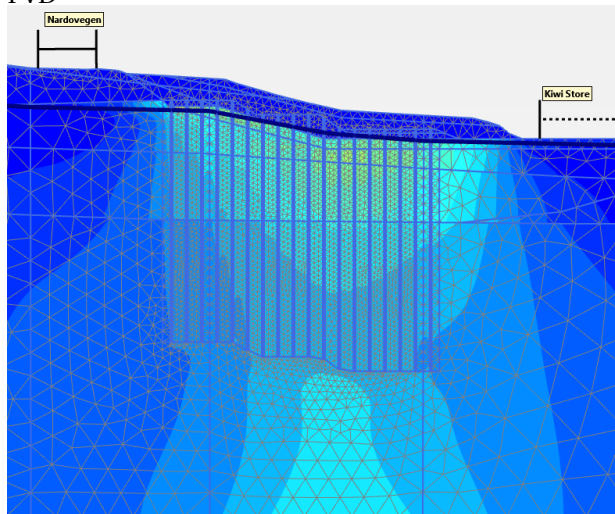


Figure 8.8: Excess pore pressures after filling with PVD installed

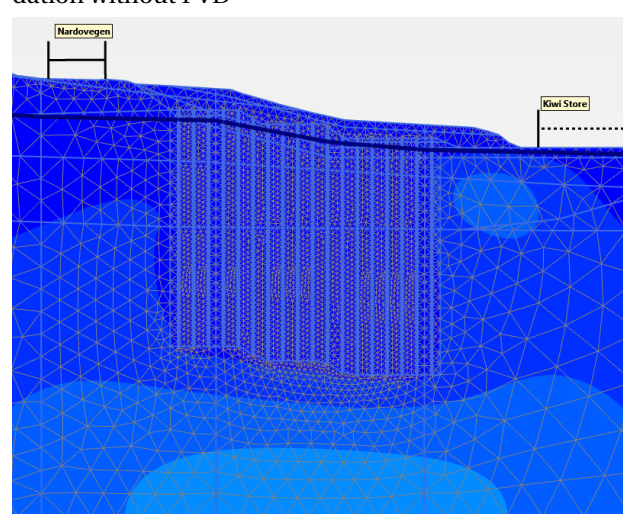


Figure 8.9: Excess pore pressures after 265 days consolidation with PVD installed

slope). The calculated displacements have been normalised are given for the end of the settlement monitoring period, i.e. 267 days after fill placement. The have been normalised over both the settlement, and height of placed fill.

No monitoring data is available to verify the calculated values.

All plots show increasing displacements in the up-slope direction; and as expected, the displacements area greatest at -15m from the centre-line, close to the maximum up-slope extent of the fill. Displacements beneath Profile A are greatest as a rapid decrease in fill height exists on the left side of the model, creating stress concentrations in this location. Profile B is noted to have much more gradual decrease in fill height, particularly on the down-slope side where the geometry is similar to a berm which results in a much closer grouping of lateral deformation and

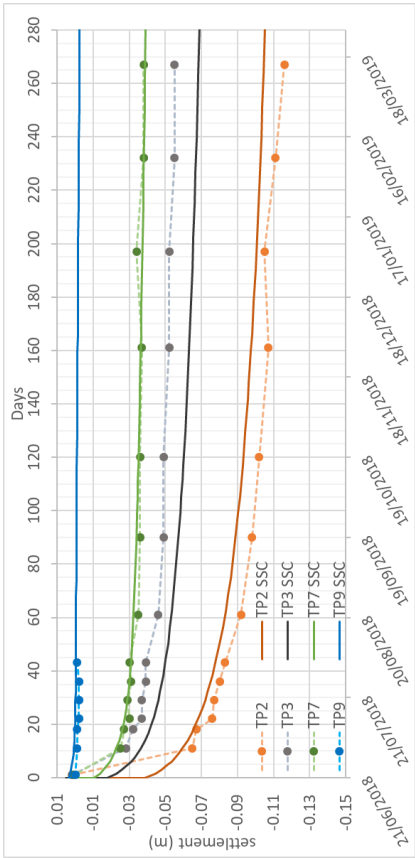


Figure 8.10: Predicted and measured settlements Section A

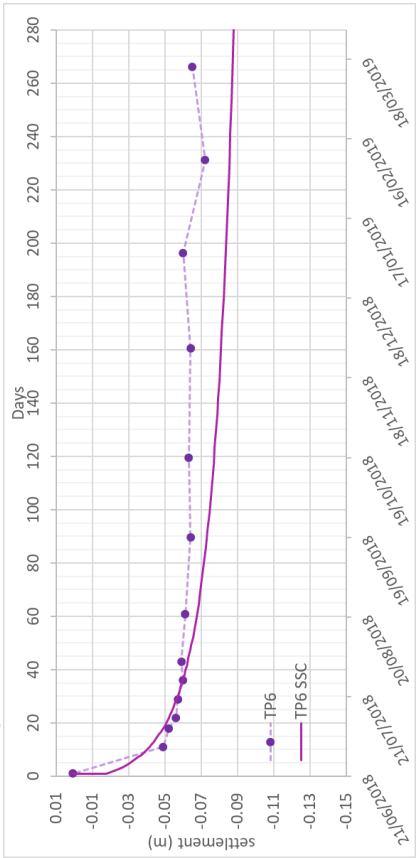


Figure 8.12: Predicted and measured settlements Section C

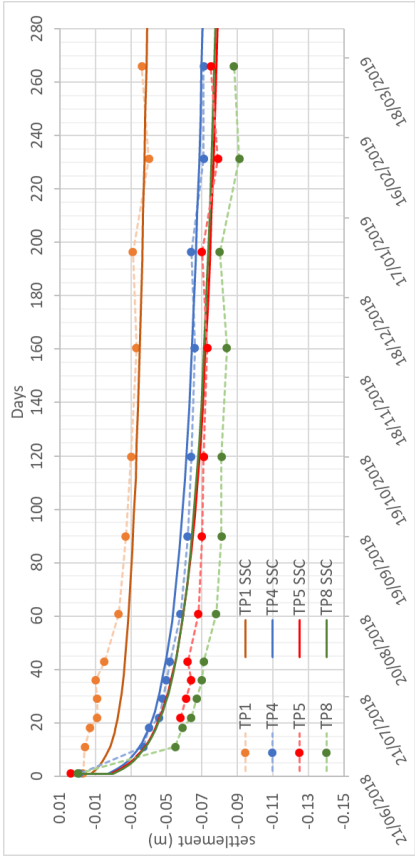


Figure 8.11: Predicted and measured settlements Section B

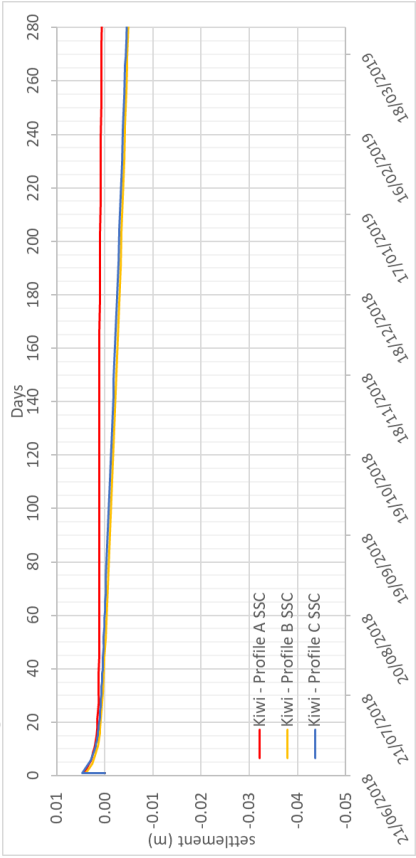


Figure 8.13: Predicted settlements at Kiwi

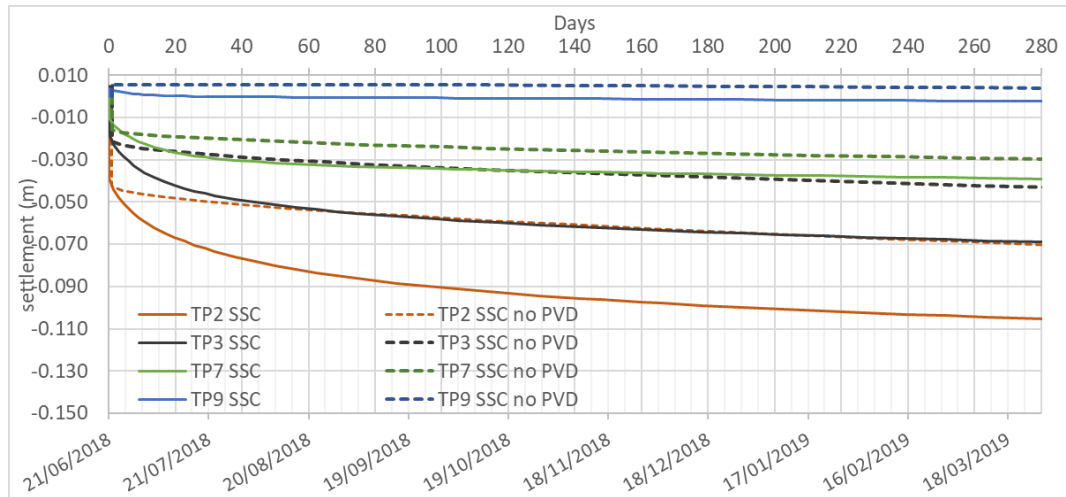


Figure 8.14: Settlement along Profile A, with and without PVD

increasing stability.

8.5 Safety

The lateral displacements for the case of with and without PVD at the end of consolidation shows how by increasing the rate of consolidation stability of the embankment is increased

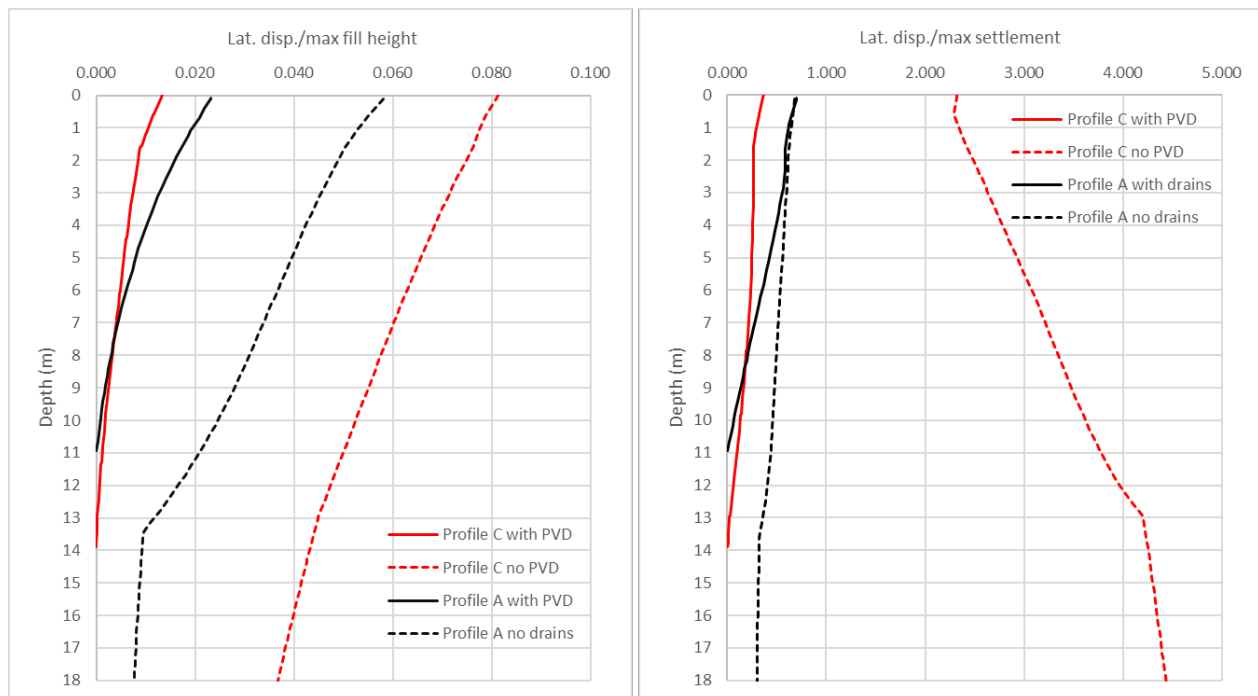


Figure 8.18: Comparison of lateral displacements at 15m from the fill centre-line, with and without PVD

An additional c' - ϕ reduction calculation was carried out, with and without PVD. in all cases the material safety factor was shown to increase with the introduction of PVD.

Profile	FoS no drains	FoS PVD
A	1.21	1.42
B	1.23	1.58
C	1.24	1.57

Table 8.1: Factor of safety against base failure

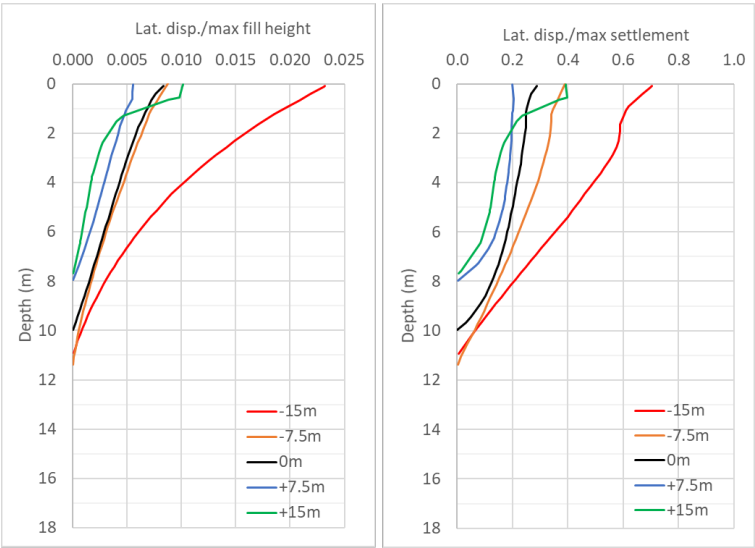


Figure 8.15: Normalised lateral displacements along Profile A

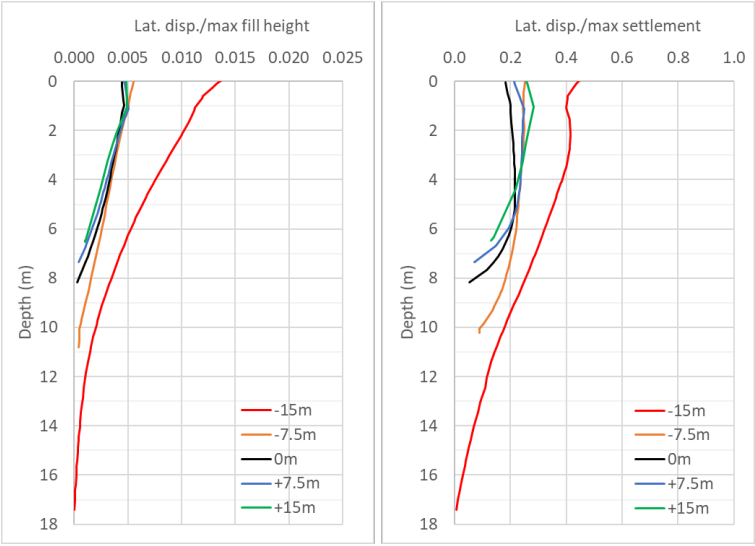


Figure 8.16: Normalised lateral displacements along Profile B

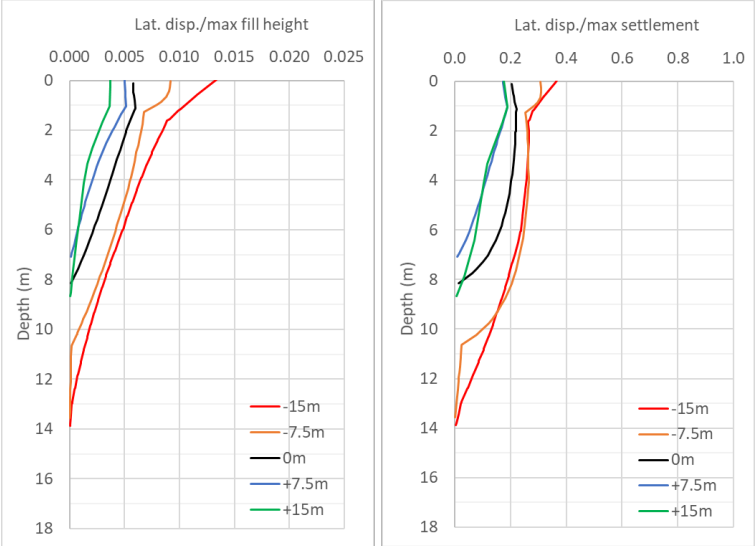


Figure 8.17: Normalised lateral displacements along Profile C

Chapter 9

Conclusions and Discussion

9.1 Summary and Conclusions

Results clearly show the benefit of PVD of decreasing the primary consolidation time by, on average, over 4 years. Additionally, PVD provide the benefit of increasing stability of the foundation by decreasing lateral strains.

A very good fit between predicted and observed pore-pressure response was achieved through matching permeability values, although the initial excess pore pressure was always slightly underestimated. Including the e -log k relationship of $C_k=0.5e_0$ proposed by [Tavenas et al. \(1983b\)](#) provides an increase in precision for predicting pore pressure decay. However, the most significant increase is to be found by using a stress dependant stiffness.

A potential problem with the PVD application to slope stability has been identified. It was observed that pore pressures in all piezometers reached equilibrium at an increased pressure after installation of PVD. This increase gives cause for consideration, given the context of a slope stabilisation scheme. These identified effects on steady pore pressure should be considered when PVD are to be installed in a situation with large over-hydrostatic pore pressures.

9.2 Discussion of Results

9.2.1 Uncertainty of the Ground Conditions

The ratio k_h/k_v was assumed to be 3 and the ratio k'_h/k_v was assumed to be unity which achieved results which closely matched observed behaviour. However, it is possible that CRS derived k_v was an under estimate, and therefore $k_h/k_v=3$ may be too high; indeed there is evidence to sug-

gest the ratio may range from close to unity ((Bergado et al., 1991), (Tavenas et al., 1983a)) to as high as 15 Jamiolkowski et al. (1983).

Consolidation rates have been shown to be more sensitive to permeability within the smear zone, rather than the dimensions of the smear zone itself. Notwithstanding this, the diameter of the smear zone is not known and is another potential source of error.

The reasons for slightly under-hydrostatic pore pressures at positions A2 and C2 were not fully identified. The most probable cause would be under-drainage from a more permeable layer, although the site investigation does not give strong evidence for this. A very close to hydrostatic condition was created following the installation of deep PVD, suggesting under-drainage did not effect soils to a great depth and therefore extrapolating the initial condition to soils above or below may give unrealistic estimates of pore pressure.

9.2.2 Accuracy of the Numerical Model

The numerical analysis has shown that PVD have significantly reduced the time of consolidation and increased stability beneath the fill as expected.

The settlements calculated by SSC were within $\pm 8\text{mm}$ of measured values, a normalised error of $\pm 15\%$. The pore pressures were also slightly underestimated.

Excess pore pressures appear to have largely dissipated with an excess of $<1\text{kPa}$ remaining within the PVD influence zone at the end of consolidation period. Some 15kPa of excess pore pressure remains below the PVDs.

Some inaccuracy was introduced by averaging POP over along the slope profile which results in a slight misrepresentation of yield stress and reduced accuracy of strains created for a given load increment.

9.2.3 Efficacy as a Slope Stabilisation Technique

The increasing lateral stresses down-slope act to increase confinement the the soils downslope resulting in a decreased lateral strains for an applied load. The PVD have acted to decrease lateral strains within the soil mass, further stabilising it. Additionally, the reduced time for consolidation creates a faster increase in effective normal stresses and shear strength, so there is less time for shear strains to develop.

Rise in groundwater may in fact decrease slope stability in the drained case.

When considering the increase in restoring moments and increase, a considerable increase in safety is calculated, satisfying the design codes.

9.3 Recommendations for Future Work

The installation effects of the PVD have not been fully considered in this study and there is evidence to show that excess pore pressures of up to 45 kPa, or possibly more, are generated due to drain installation. Further study of this effect is needed to better understand what implications there are for installing a PVD array (comprising several thousand drains) close to a slope.

It would be interesting to undertake constant head permeability tests on cores of vertical and horizontal orientation, as well as remoulded samples, as the plane-strain model is particularly sensitive to input permeability values within the smear zone and ratio k_{hp}/k'_{hp} .

At the time of this study, the surcharge load has not yet been removed. Verification of with field data of SSC ability to predict pore pressure changes and heave as a result of unloading would further verify the model.

Bibliography

- Asaoka, T. (1978). Observational procedure of settlement prediction. *Soils and Foundations*, 18:87–101.
- Barron, R. A. (1948). Consolidation of fine grained soils by drain wells. *Transactions of the American Society of Civil Engineers*, 113:718–724.
- Bergado, D., Asakami, H., Alfaro, M., and Balasubramaniam, A. (1991). Smear effects of vertical drains on soft bangkok clay. *Journal of Geotechnical Engineering*, 117:1509–1530.
- Bjerrum, L. (1972). Embankments on soft ground. *Proceedings of the American Society of Civil Engineers Speciality Conference on Performance of Earth and Earth-Retaining Structures*, 2:1–54.
- Burland, J. B. (1990). On the compressibility and shear strength of natural clays. *Geotechnique*, 40:329–378.
- Degago, S., Grimstad, G., Jostad, H., Nordal, S., and Olsson, M. (2011). Use and misuse of the isotache concept with respect to creep hypotheses a and b. *Géotechnique*, 61(10):897–908.
- Hansbo, S. (1981). Consolidation of fine-grained soils by prefabricated drains. *Proceedings of the 10th international conference on soil mechanics and foundation engineering*, 6:677–682.
- Holtz, R. (1987). Preloading with prefabricated vertical strip drains. *Geotextiles and Geomembranes*, 6:109–131.
- Holtz, R., Jamiolkowski, M., Lancellota, R., and Pedroni, R. (1991). Ciria ground engineering report: Prefabricated vertical drains design and performance.
- Indraratna, B. and Redana, I. W. (1997). Plane-strain modelling of smear effects associated with vertical drains. *Journal of Geotechnical and Geoenvironmental Engineering*, 123:474–478.
- Indraratna, B. and Redana, I. W. (2000). Numerical modelling of vertical drains with smear and well resistance installed in soft clay. *Canadian Geotechnical Journal*, 37:132–145.

- Jamiolkowski, M., Lancellotta, R., and Wolski, W. (1983). Precompression and speeding up consolidation. *Proceedings of the Eighth European Conference on Soil Mechanics and Foundation Engineering*, 3:1201–1226.
- Johnson, S. J. (1970). Precompression for improving foundation soils. *Journal of the Soil Mechanics and Foundations Division, Proceedings of the ASCE*, 96:111–144.
- Karlsrud, K. and Hernandez-Martinez, G. (2013). Strength and deformation properties of norwegian clays from laboratory tests on high-quality block samples. *Canadian Geotechnical Journal*, 50:1273–1293.
- Kjellman, W. (1948). Accelerating consolidation of fine grained soils by means of cardboard wicks. *Proceedings of the 2nd International Conference on Soil Mechanics and Foundation Engineering*, 2:302–305.
- Kommune, T. (1988). Bru torbjørn bratts veg, grunnundersøkelser datarapport.
- Ladd, C., Foot, R., Ishihara, K., Schlosser, F., and Poulos, H. (1977). Stress-deformation and strength characteristics: state-of-the-art report. *Proceedings of the Ninth International Conference on Soil Mechanics and Foundation Engineering*, 2:421–94.
- Levadoux, J. and Baligh, M. (1980). Pore pressure during cone penetration in clays. *Massachusetts Institute of Technology Research Report R80-15*.
- Lunne, T., Berre, T., and Strandvik, S. (1997). Sample disturbance effects in soft low plastic norwegian clay. *Proc. of the Symp. on Recent Develop. in Soil and Pavement Mech., Rio de Janeiro*.
- NGU (2013). *Quaternary geology of Norway, Geological Survey of Norway Special Publication, 13*. Norges geologiske undersøkelse.
- NVE (2014). *Sikkerhet mot kvikkleireskred*. Norges vassdrags og energidirektorat.
- PLAXIS (2018). *PLAXIS 2D Material Models Manual*. PLAXIS.
- Reite, A., Sveian, H., and Erichsen, E. (1999). *Trondheim fra istid til nåtid -landskaps-historie og løsmasser, Gråsteinen 5*. Norges geologiske undersøkelse.
- Reite, A. J., Selnes, H., and Sveian, H. (1982). A proposed deglaciation chronology for the trondheimsfjord area, central norway. *Geological Survey of Norway Bulletin*, 375:75–84.
- Sand, K. (1999). *Fra istid til nåtid*. NGF.
- Schädlich, B. and Schweiger, H. (2012). Influence of non-local strain regularisation on the evolution of shear bands. *Institute for Soil Mechanics and Foundation Engineering, Graz University of Technology, Austria*.

- Stolle, D., Vermeer, P., and Bonnier, P. (1999). A consolidation model for creeping clay. *Canadian Geotechnical Journal*, 36(4):754–759.
- Strand, S., Thakur, V., L'Heureux, J., Lacasse, S., Karlsrud, K., Nyheim, T., Aunaas, K., Ottesen, H., Gjelsvik, V., Fauskerud, O., Sandven, R., and Åkershul, A. (2017). Runout of landslides in sensitive clays. *Landslides in Sensitive Clays From Research to Implementation*, pages 289–300.
- Tavenas, F., Leblonde, P., Jean, P., and Leroueil, S. (1983a). The permeability of natural soft clays. part i: Methods of laboratory measurement. *Canadian Geotechnical Journal*, 20(4):629–644.
- Tavenas, F., Leblonde, P., Jean, P., and Leroueil, S. (1983b). The permeability of natural soft clays. part ii: Permeability characteristics. *Canadian Geotechnical Journal*, 20(4):645–660.
- Terzaghi, K., Peck, R., and Mesri, G. (1996). *Soil Mechanics in Engineering Practice*. John Wiley & Sons, Inc.

Acronyms

CAUC Consolidated Anisotropic Undrained Compression triaxial test

CAUP Consolidated Anisotropic Undrained Passive triaxial test

CPT Cone Penetration Test

CRS Constant Rate of Strain

moh Meters above sea level (Norwegian: meter over havet)

POP Previous Overburden Pressure

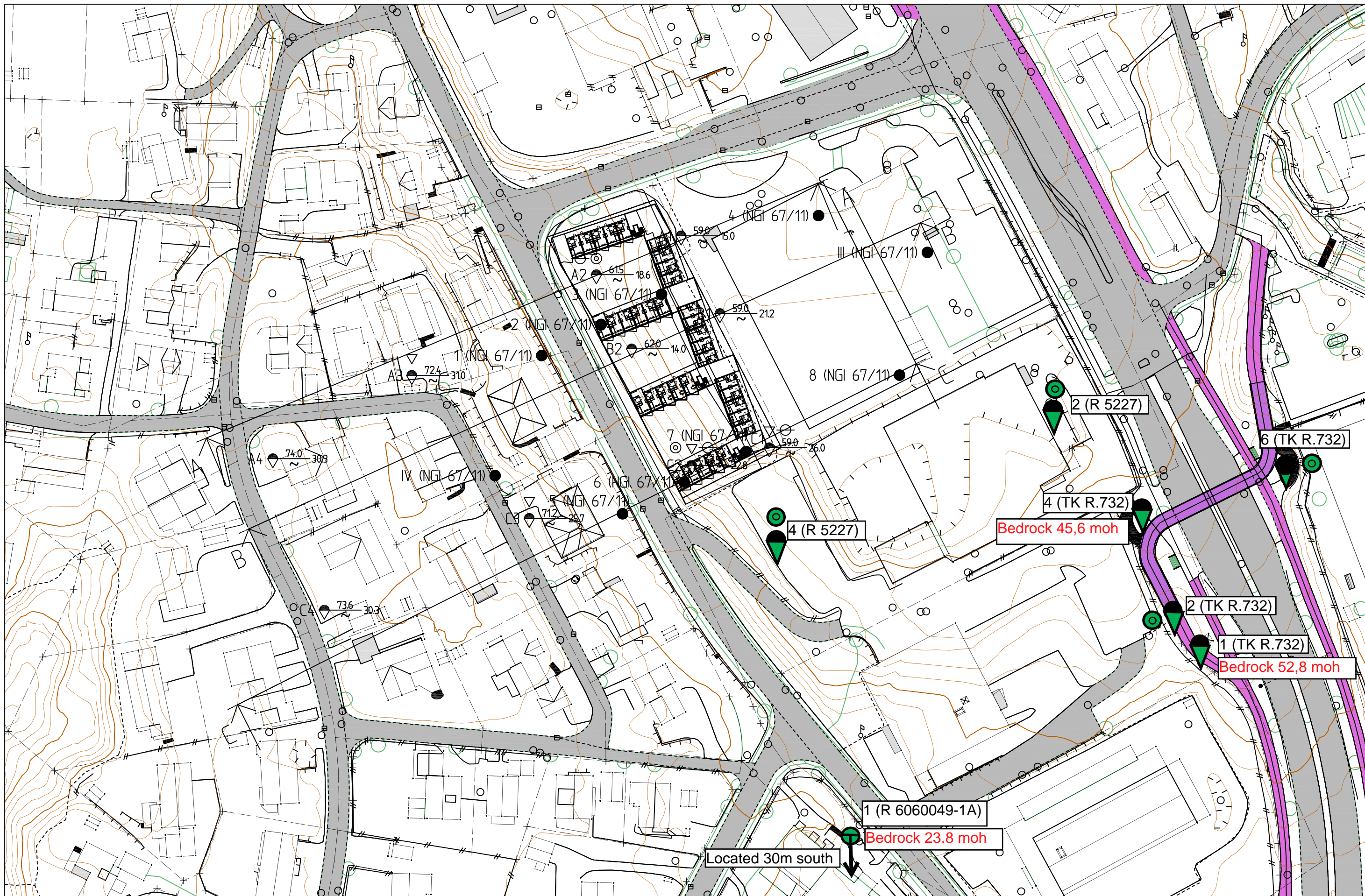
PSD Particle Size Distribution

PVD Prefabricated Vertical Drain

SSC Soft Soil Creep model

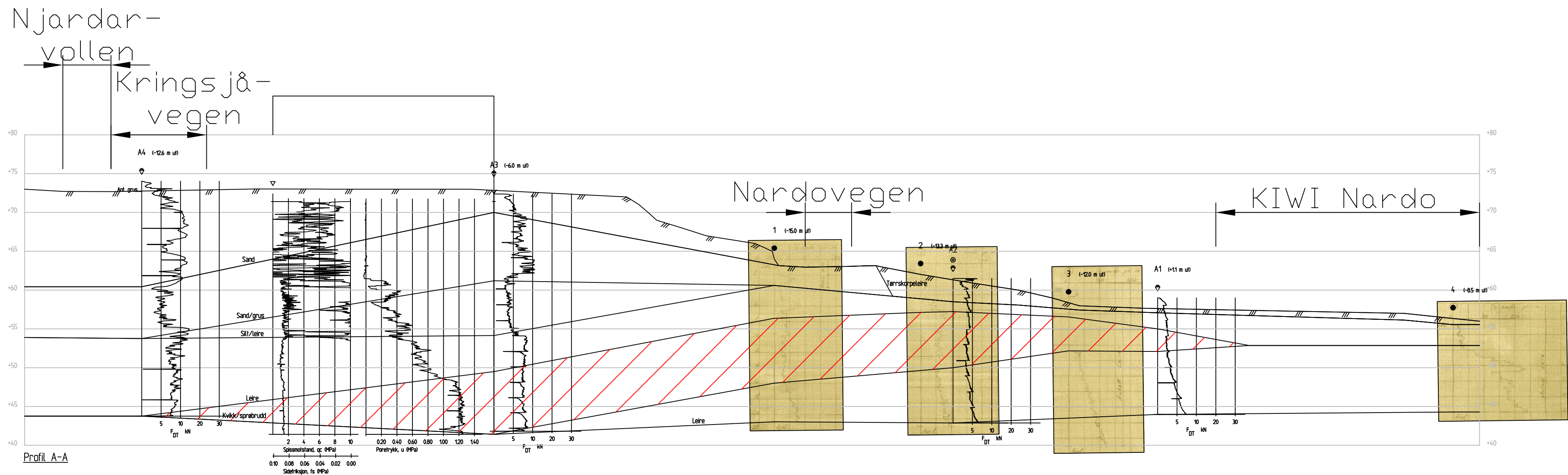
Appendix A

Site Plan and Slope Profiles



						OPPDRAG		INNHOOLD		OPPDRAG NR.		MÅLESTOKK	BLAD NR.	AV
						Nardobakken		SITUASJONSPLAN		1350020995		1:1000	01	01
						OPPDRAGSGIVER		Dreietrykksondering		Trykksondering (CPTU)		TEGNING NR.		REV.
						Nardobakken Eiendom AS		Dreiesondering		Piezometer		202		0
								Historic sounding						

RAMBOLL
Rambøll AS - Region Midt-Norge
P.b. 9420 Sluppen
Mellomila 79, N-7493 Trondheim
TLF: 73 84 10 00 - FAX: 73 84 10 60
www.ramboll.no



00	28.04.2017		BAGJ	KEG	BAGJ
REV.	DATO	ENDRING	TEGN	KONTR	GODKJ
TEGNINGSSTATUS					

RAMBOLL

Rambøll AS - Region Midt-Norge
P.b. 9420 Sluppen
Mellomila 79, N-7493 Trondheim
TLF: 73 84 10 00 - FAX: 73 84 10 60
www.ramboll.no

OPPDRA Nardobakken	INNHO Profil A
OPPDRA Nardobakken Eiendom AS	Terreng og sonderinger

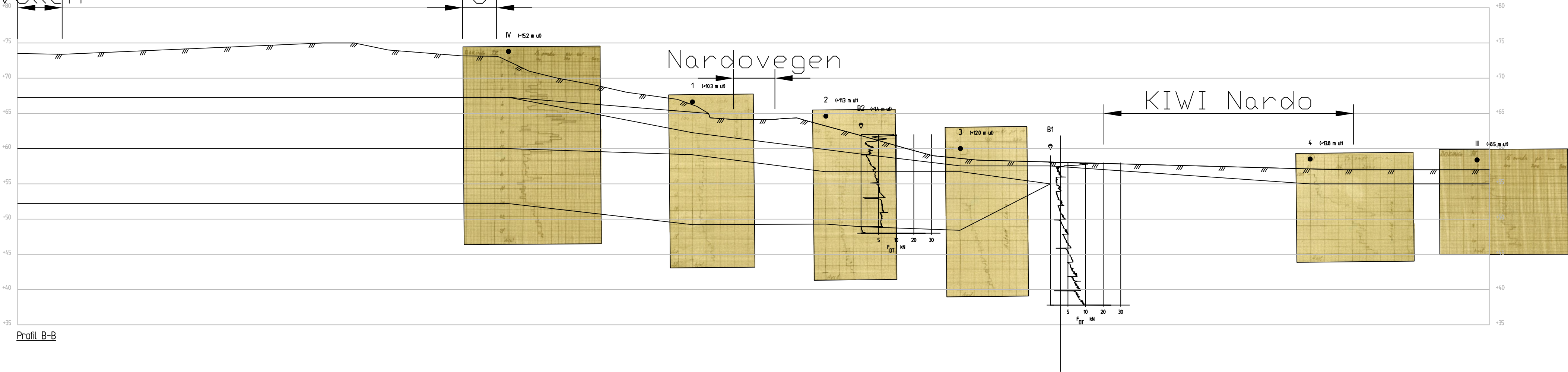
OPPDRA NR. 1350020995	MÅLESTOKK 1:400	BLAD NR. 01	AV 01
TEGNING NR. 203			REV. 0

Njardar-
vollen

Kringsjå-
vegen

Nardovegen

KIWI Nardo



Profil B-B

00	28.04.2017		BAGJ	KEG	BAGJ
REV.	DATO	ENDRING	TEGN	KONTR	GODKJ
TEGNINGSSTATUS					

RAMBOLL

Rambøll AS - Region Midt-Norge
P.b. 9420 Sluppen
Mellomila 79, N-7493 Trondheim
TLF: 73 84 10 00 - FAX: 73 84 10 60
www.ramboll.no

OPPDRA

Nardobakken

OPPDRA

Nardobakken Eiendom AS

INN

Profil B

Terreng og sonderinger

OPPDRA NR.
1350020995

MÅLESTOKK
1:400

BLAD NR.
01

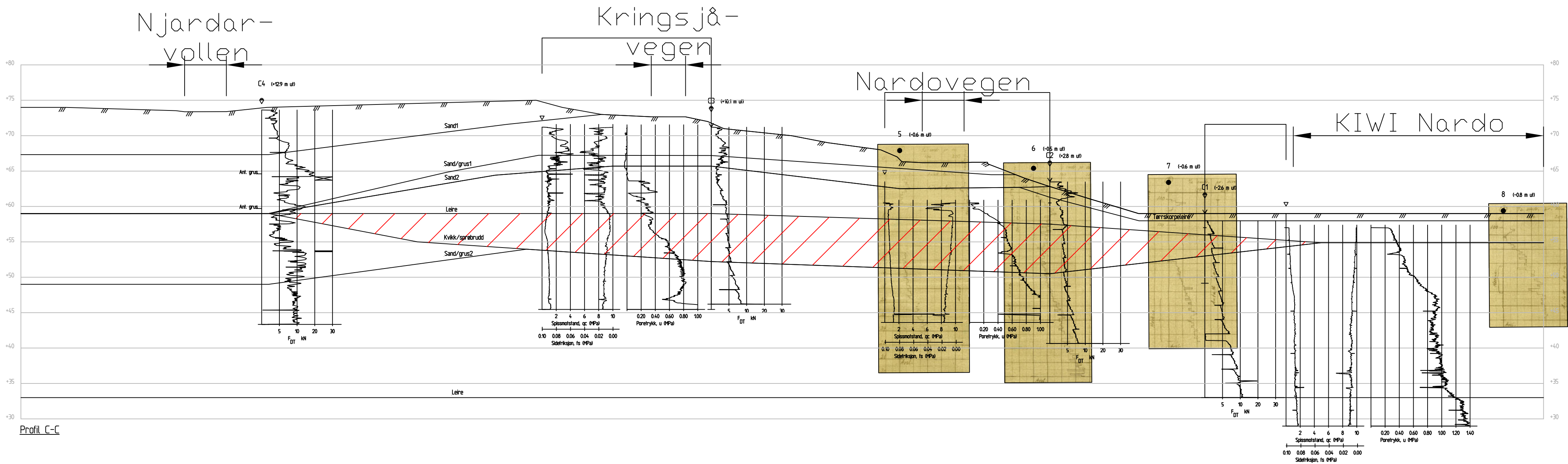
AV
01

TEGNING NR.

204

REV.

0



Profil C-C

00	28.04.2017		BAGJ	KEG	BAGJ
REV.	DATO	ENDRING	TEGN	KONTR	GODKJ
TEGNINGSSTATUS					

RAMBOLL

Rambøll AS - Region Midt-Norge
P.b. 9420 Sluppen
Mellomila 79, N-7493 Trondheim
TLF: 73 84 10 00 - FAX: 73 84 10 60
www.ramboll.no

OPPDRA Nardobakken	OPPDRA Nardobakken Eiendom AS
OPPDRA Nardobakken Eiendom AS	

INN Profil C	Terreng og sonderinger
Terreng og sonderinger	

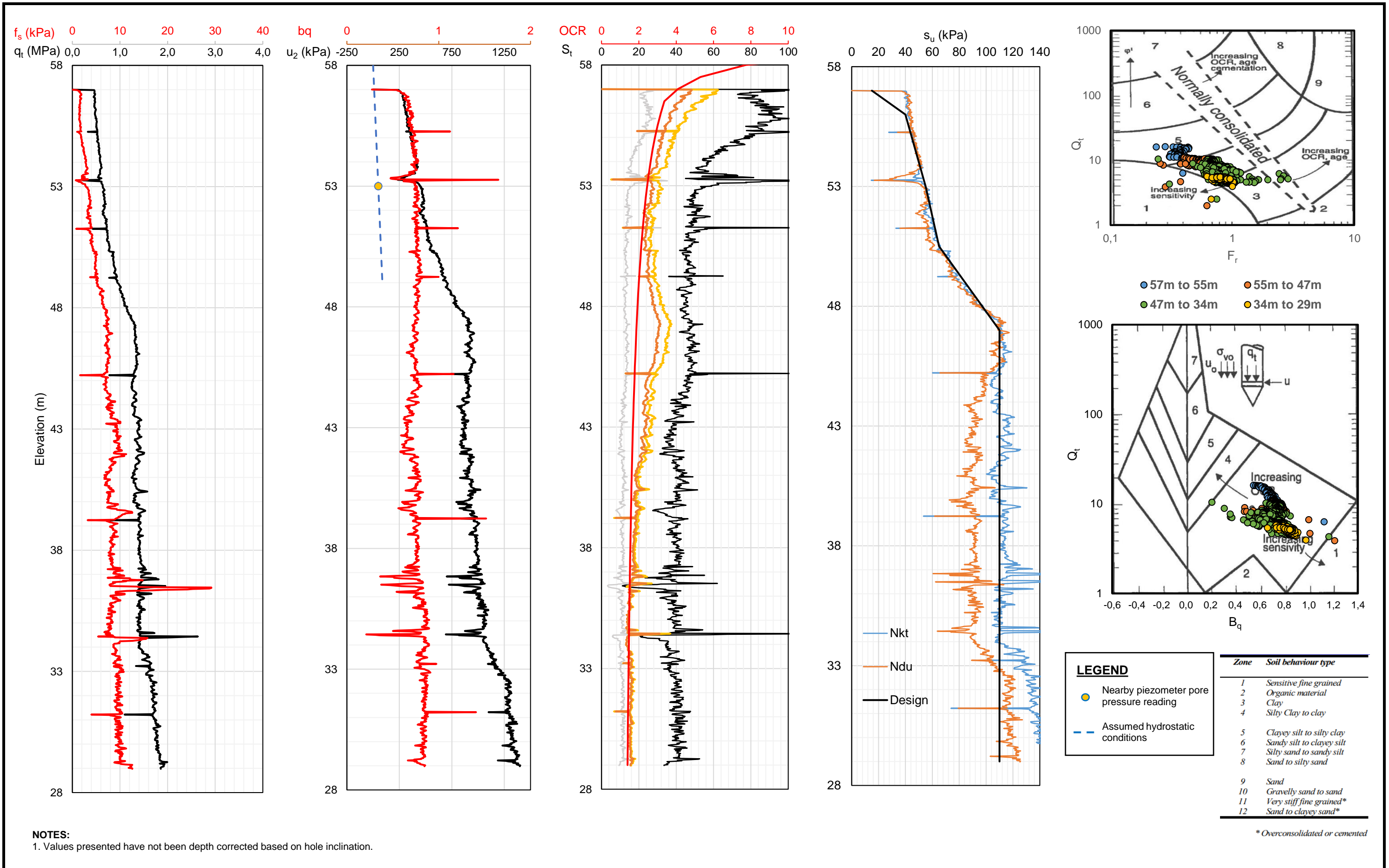
OPPDRA NR. 1350020995	MÅLESTOKK 1:400	BLAD NR. 01	AV 01
TEGNING NR. 205			REV. 0

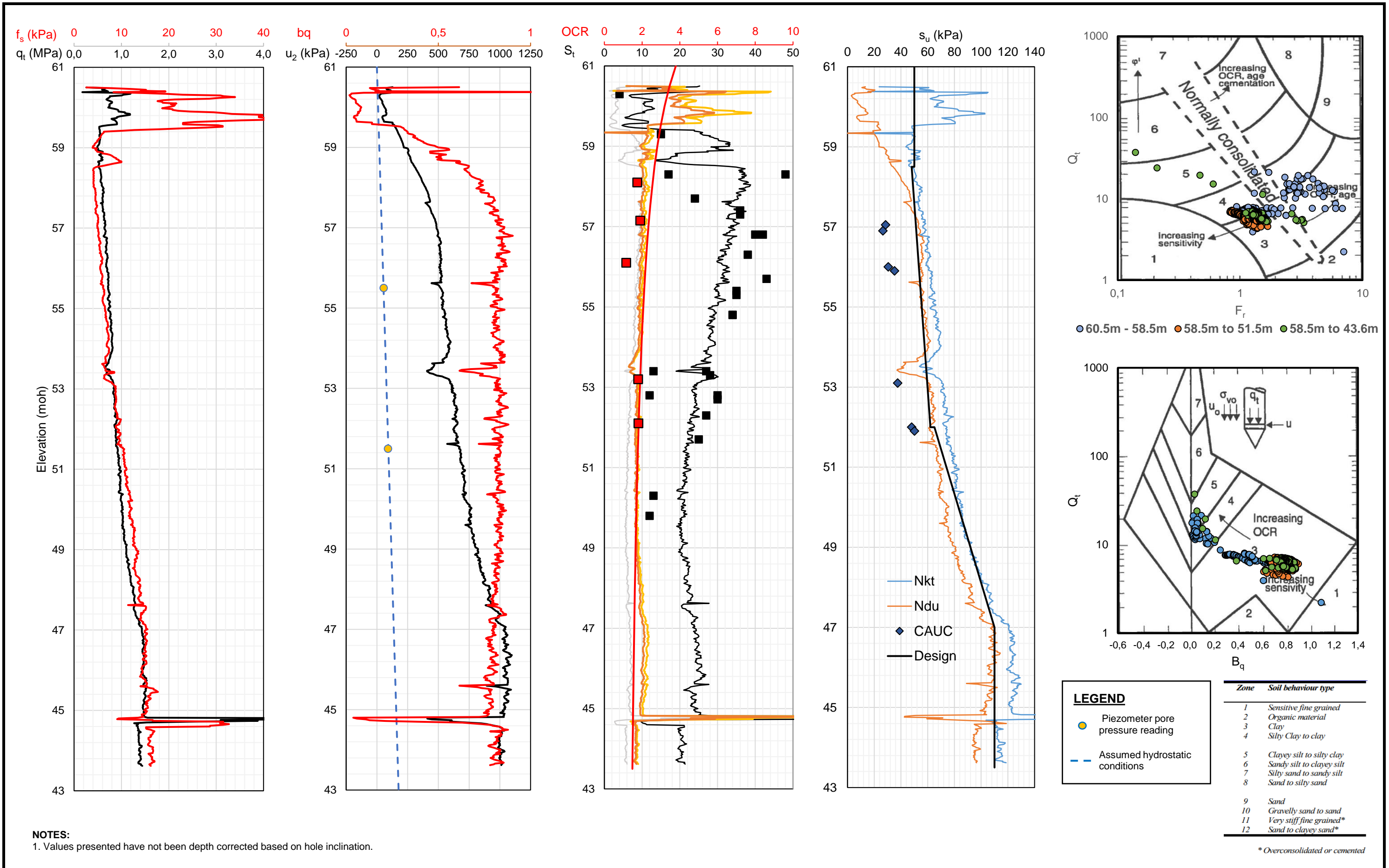
Appendix B

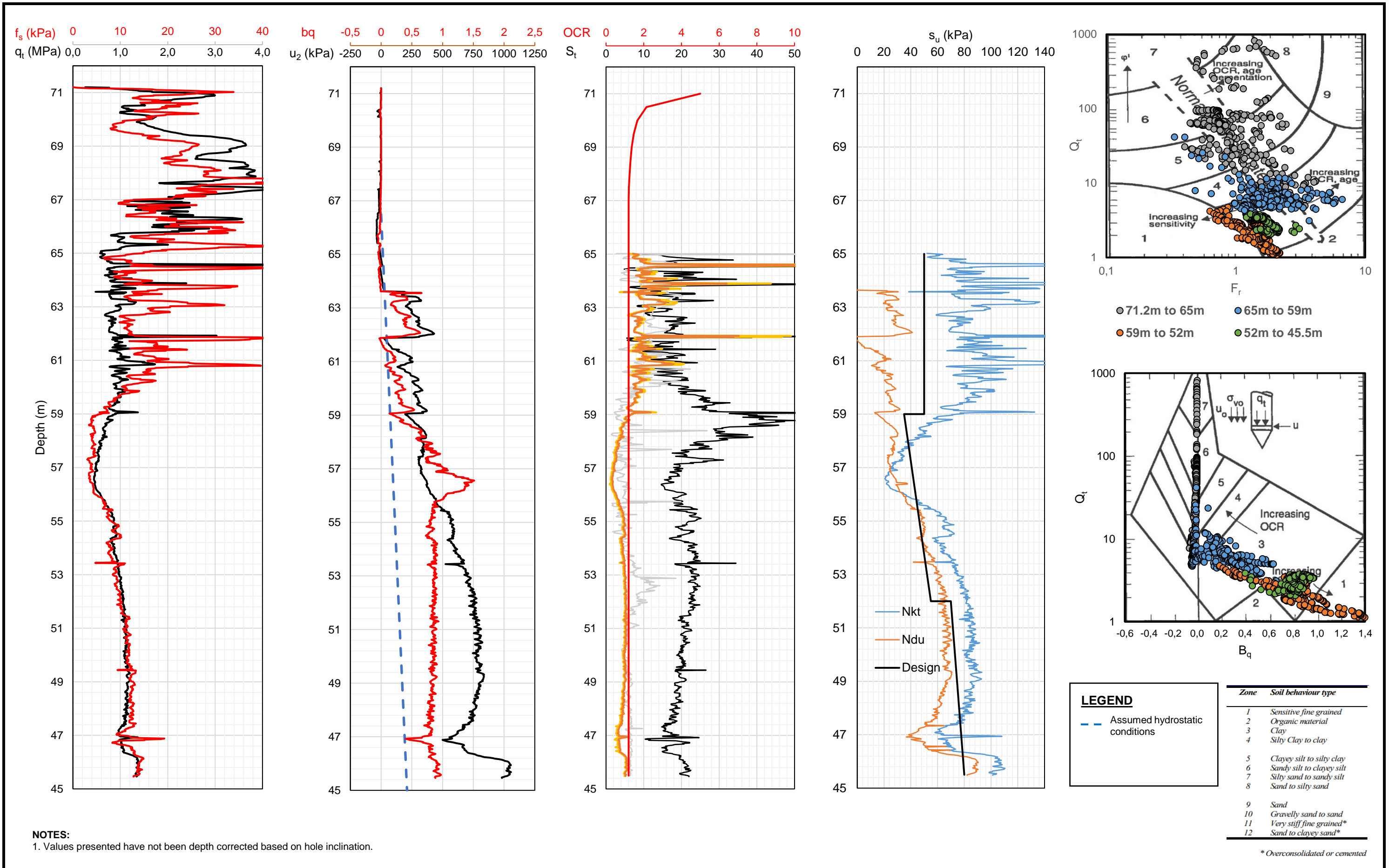
Interpreted Site Investigation Data

Reference	Current SI? / On site?	Sounding type	Max depth (m)	Lab testing
A1	Y Y	RP	15	
A2	Y Y	RP, 54, PZ	18.5	w, γ , FC, UC
A3	Y Y	RP, CPTU	31	
A4	Y Y	RP	30	
B1	Y Y	RP	21	
B2	Y Y	RP	14	
C1	Y Y	RP, CPTU, PZ	30	
C2	Y Y	RP, 54, CPTU, PZ	23	w, Att, γ , FC, UC, CAUC, CAUP, Oed
C3	Y Y	RP, CPTU	25.5	
C4	Y Y	RP	30	
1 (NGI 67/11)	N Y	RS	21	
2 (NGI 67/11)	N Y	RS	21	
3 (NGI 67/11)	N Y	RS	21	
4 (NGI 67/11)	N Y	RS	12	
5 (NGI 67/11)	N Y	RS	28	
6 (NGI 67/11)	N Y	RS	28	
7 (NGI 67/11)	N Y	RS	21	
8 (NGI 67/11)	N Y	RS	14	
III (NGI 67/11)	N Y	RS	11	
IV (ngi 67/11)	N Y	RS	25	
2 (R 5227)	N N	RP, 54	18	w, γ , FC, UC, Oed
4 (R 5227)	N N	RP, 54	11	w, γ , FC, UC, CIUC
1 (TK R.732)	N N	RP	11	
2 (TK R.732)	N N	RP, 54	10	w, γ , PSD, FC, UC, CAUC, Oed
4 (TK R.732)	N N	RP	15	
6 (TK R.732)	N N	RP, 54	10	w, γ , PSD, FC, UC
1 (R 6060049-1A)	N N	TS	46	
RP = rotary pressure, 54 = 54mm piston, PZ = piezometer, CPTU = cone penetration test with pore pressure measurement, RS = rotary sounding, TS = total sounding				
w = moisture content, Att = atterberg limits, γ = bulk density, FC = fall cone shear strength, UC = uniaxial compression, C(A/I)U(C/P) = consolidated (anisotropic/isotropic) undrained (compression/passive), PSD = particle size distribution				

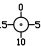
Table B.1: Summary of soundings referenced within this study







Dybde, m	Jordart	Sign.	Lab. nr	Vanninnhold (w) i %				γ kN/m ³	Skjærfasthet (C_u) i kPa				S_t
				10	20	30	40		10	20	30	40	
5	sprøbrudd	/	1					• 17.0	▼		▼	⊙	39
								• 17.5	▼	⊙	▼		21
10													
15													
20													

Enkelt trykkforsøk :  (strek angir def.% v/brudd)

Konusforsøk - Omrørt/uforstyrret: ▼ / ▽

Penetrometerforsøk ☐ Konsistensgrense w_p ———— w_L Andre forsøk:

T= Treaksialforsøk

Ø= Ødometerforsøk

K= Kornfordeling

00	04.05.2017		BAGJ	KEG	PAW
Rev.	Dato	Tekst	Utarb	Kontr	Godkj

Oppdrag nr. 1350020995 Målestokk: 1:100 Status: Datarapport

Nardobakken
Nardobakken Eiendom AS

BORPROFIL HULL NR.: A1

TERRENGHØYDE: +59,0 PRØVETYPE: 54 mm



Rambøll AS - Region Midt-Norge
P.b. 9420 Sluppen
Mellomila 79, N-7493 Trondheim
TLF: 73 84 10 00 - FAX: 73 84 10 60
www.ramboll.no

Tegning nr.

Rev.

109

0

Dybde, m	Jordart	Sign.	Lab. nr.	Vanninnhold (w) i %				γ kN/m ³	Skjærfasthet (C_u) i kPa				S_t
				10	20	30	40		10	20	30	40	
5	matjord		06		•								
	TØRRSKORPELEIRE		07			•						▼	
			08				•			▼			
	LEIRE		09				•	17.6 17.7	▼		▽	○	18 35
10													
			10				•	17.4 17.4	▼		▽	○	40 40
	enkelte små gruskorn		11				•	17.4 17.6	▼		▽	○	25 23
15													
			12				•	17.8 17.6	▼		▽	○	16 16
20													

Enkelt trykkforsøk : (strek angir def.% v/brudd)

Konusforsøk - Omrørt/uforstyrret: ▼ / ▽

Penetrometerforsøk ☐ Konsistensgrense w_p ———— w_L Andre forsøk:

T= Treksialforsøk

Ø= Ødometerforsøk

K= Kornfordeling

00	04.05.2017		BAGJ	KEG	PAW
Rev.	Dato	Tekst	Utarb	Kontr	Godkj

Oppdrag nr. 1350020995

Målestokk: 1:100

Status: Datarapport

Nardobakken
Nardobakken Eiendom AS

BORPROFIL HULL NR.: A2

TERRENGHØYDE: +61,5 PRØVETYPE: Naver/54 mm



Rambøll AS - Region Midt-Norge
P.b. 9420 Sluppen
Mellomila 79, N-7493 Trondheim
TLF: 73 84 10 00 - FAX: 73 84 10 60
www.ramboll.no


Tegning nr.

Rev.

110

0

Dybde, m	Jordart	Sign.	Lab. nr	Vanninnhold (w) i %				γ kN/m ³	Skjærfasthet (C _u) i kPa				S _t		
				10	20	30	40		10	20	30	40			
5	Siltig leire	1 x 1	1		●			19.5	▼			->95.0	->52.0	16	
			2		●			19.0	▼		▽	⊙		11	
			3		●			19.0	▼		⊙		▽	9	
10															

Enkelt trykkforsøk :  (strek angir def.% v/brudd)

Konusforsøk - Omrørt/uforstyrret: ▼ / ▽

Penetrometerforsøk ☐ Konsistensgrense w_P w_L

Andre forsøk:

T= Treksialforsøk

Ø = Ødometerforsøk

K= Kornfordeling

00	04.05.2017		BAGJ	KEG	PAW
Rev.	Dato	Tekst	Utarb	Kontr	Godk

Oppdrag nr. 1350020995

Målestokk: 1:100

Status: Datarapport

Nardobakken

Nardobakken Eiendom AS

BORPROFIL HULL NR.: B2

TERRENGHØYDE: +62,0 PRØVETYPE: 54 mm



Rambøll AS - Region Midt-Norge
P.b. 9420 Sluppen
Mellomila 79, N-7493 Trondheim
TLF: 73 84 10 00 - FAX: 73 84 10 60
www.ramboll.no

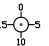
Tegning nr.

Rev.

111

0

Dybde, m	Jordart	Sign.	Lab. nr.	Vanninnhold (w) i %				γ kN/m ³	Skjærfasthet (C_u) i kPa				S_t
				10	20	30	40		10	20	30	40	
5	Blandet	∞	1		•								
		1 x 1	2		•			20.0	▼			->55.0	4
		/	3		•							○	
	Sprøbrudd?	///	4			•	->52.0	18.0	▼		▽	○	15
	Kvikkleire	///	5					18.0	▼		▽	○	48
10	delvis kvikk delvis kvikk	///	6				->52.0	17.6	▼	▽		○	36 42
	leire sprøbrudd	///	7					17.9 17.9	▼		▽	○	35 34
	leire leire leire	///	8			•		18.7 18.2	▼		▽	○	28 30
	leire leire	///	9			•		18.2	▼		▽	->55.0	13 12
15													
20													

Enkelt trykkforsøk :  (strek angir def.% v/brudd)

Konusforsøk - Omrørt/uforstyrret: ▼ / ▽

Penetrometerforsøk  Konsistensgrense w_p ——— w_L Andre forsøk:

T= Treksialforsøk

Ø= Ødometerforsøk

K= Kornfordeling

00	04.05.2017		BAGJ	KEG	PAW
Rev.	Dato	Tekst	Utarb	Kontr	Godkj

Oppdrag nr. 1350020995 Målestokk: 1:100 Status: Datarapport

Nardobakken
Nardobakken Eiendom AS

BORPROFIL HULL NR.: C2

TERRENGHØYDE: +63,5 PRØVETYPE: 54 mm



Rambøll AS - Region Midt-Norge
P.b. 9420 Sluppen
Mellomila 79, N-7493 Trondheim
TLF: 73 84 10 00 - FAX: 73 84 10 60
www.ramboll.no

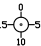
Tegning nr.

Rev.

112

0

Dybde, m	Jordart	Sign.	Lab. nr.	Vanninnhold (w) i %				γ kN/m ³	Skjærfasthet (C_u) i kPa				S_t
				10	20	30	40		10	20	30	40	
5													
	KVIKKLEIRE		01					17.6					36
	LEIRE							17.6					40
			02					17.9					35
								17.9					34
10			03					18.7					27
								18.2					30
			04					18.7					13
								19.2					12
15													
20													

Enkelt trykkforsøk :  (strek angir def.% v/brudd)

Konusforsøk - Omrørt/uforstyrret: ▼ / ▽

Penetrometerforsøk ☐ Konsistensgrense w_p ———— w_L Andre forsøk:

T= Treksialforsøk

Ø= Ødometerforsøk

K= Kornfordeling

00	04.05.2017		BAGJ	KEG	PAW
Rev.	Dato	Tekst	Utarb	Kontr	Godkj

Oppdrag nr. 1350020995 Målestokk: 1:100 Status: Datarapport

Nardobakken
Nardobakken Eiendom AS

BORPROFIL HULL NR.: C2, Rambøll
TERRENGHØYDE: +63,5 PRØVETYPE: 54 mm



Rambøll AS - Region Midt-Norge
P.b. 9420 Sluppen
Mellomila 79, N-7493 Trondheim
TLF: 73 84 10 00 - FAX: 73 84 10 60
www.ramboll.no

Tegning nr. Rev.

113 0

Dybde, m	Jordart	Sign.	Lab. nr	Vanninnhold (w) i %				γ kN/m ³	Skjærfasthet (C_u) i kPa				S_t
				10	20	30	40		10	20	30	40	
5	matjord(silt,leirig,humusholdig)		01										
	oppfyll masse		02										
	tørreskorpeleire,sand,grus												
	TØRRSKORPELEIRE												
10	LEIRE		03										
			04										
	KVIKKLEIRE												
	LEIRE												
	enkelte små gruskorn												
15													
20													

Enkelt trykkforsøk : (strek angir def.% v/brudd)

Konusforsøk - Omrørt/uforstyrret: ▼ / ▽

Penetrometerforsøk ☐ Konsistensgrense w_p ——— w_L

Andre forsøk:

T= Treaksialforsøk

Ø= Ødometerforsøk

K= Kornfordeling

00	04.05.2017		BAGJ	KEG	PAW
Rev.	Dato	Tekst	Utarb	Kontr	Godkj

Oppdrag nr. 1350020995

Målestokk: 1:100

Status: Datarapport

Nardobakken
Nardobakken Eiendom AS

BORPROFIL HULL NR.: C2, supplerende

TERRENGHØYDE: +63,5

PRØVETYPE: Naver/54 mm



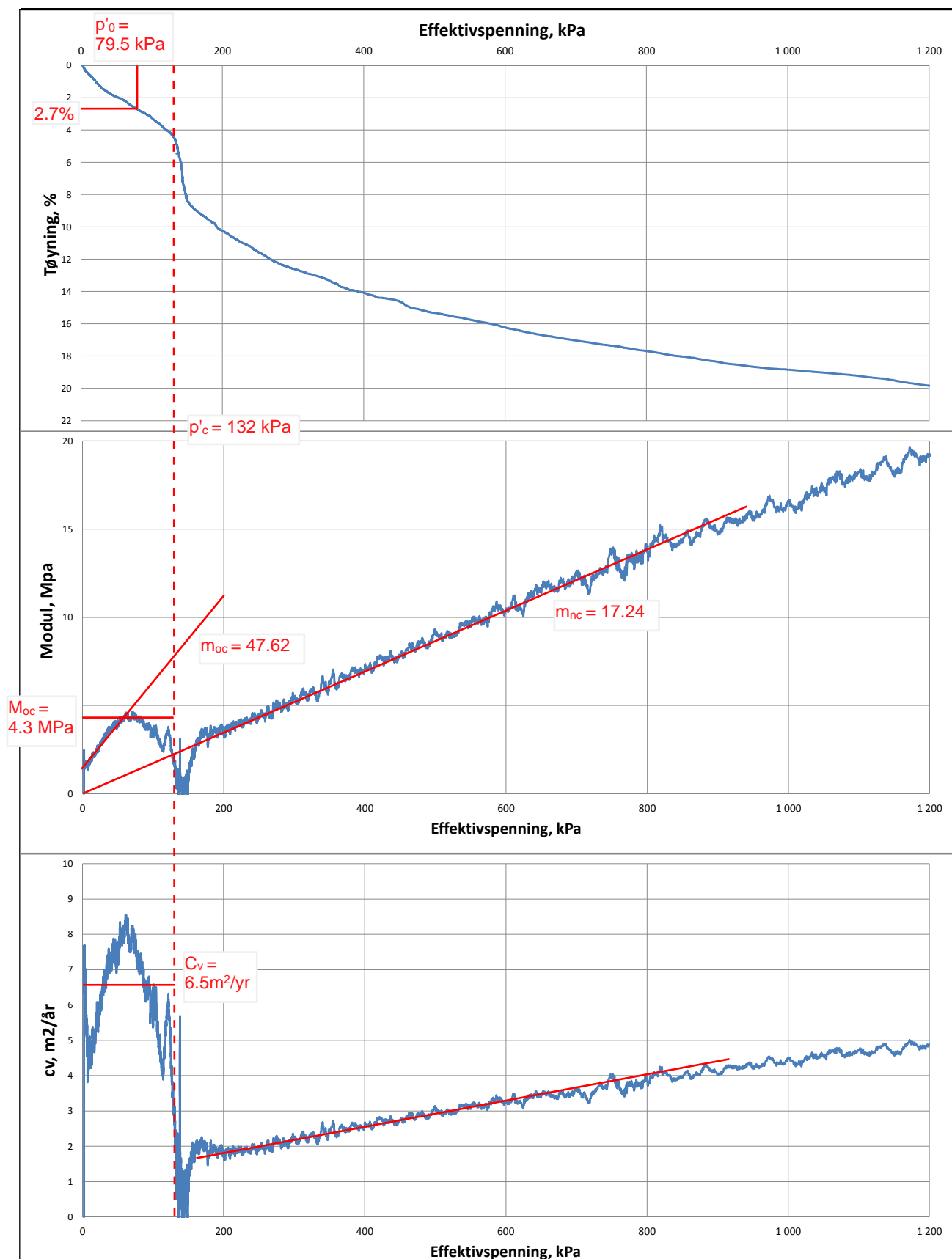
Rambøll AS - Region Midt-Norge
P.b. 9420 Sluppen
Mellomila 79, N-7493 Trondheim
TLF: 73 84 10 00 - FAX: 73 84 10 60
www.ramboll.no

Tegning nr.

Rev.

114

0



pkt C2 lab 1 dybde 6,35m Leire



Nardobakken

Nardobakken Eiendom AS

Ødometerforsøk

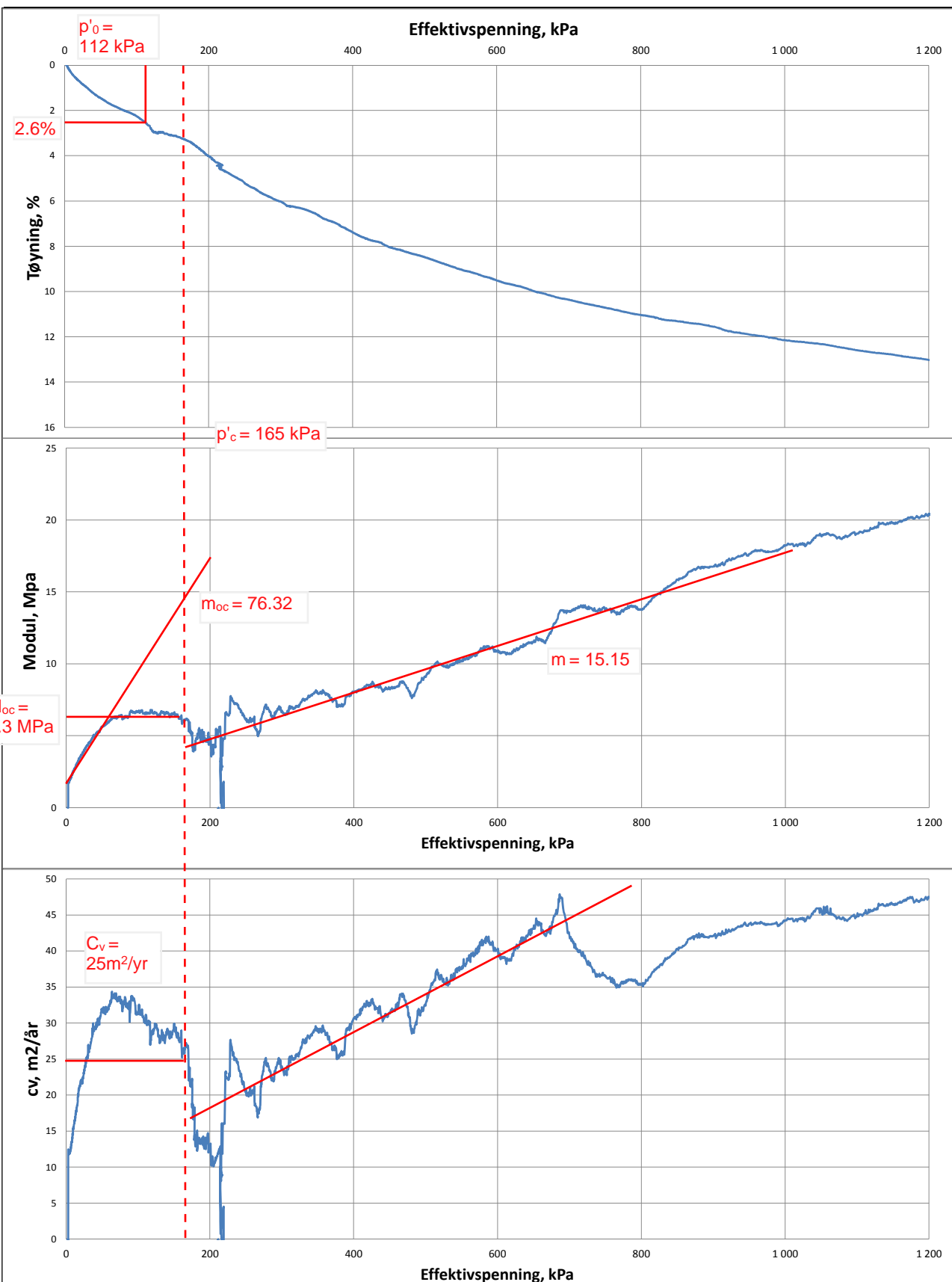
Oppdrag
1350020995

Tegn./kontr.
BAGJ/KEG

Dato
22.11.2016

Bilag
-

Tegn. Nr.
119



pkt C2 lab 3 dybde 10,30m Leire



Nardobakken

Nardobakken Eiendom AS

Ødometerforsøk

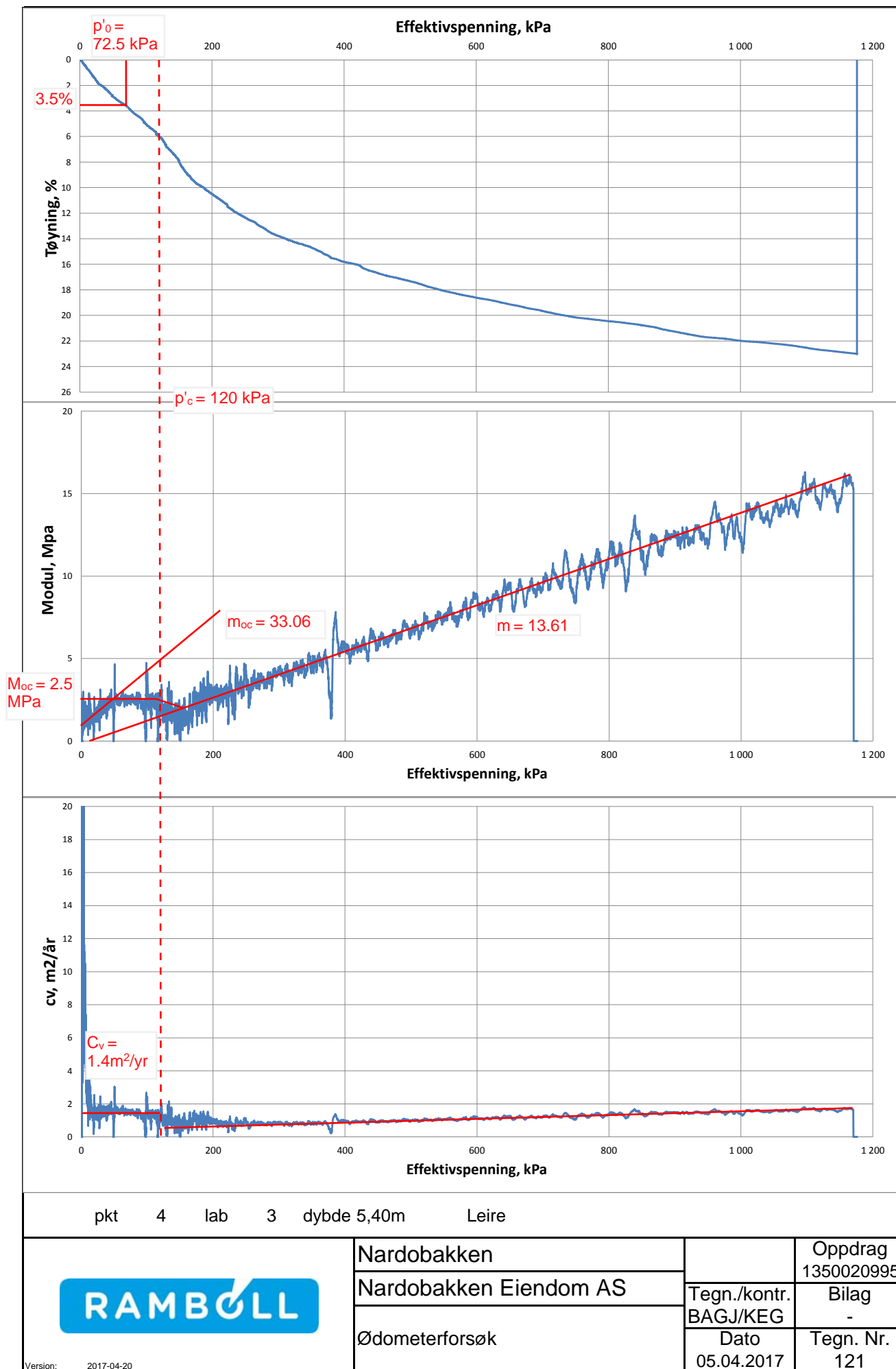
Oppdrag
1350020995

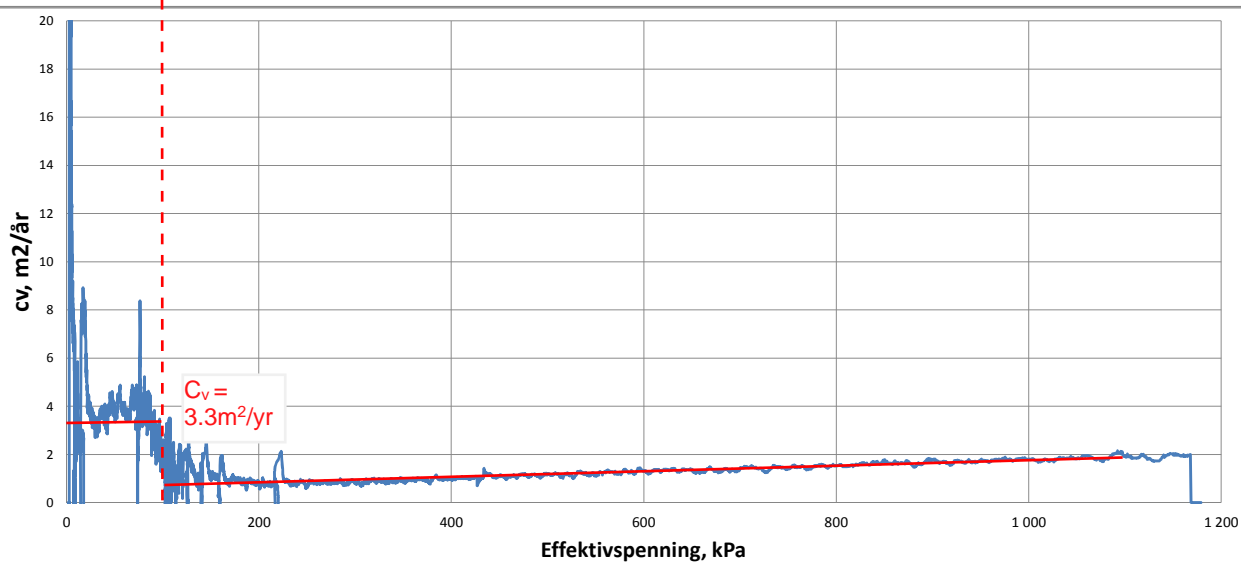
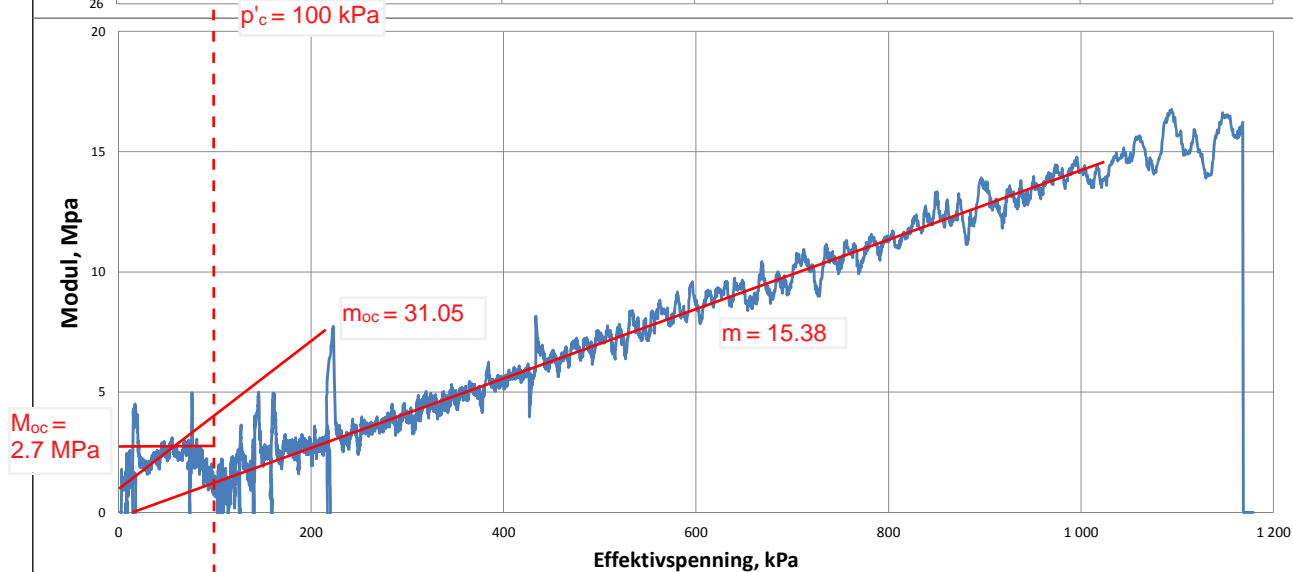
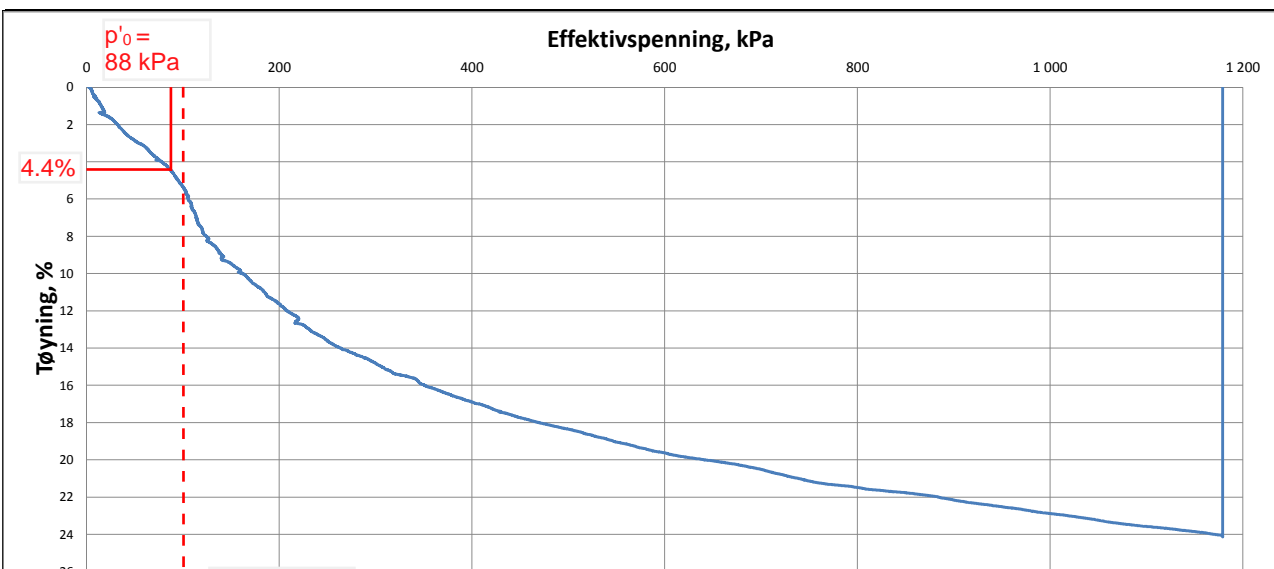
Tegn./kontr.
BAGJ/KEG

Dato
22.11.2016

Bilag
-

Tegn. Nr.
120





pkt 4 lab 4 dybde 7,40m Leire,(Kvikk)



Nardobakken

Nardobakken Eiendom AS

Ødometerforsøk

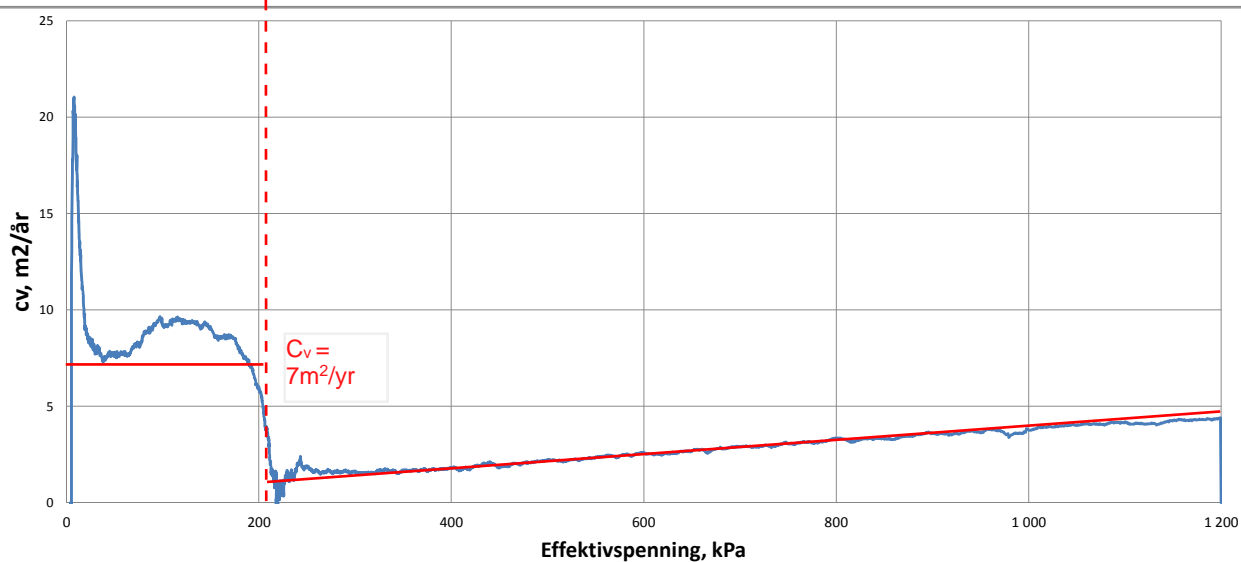
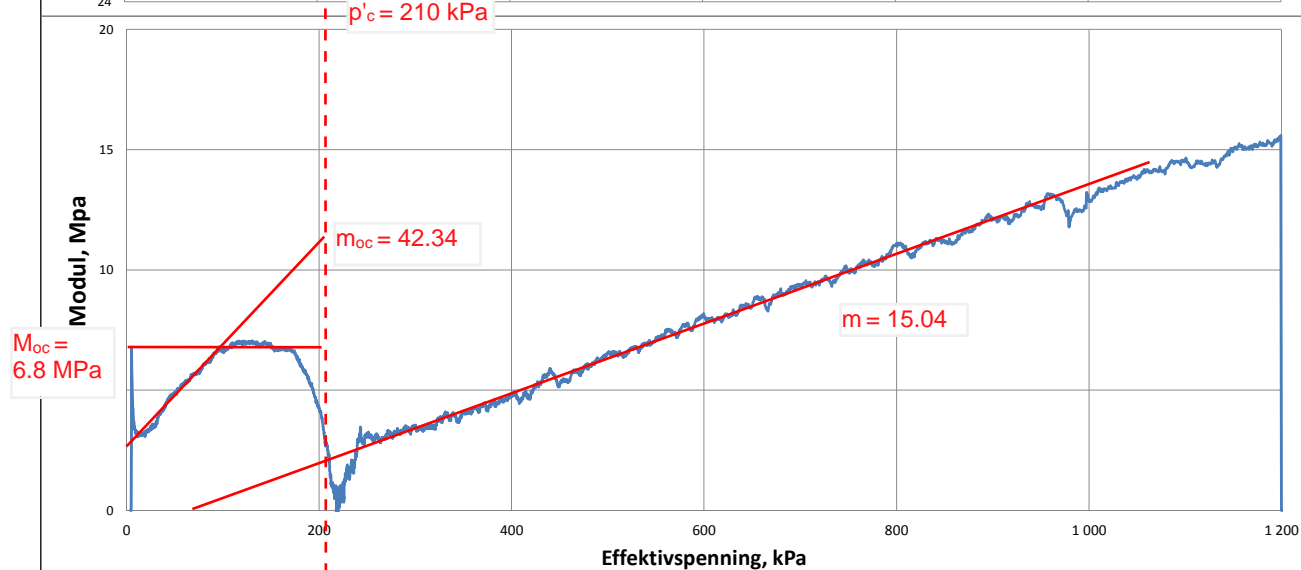
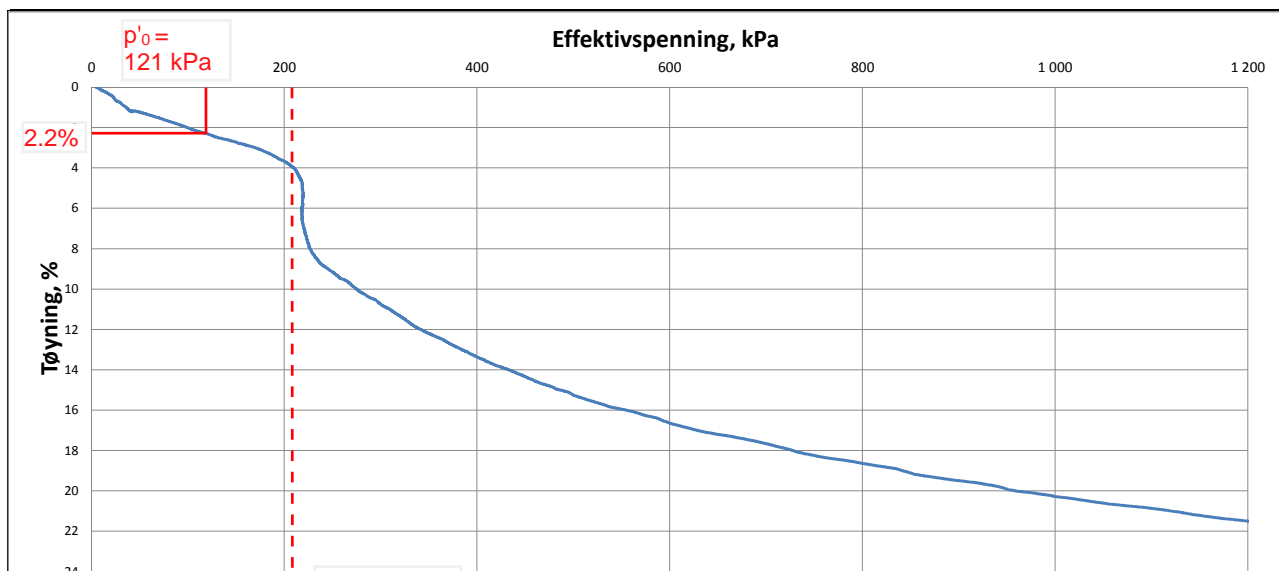
Oppdrag
1350020995

Tegn./kontr.
BAGJ/KEG

Dato
03.04.2017

Bilag
-

Tegn. Nr.
122



pkt 4 lab 5 dybde 11,40m Leire



Nardobakken

Nardobakken Eiendom AS

Ødometerforsøk

Oppdrag
1350020995

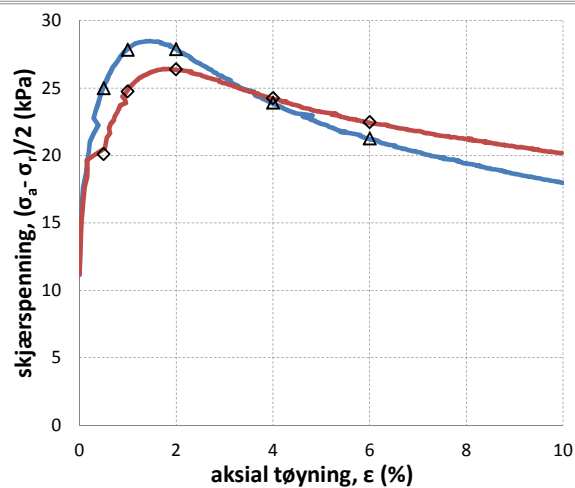
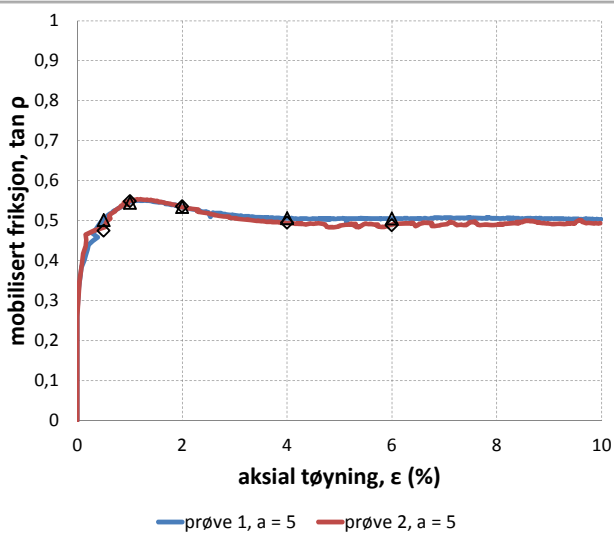
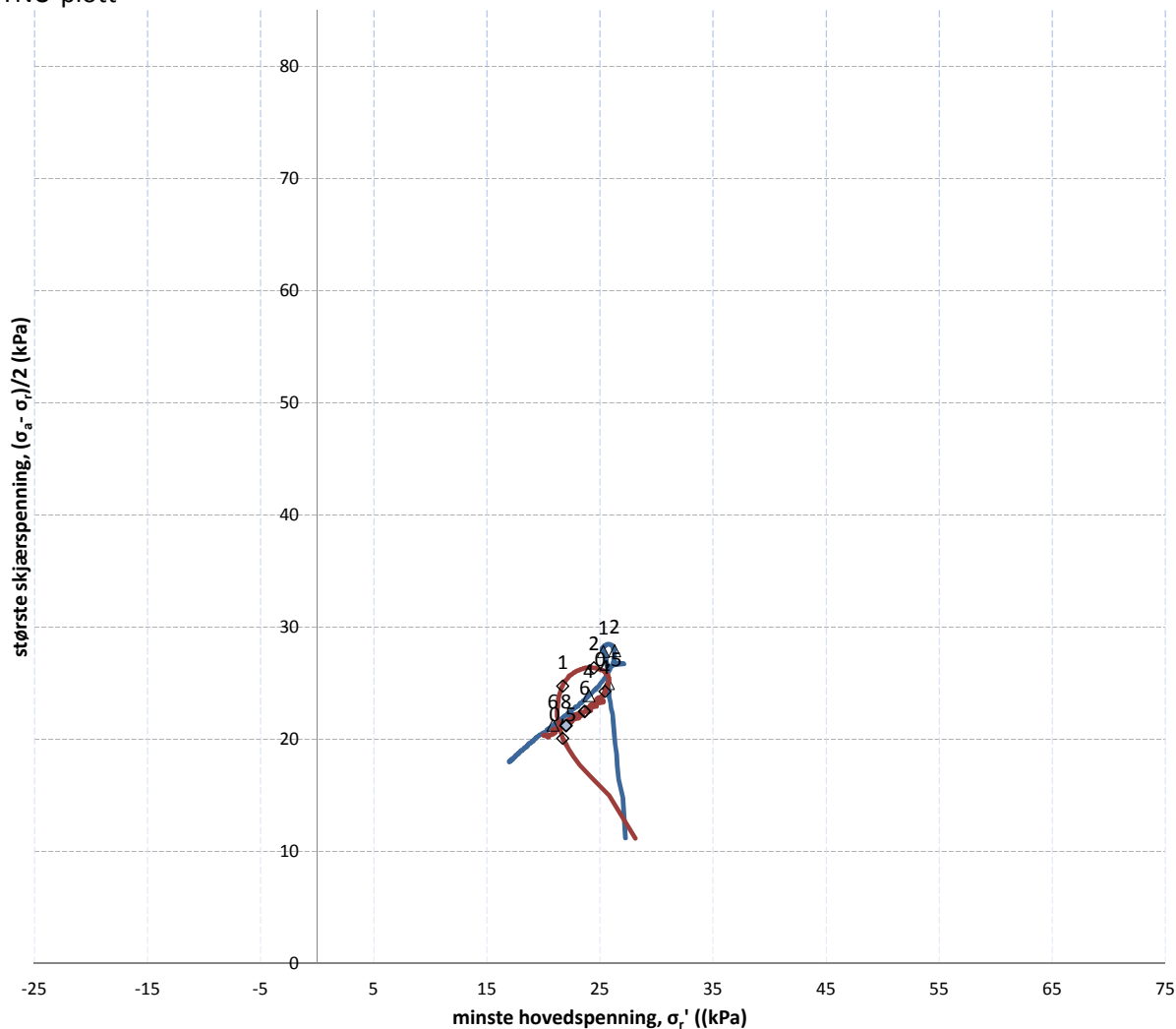
Tegn./kontr.
BAGJ/KEG

Dato
03.04.2017

Bilag
-

Tegn. Nr.
123

NTNU-plott



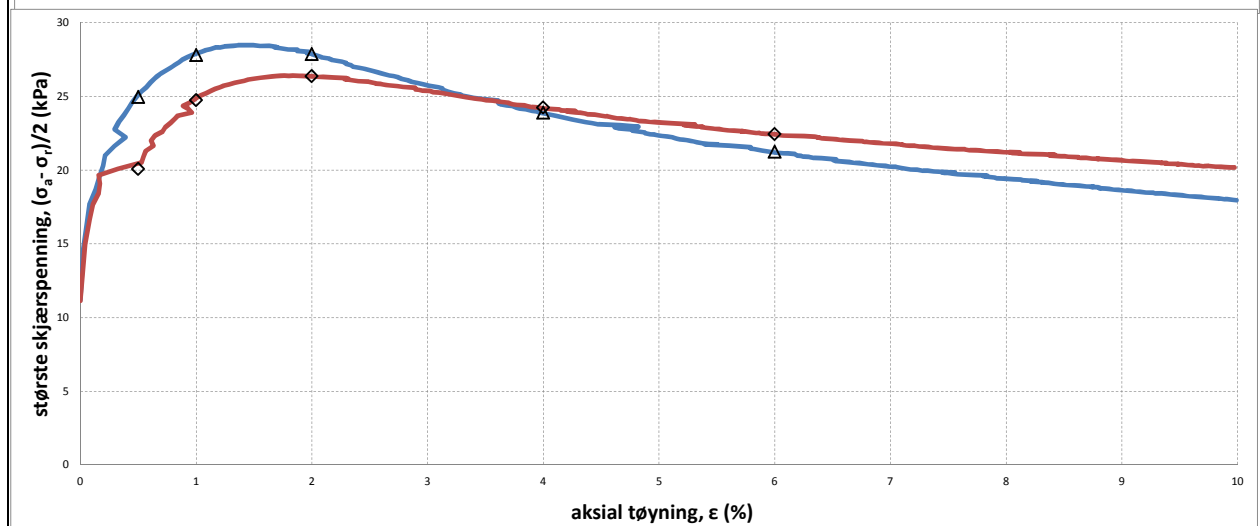
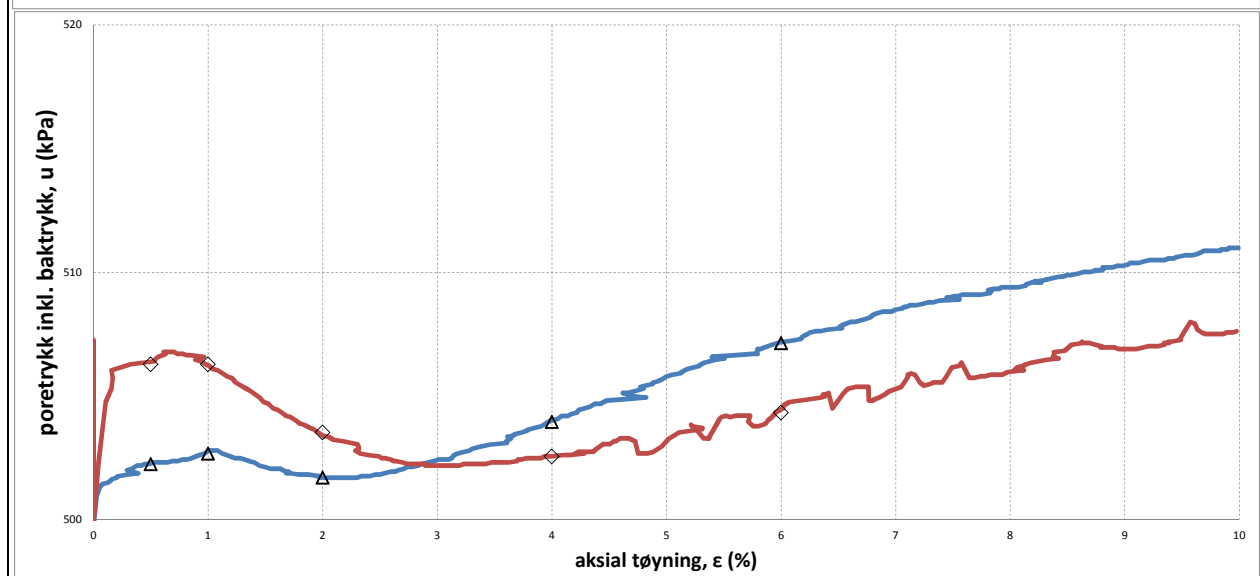
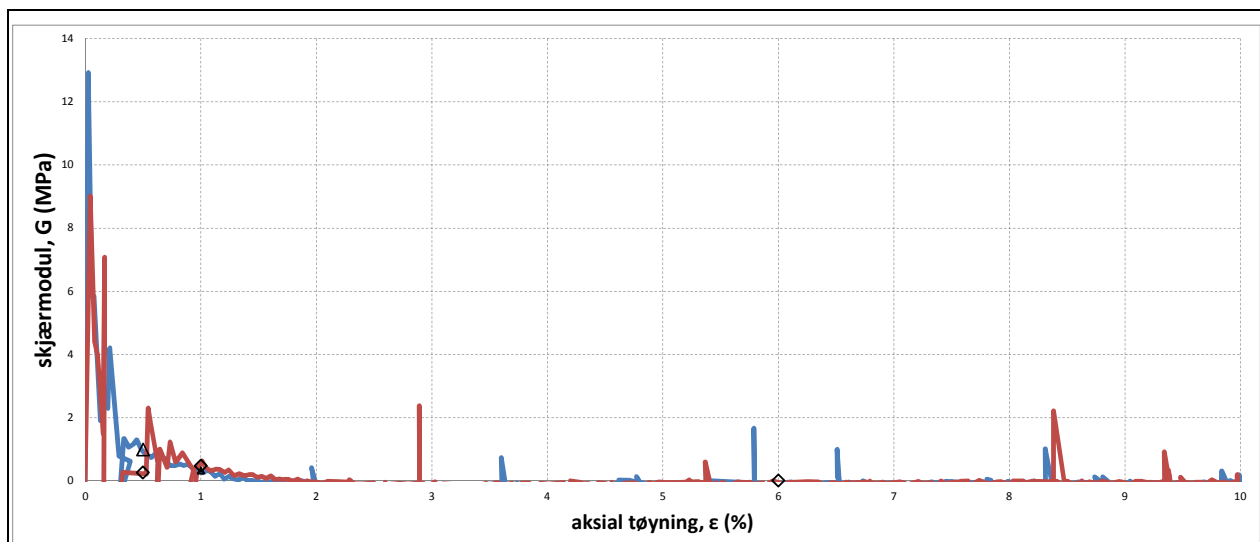
PRØVE	SYMBOL	PUNKT	LAB	DYBDE	TYPE	w(vekt%)	dV (%)	de/e ₀	Konsolideringsspenninger			KOMMENTAR
									p ₀ ' (kPa)	p _a ' (kPa)	p _r ' (kPa)	
1	Δ	C2	1	6,45m	CAUc	58,5	1,5	0,021	77	50	28	Leire
2	◇	C2	1	6,60m	CAUc	48,9	1,5	0,025	77	50	28	Leire



Nardobakken
Nardobakken Eiendom AS
TREAKSIALFORSØK

Tegn./kontr.
BAGJ/KEG
Dato
03.01.2017

Oppdrag
1350020995
Bilag
-
Tegn. Nr.
115



PRØVE	SYMBOL	PUNKT	LAB	DYBDE	TYPE	w(vekt%)	dV (%)	de/e₀	Konsolideringsspenninger			KOMMENTAR
									p₀' (kPa)	pₐ' (kPa)	pᵣ' (kPa)	
1	△	C2	1	6,45m	CAUc	58,5	1,5	0,021	77	50	28	Leire
2	◇	C2	1	6,60m	CAUc	48,9	1,5	0,025	77	50	28	Leire



Nardobakken

Nardobakken Eiendom AS

TREAKSIALFORSØK

Oppdrag
1350020995

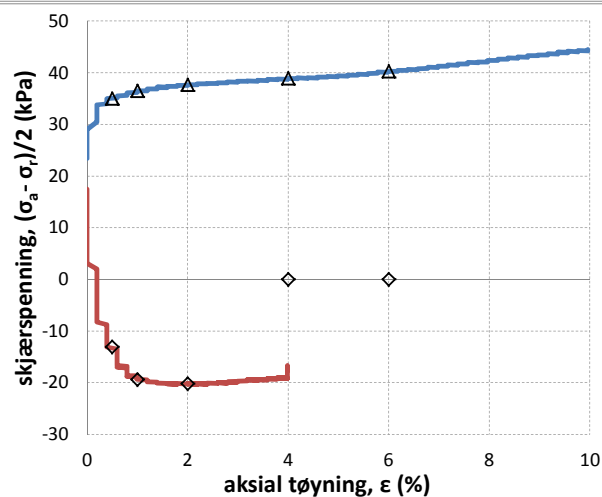
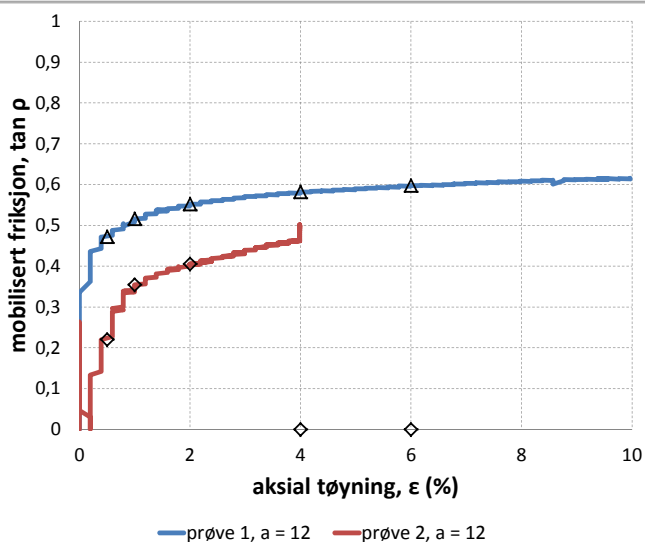
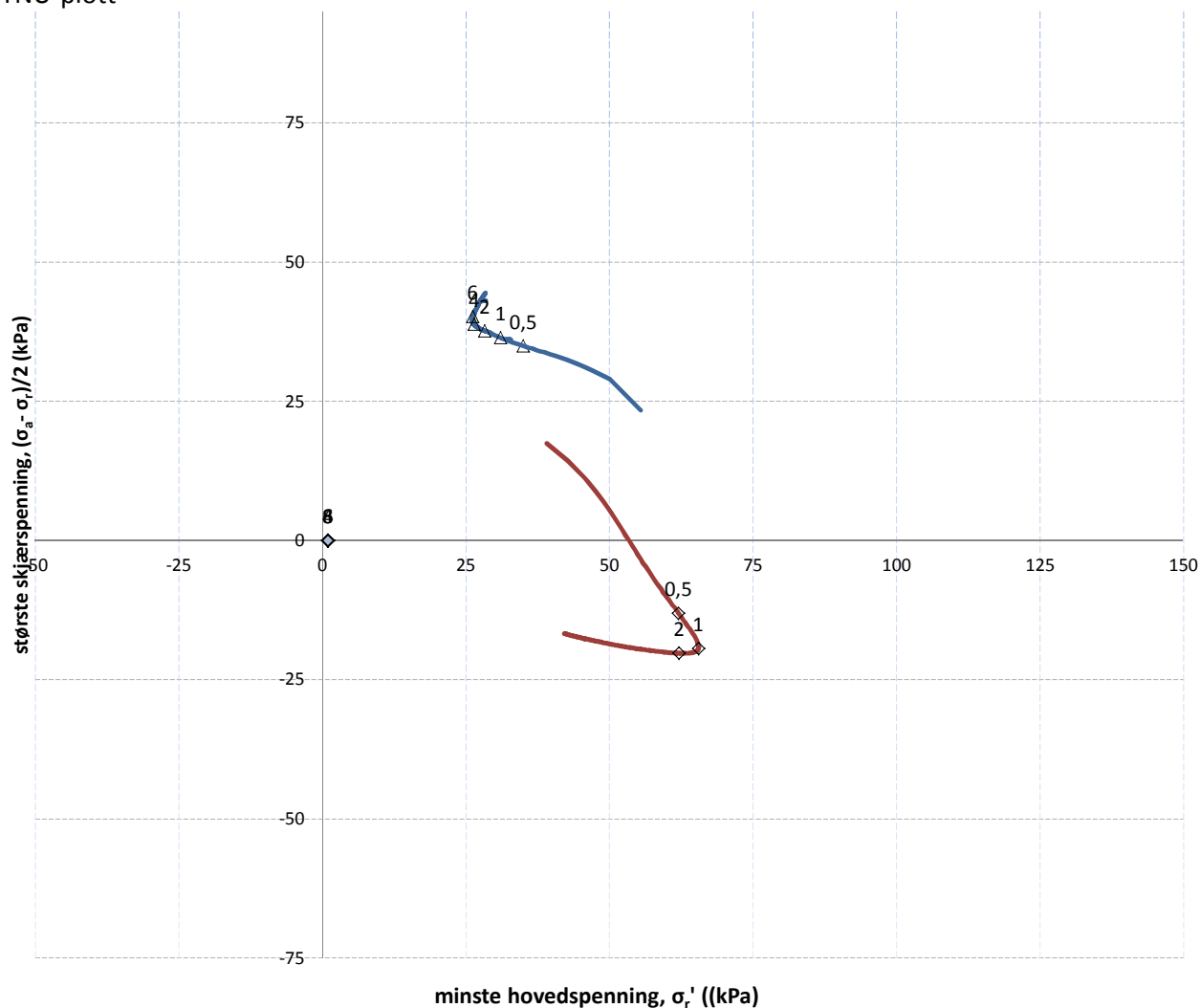
Tegn./kontr.
BAGJ/KEG



Dato
03.01.2017

Bilag
-

Tegn. Nr.
115

NTNU-plott



PRØVE	SYMBOL	PUNKT	LAB	DYBDE	TYPE	w(vekt%)	dV (%)	de/e ₀	Konsolideringsspenninger			KOMMENTAR
									p ₀ ' (kPa)	p _a ' (kPa)	p _r ' (kPa)	
1		C2	3	10,40m	CAUc	33,2	3,8	0,080	109	102	56	Leire
2		C2	3	10,55m	CAUp	41,7	1,3	0,024	109	73	39	Leire



Nardobakken

Nardobakken Eiendom AS

TREAKSIALFORSØK

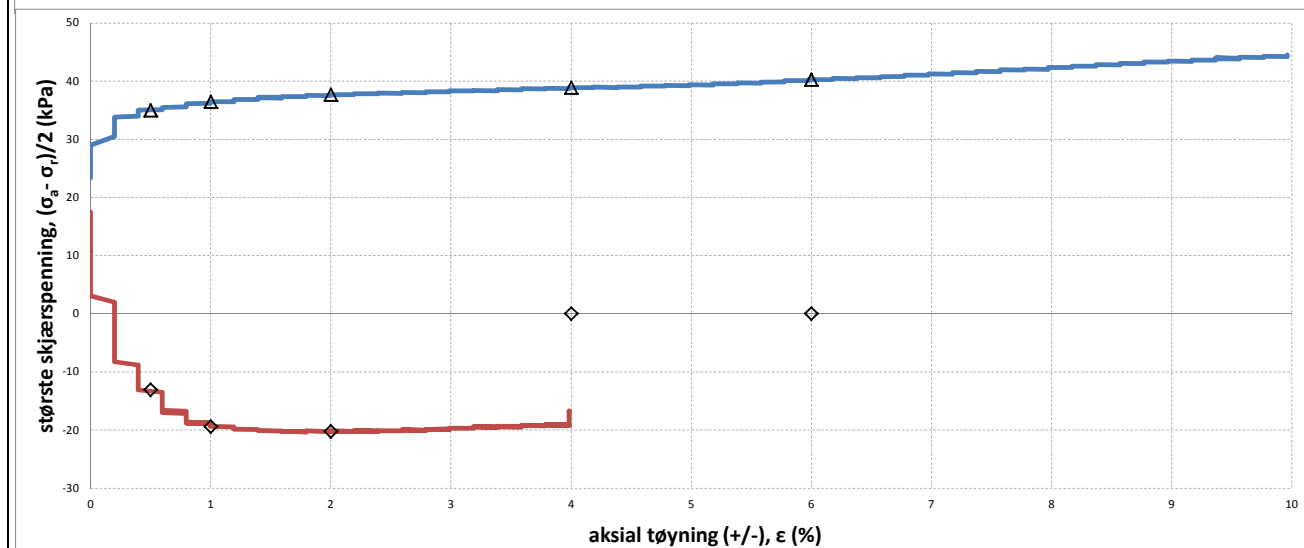
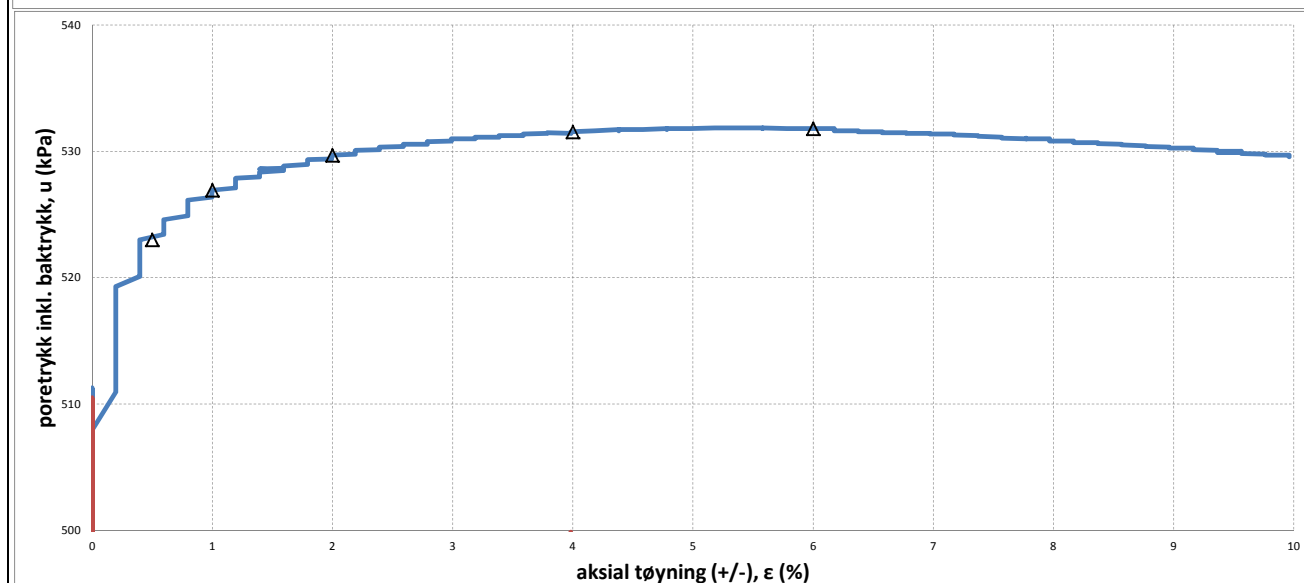
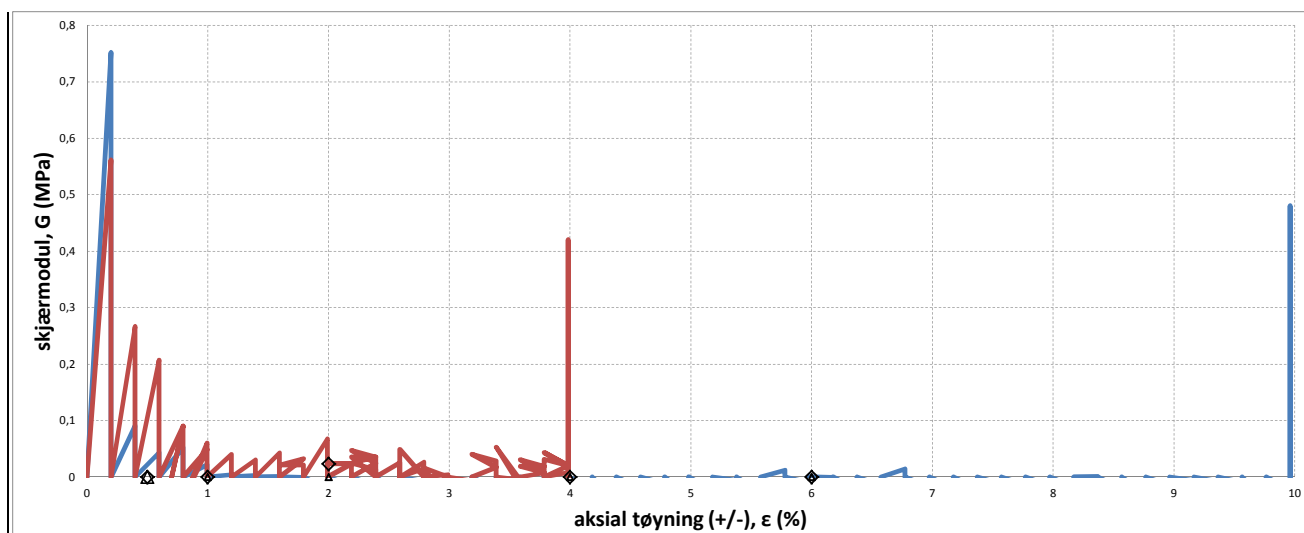
Oppdrag
1350020995

Tegn./kontr.	BAGJ/KEG
--------------	----------

Dato
05.01.2017

Bilag
-

Tegn. Nr.
116



PRØVE	SYMBOL	PUNKT	LAB	DYBDE	TYPE	w(vekt%)	dV (%)	de/e ₀	Konsolideringsspenninger			KOMMENTAR
									p ₀ ' (kPa)	p _a ' (kPa)	p _r ' (kPa)	
1	Δ	C2	3	10,40m	CAUc	33,2	3,8	0,080	109	102	56	Leire
2	◇	C2	3	10,55m	CAUp	41,7	1,3	0,024	109	73	39	Leire



Nardobakken

Nardobakken Eiendom AS

TREAKSIALFORSØK

Oppdrag
1350020995

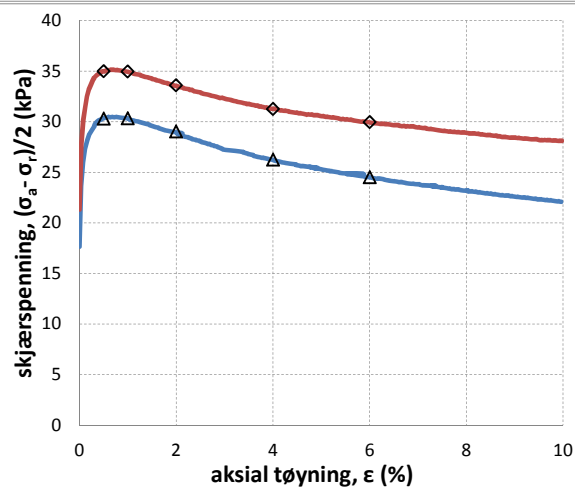
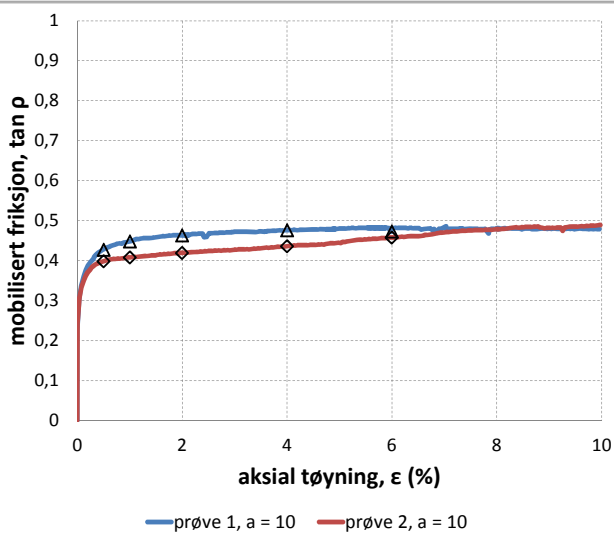
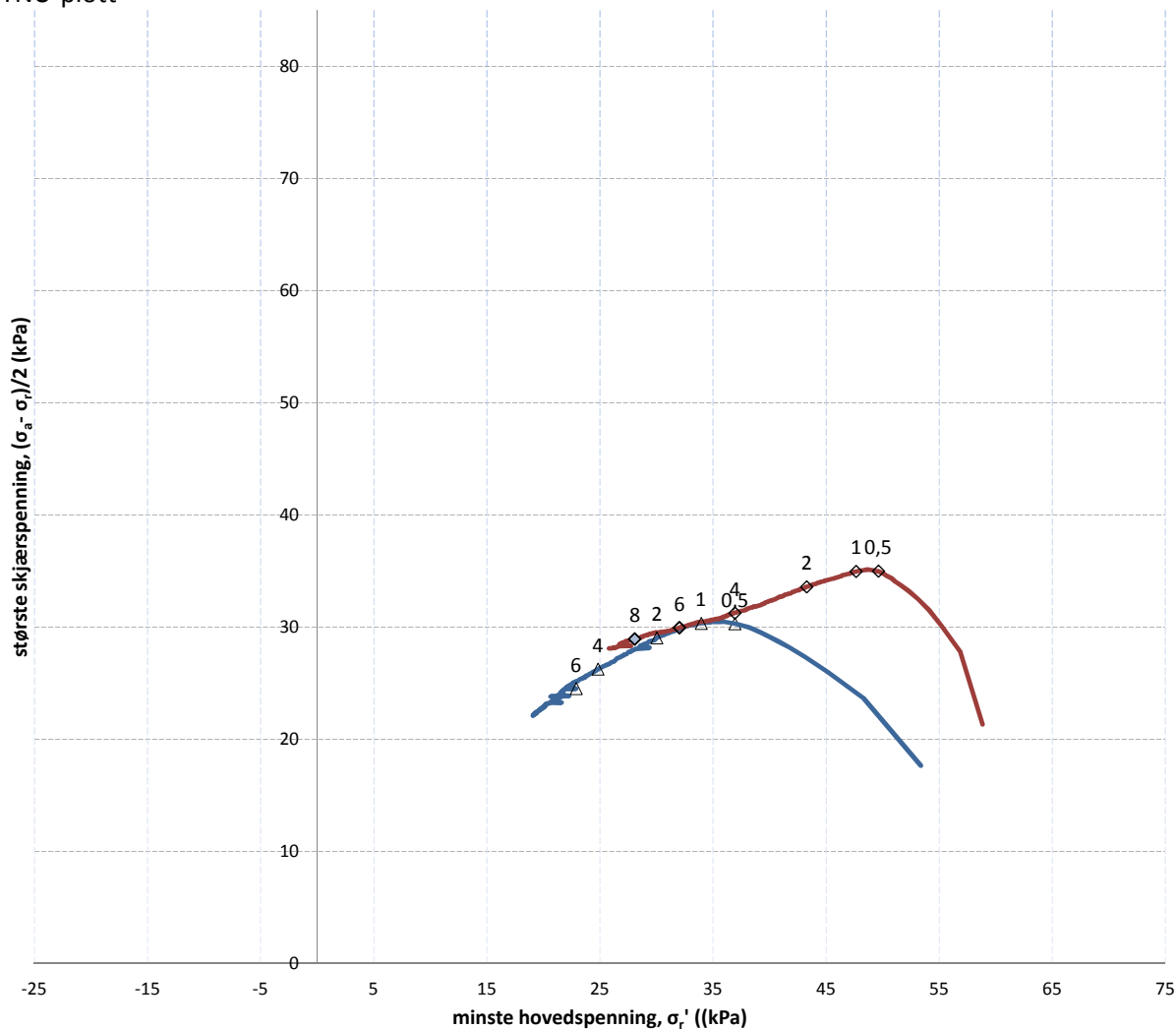
Tegn./kontr.
BAGJ/KEG

Dato
05.01.2017

Bilag
-

Tegn. Nr.
116

NTNU-plott



PRØVE	SYMBOL	PUNKT	LAB	DYBDE	TYPE	w(vekt%)	dV (%)	de/e ₀	Konsolideringsspenninger			KOMMENTAR
									p ₀ ' (kPa)	p _a ' (kPa)	p _r ' (kPa)	
1	Δ	4	4	7,50m	CAUc	42,5	3,2	0,058	85	87	53	Kvikkleire
2	◊	4	4	7,60m	CAUc	46,1	3,1	0,055	85	100	59	Kvikkleire



Nardobakken

Nardobakken Eiendom AS

TREAKSIALFORSØK

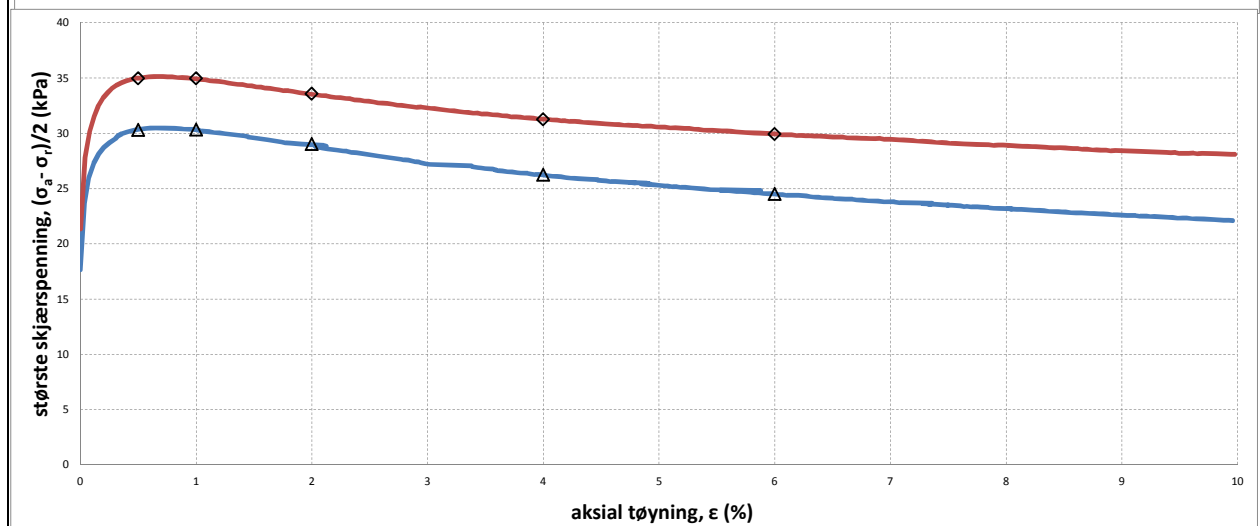
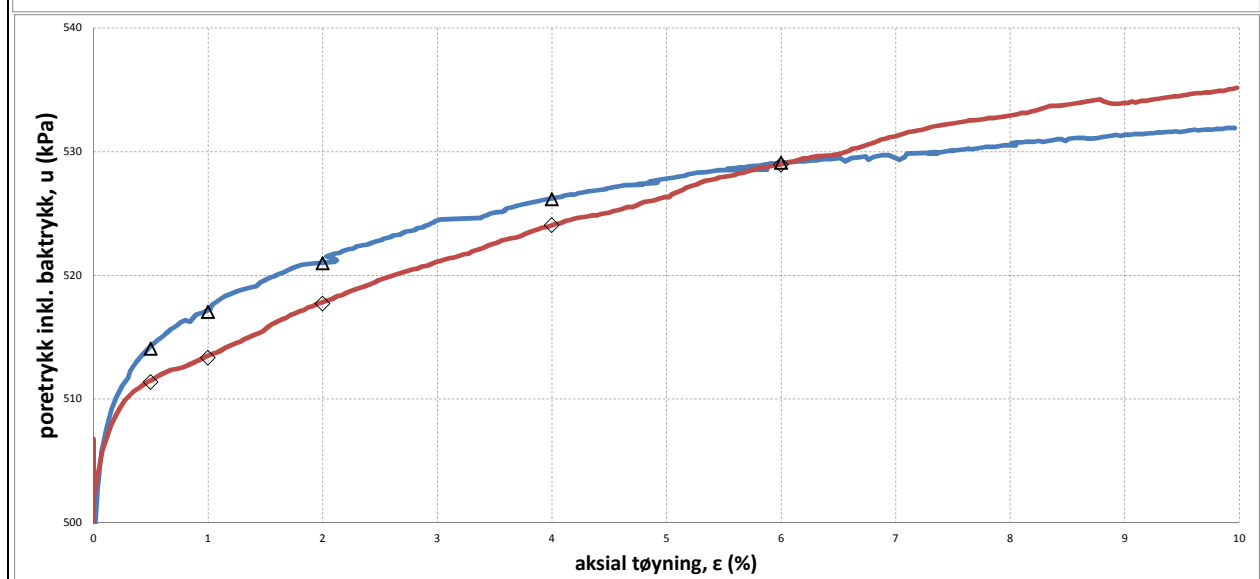
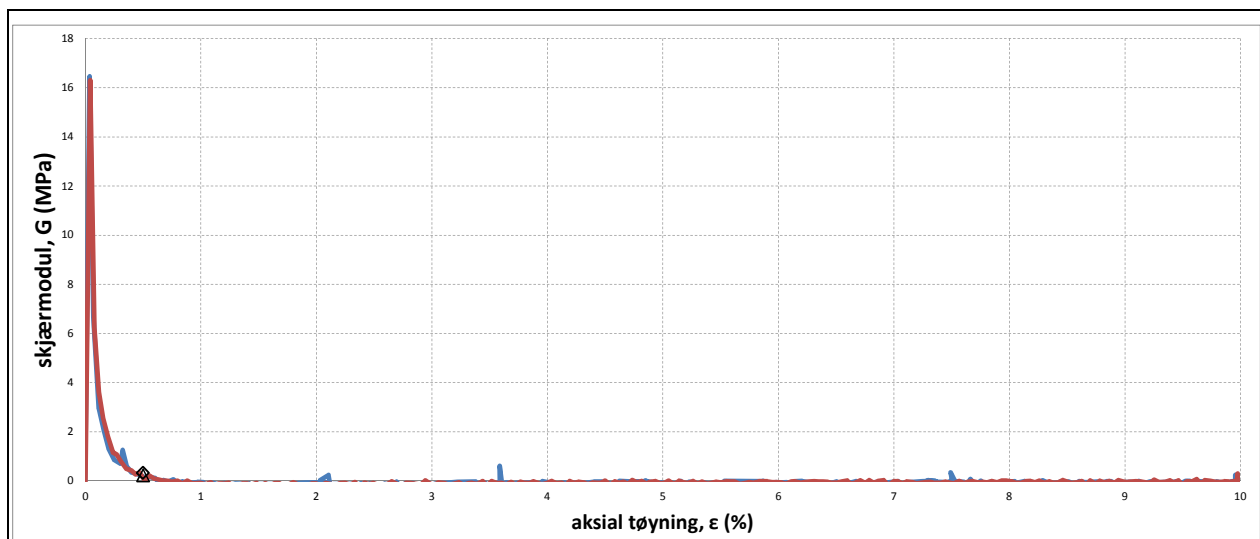
Tegn./kontr.
BAGJ/KEG

Dato
20.04.2017

Oppdrag
1350020995

Bilag
-

Tegn. Nr.
117



PRØVE	SYMBOL	PUNKT	LAB	DYBDE	TYPE	w(vekt%)	dV (%)	de/e₀	Konsolideringsspenninger			KOMMENTAR
									p₀' (kPa)	pₐ' (kPa)	pᵣ' (kPa)	
1	△	4	4	7,50m	CAUc	42,5	3,2	0,058	85	87	53	Kvikkleire
2	◇	4	4	7,60m	CAUc	46,1	3,1	0,055	85	100	59	Kvikkleire



Nardobakken

Nardobakken Eiendom AS

TREAKSIALFORSØK

Oppdrag
1350020995

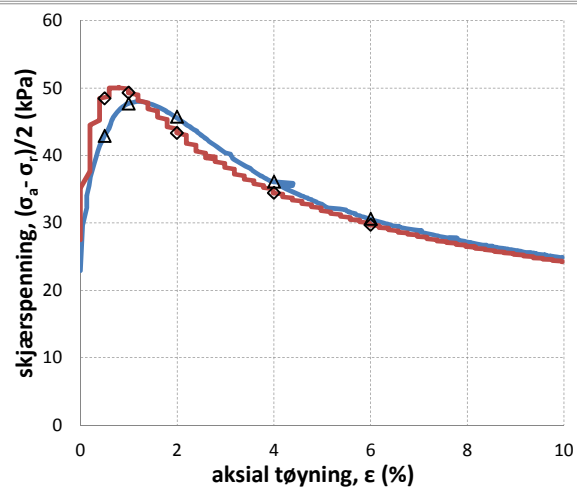
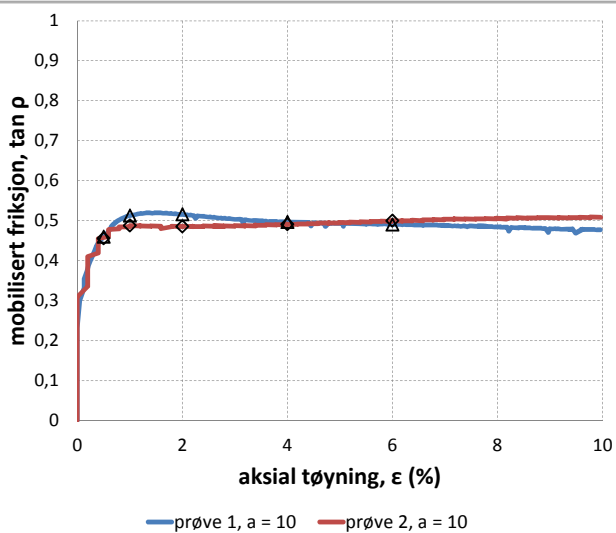
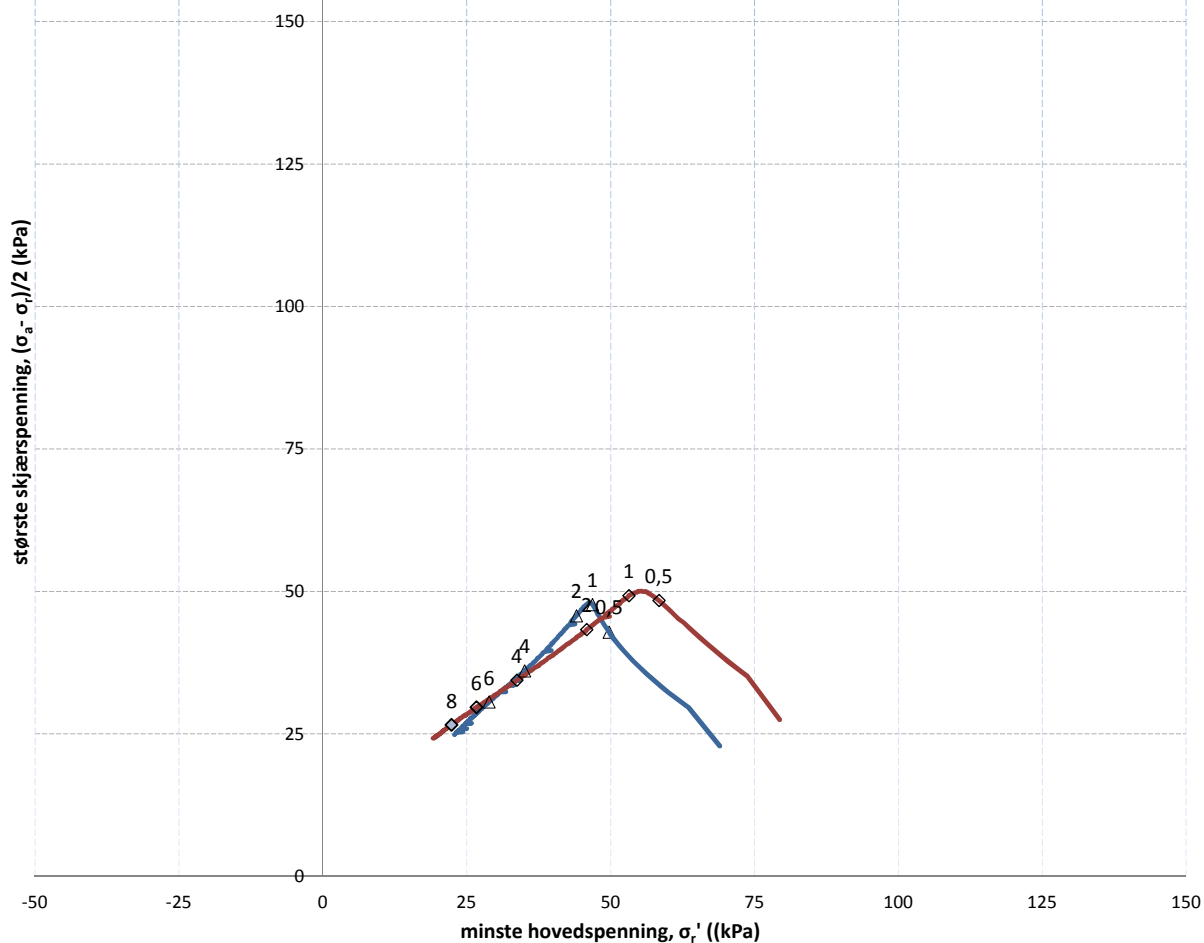
Tegn./kontr.
BAGJ/KEG

Dato
20.04.2017

Bilag
-

Tegn. Nr.
117

NTNU-plott



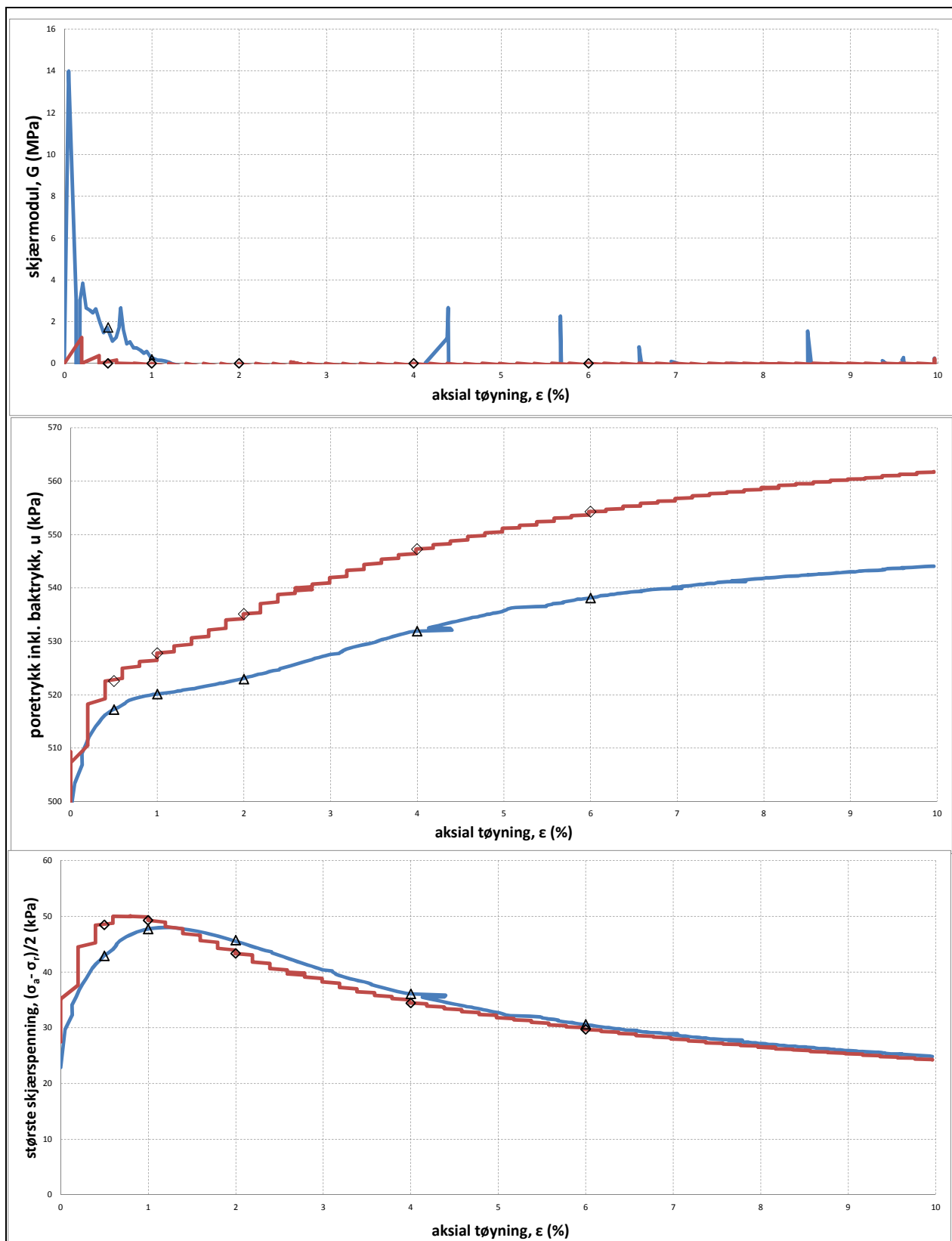
PRØVE	SYMBOL	PUNKT	LAB	DYBDE	TYPE	w(vekt%)	dV (%)	de/e ₀	Konsolideringsspenninger			KOMMENTAR
									p ₀ ' (kPa)	p _a ' (kPa)	p _r ' (kPa)	
1	Δ	4	5	11,50m	CAUc	43,8	1,9	0,034	112	114	69	Leire
2	◇	4	5	11,60m	CAUc	43,6	1,8	0,033	112	133	79	Leire



Nardobakken
Nardobakken Eiendom AS
TREAKSIALFORSØK

Tegn./kontr.
BAGJ/KEG
Dato
18.04.2017

Oppdrag
1350020995
Bilag
-
Tegn. Nr.
118



PRØVE	SYMBOL	PUNKT	LAB	DYBDE	TYPE	w(vekt%)	dV (%)	de/e ₀	Konsolideringsspenninger			KOMMENTAR
									p ₀ ' (kPa)	p _a ' (kPa)	p _r ' (kPa)	
1	△	4	5	11,50m	CAUc	43,8	1,9	0,034	112	114	69	Leire
2	◇	4	5	11,60m	CAUc	43,6	1,8	0,033	112	133	79	Leire



Nardobakken

Nardobakken Eiendom AS

TREAKSIALFORSØK

Oppdrag
1350020995

Tegn./kontr.
BAGJ/KEG

Dato
18.04.2017

Bilag
-

Tegn. Nr.
118